POLITECNICO DI TORINO

Master of Science in Physics of Complex Systems

Final dissertation

Nuclear Quantum Effects on Hydrogen diffusion via Langevin-based Molecular Dynamics

Supervisors
Prof. Alessandro PELIZZOLA
Dr. Fabio FINOCCHI
Dr. Simon HUPPERT

Candidate
Niccolò AVALLONE

ACADEMIC YEAR 2019 - 2020

Summary

In condensed matter and molecules, light nuclei, mainly hydrogen, exhibit the so called Nuclear Quantum Effects (NQEs), such as zero-point energy motion and tunneling, due to their intrinsic quantum delocalization. NQEs can have a large impact on the structure and the dynamics of materials. Any approximated method that treats light nuclei as classical objects cannot reproduce correctly predict their quantum behaviour. Real applications of this problem are, for example, solid fuel cells, which are relevant for energy harvesting.

The most used approach to study the NQEs is the Feynman Path Integral (PI) formalism, which conserves the concept of trajectories in the quantum picture, hence the use of Molecular Dynamics simulation techniques, such as Ring Polymer Molecular Dynamics. However, PI-based methods present high computational costs, urging the development of simpler alternative techniques. A promising method is the Quantum Thermal Bath (QTB). Its main idea is to maintain the classical equations of motion and trajectories, but to use a generalized Langevin equation with colored noise to mimic quantum delocalization of light nuclei. Although QTB has proven efficient for a variety of problems, it suffers from a major drawback, namely the Zero-Point Energy Leakage. Therefore, the method is refined into the Adaptive Quantum Thermal Bath (adQTB), thanks to the Quantum Fluctuation-Dissipation theorem, which allows to recover the correct quantum energy distribution during the simulation.

This work is a comparative study of these methods on a simple model of a 2D solid material, in which protons or hydrogen can diffuse. We have designed the model system in a way to set various time and energy scales that are connected to hydrogen diffusion in real materials. By using this model, we discuss classical diffusion (used as a reference) and approximate quantum simulation methods (QTB and adQTB). We show that nuclear quantum effects can play an important role on diffusion and modify the rate constants substantially. Before discussing the results of numerical simulations in Chapter 4, we present in Chapters 2 and 3 the main methods in statistical physics that are relevant in this context.

Acknowledgements

I thank for this work the research group of Low-dimensional Oxides at Institut des NanoSciences de Paris (INSP) - Sorbonne Université - in particular Dr. Fabio Finocchi, Dr. Simon Huppert and Dr. Philippe Depondt, which dedicated much of their time to explain me their work and help me during my research internship. I thank also Erika Fallacara for her support during the internship and Thomas Plé for his suggestions.

At the end of my formation as a university student, I wish to heartly thank all people who helped me and supported me along the path of my Bachelor in Physics and my Master in Physics of Complex Systems. In particular, my parents - Vincenzo and Serenella - and my sister Arianna, who have always believed in me. Adele Ravagnani, who has been at my side for all these years. My companions and friends Riccardo Corno, Dario D'Asaro, Maria Giorgi, Ivan De Carlo, Gianluca Boni and Emanuele Massa. I thank also Sergio Scibilia, Adele Biscotti, Matteo Sabbatini and Prof. Enzo Novara for their friendship.

I am grateful to Università di Torino, Politecnico di Torino, Sorbonne Université for the knowledge and the abilities which will be the basis of my career.

Table of Contents

List of Tables

List of Figures

Chapter 1

Introduction

1.1 Nuclear Quantum Effects

Even if the laws of Quantum Mechanics are well known and formulated, many-body quantum physics still presents a major theoretical challenge. Indeed, when it is necessary to deal with a system of many quantum particles, it is practically impossible to solve the Schrödinger equation for an high number of degrees of freedom. Therefore, one first step to deal with complex quantum multi-atomic systems is to decouple the electronic and nuclei degrees of freedom i.e. assuming an adiabatic separation between the electronic and nuclear time scales. This is the so-called Born-Oppenheimer approximation, which is based on the assumption that all nuclei of a quantum system are much heavier than the electrons, so their behaviour can be considered classical and simply Newton's second law describes their dynamics. Electrons are considered to be always in the ground state configuration corresponding to a given nuclear configuration. This electronic ground state can be approximated using a variety of methods, depending on the required accuracy and on the computational resources available. Some approaches rely on an explicit calculation of the ground state energy (within certain approximations, such as the Density Functional Theory which allows to treat relatively large systems - up to hundreds of atoms - at a limited computational cost). In other cases, the Born Oppenheimer energy is modeled through analytical expressions, that depend on the nuclei position and on parameters that are fitted to best reproduce the experimental observation. Once the electronic ground state energy is determined, the nuclei, because of their mass, are often considered as classical objects, following Newton's law of motion in the potential energy landscape given by the Born Oppenheimer approximation. This classical representation of the atomic nuclei allows to dramatically simplify the calculations and it provides good results for heavy atoms. However, when light atoms are considered in the systems, classical framework cannot provide an exhaustive description of the microscopic phenomena. Indeed, light nuclei present a number of purely quantum properties, known as **Nuclear Quantum Effects** (NQEs).

Experimental evidences of NQEs have shown that they are present not only in typical quantum regimes, such as at low temperature [1], or in extreme conditions, like high pressure [2], but also surprisingly close to ambient conditions, as in the case of reactions involving proton transfer [3] or displaying isotopic effects [4, 5]. Therefore, the understanding of NQEs and in general of quantum dynamics has become crucial for the development of numerous applications in material science and energy storage [6, 7].

There is no general classification of light and heavy nuclei. Therefore, in order to have an approximate idea of the elements that could present some NQEs, it is possible to consider the de Broglie thermal wavelength, where, k_B is the Boltzmann constant, T the temperature, m the mass of the particle and h the Planck constant

$$\lambda = \frac{h}{\sqrt{2\pi k_B T}} \tag{1.1}$$

If de Broglie wavelength is of the order of magnitude of the characteristic length scale of the system (lattice parameters, inter-atomic distances, mean free path ...), the quantum nature of the nuclei cannot be neglected.

In this thesis, we consider mainly hydrogen as light nuclei and the aim is to illustrate and study new methods that allow the simulation of its diffusion properties in solids. Although its mass is much heavier than the electron mass ($m_H = 1836 m_e$) hydrogen has a De Broglie wavelength at room temperature of the order of the Å. For a generic solid material, we then expect that the quantum delocalization of the hydrogen has a major impact on the properties of the system and the NQEs cannot be neglected [8], and more particularly zero-point motion which allows the hydrogen to diffuse even in a very low temperature regime. Tunnelling, another typical quantum phenomena, can also influence hydrogen diffusion. In the following paragraphs, review some examples of NQEs in real systems, in order to explain their importance and motivate the field of research.

1.1.1 Quantum-driven phase transitions

NQEs are necessary to reproduce accurately the phase diagram of many molecular materials, such as ferroelectric crystals like $BaTiO_3$ [9] or even simple molecules like water. Indeed, ice presents many exotic phases under pressure, which can be observed for examples on planets inside [10] and outside [11] our Solar systems. In many of these phases, NQEs play a major role in both the structural properties and in the phase transitions [12].

Let us consider an example more in details [13, 2]. Ice under pressure has a quantum-driven phase transition between the so-called Phase VII and the Phase X. In the former, ice has a cubic structure with disordered hydrogen bonding. As pressure increases to $65GPa$, Raman and infrared spectra show a transition towards a more symmetric phase, namely ice Phase X. At the atomic scale, simulations show that the distance d_{OO} between the oxygens atoms decreases and that for $d_{OO} \simeq 2.42$Å, the proton sits at mid-distance of the two oxygen atoms instead of off-centre. This proton-centered structure shows that the difference between covalent and hydrogen bond does not apply in this symmetrized state as in ordinary ice.

This quantum phase transition can be modeled with a one-dimensional model, using the position of the hydrogen x along the oxygen-oxygen distance as coordinate and writing a potential $V(x)$, in which the pressure P is a variable parameter. The classical phase transition is simply given by the Landau picture [14] as

$$F(x; P) = Ax^4 + B(P - P_c)x^2$$

where A and B are two parameters, the pressure plays the same role as the temperature in typical phase transitions and x is the order parameter.

As P increases, a classical phase transition occurs when the form of the potential passes from a double well potential to a single well, at a $P_c \simeq 100GPa$. However, the quantum delocalization of the proton allows the quantum phase transition to occur before the classical one. The NQE at the base of the quantum phase transition is the zero-point energy E_0. As P increases, the barrier passes from $V(x) > E_0$ to values $V(x) \leq E_0$, shifting down the P_c from around 90-100 GPa in classical nuclei simulations dwon to $65GPa$ in quantum simulations (and in agreement with experimental measurements).

Therefore, in this example we have two main quantum effects: the tunneling of the proton in the Phase VII and the zero-point energy in the quantum phase transition to Phase X. Analogous quantum-driven phase transitions can be observed in salty ice as well [5].

1.1.2 Isotope effects

Most isotope effects cannot be captured within a classical description of the nuclei. These effects are therefore a signature of NQEs. They can have major impact on dynamical, elastic and thermal properties in condensed matter [15]. For example, in the case of lithium hydride (LiH) and lithium deuteride (LiD) [16], we observe changes in the vibrational spectra due to the dependence of phonons on atomic masses. The isotope masses has then an influence only on the optic modes, because they depends on the reduced mass, in which the lighter atom have an important weight. On the other hand, the acoustic modes depends in general only on the total mass, so a change from H to D does not change the phononic DOS. Moreover, isotope effects are at the base of anharmonicity differences between LiH and LiD and, in general, it is often an experimental hint of the presence of NQEs in the system.

We note that the classical Equipartition theorem, which we will review in Section 3.2, states that each degrees of freedom has a mean kinetic energy equal to $k_B T/2$.This is approximately valid at higher temperatures than Debye temperature, while below it NQEs become really relevant. Furthermore, within the Born-Oppenheimer approximation, the potential energy as well does not depend on the mass of the nuclei. Therefore, the isotope effect cannot be explained within a purely classical framework.

1.1.3 Proton diffusion in materials

An interesting quantum dynamics problem is that of proton or hydrogen diffusion in solid materials [17]. Many efforts are done in this regards because proton conduction and diffusion is at the core of the developments of hydrogen solid fuel cells [6, 7].

In general, NQEs, and particularly zero-point energy and tunneling tend to increase the proton diffusion, particularly at low temperatures: for a classical proton, diffusion is completely suppressed when $T \to 0$, whereas it is not the case for the quantum problem. In actual materials, proton and hydrogen diffusion mechanisms can be quite complex, as for instance in hydroxides, such as brucite [18]. These materials, under high pressure conditions, can have dramatic changes in their geometrical structure and therefore many interesting phenomena arise, such as proton frustration and proton diffusion. NQEs such as zero-point energy and tunneling can then enhance the diffusion and make possible the rearrangement of the protons.

Finally, possible applications of proton diffusion involving NQEs can be found also in biological system, such as water wires [19], which have also promising application in fuel cells.

1.1.4 Chemical reaction rates and hydrogen bond

The study of kinetics of chemical reactions very often involve the computation of chemical reaction constants, which determine the direction of the reactions (from reactants to products), and reaction rates, which quantify the speed at which reactants are converted to products. Reaction rates depend in general on the temperature and on the activation energy (see. in Section 2.6 Arrhenius law (2.55) [20]).

The problem can be described as a two states system, A for the reactants and B for the products, separated by an energy barrier, along a certain reaction coordinate ξ. One simple but interesting example are unimolecular dissociation [21], which can be described as a decaying process $N(t)/N(0) \propto e^{-k(T)t}$, where N is the concentration of reactants and $k(T)$ is the reaction rate. In many dissociations reaction involving light nuclei, such as hydrogen, NQEs can play a major role in the computation of reaction rates. Classical quantum simulations lead to different kinetic results, in particular the difference between classical and quantum activation energies.

1.2 The open question of Quantum Dynamics

The main fundamental problem of quantum dynamics is the impossibility of resolution of the time-dependent Schrödinger equation for large systems, due to its exponential scaling with the number of degrees of freedom. This is not only valid for electrons but also for light nuclei, even if we are not interested in the exchange and quantum coherence properties.

We have shown that NQEs of light nuclei are fundamental phenomena in a vast amount of complex systems. Despite the fact that much progress has been done, the computation of time-dependent properties of the nuclei, remains a very important theoretical challenge. These dynamical properties are captured by time correlation functions (see Section 2.3) which are of fundamental importance since they can be probed through different experimental techniques such as infrared/Raman spectroscopy or measurement of rate constants.

Many techniques and methods are being developed in recent years. However, currently, these methods are all approximations and there is not a unified quantum theory for non-static systems. Only two limit cases acan be shown to be exactly captured by most of approximated methods: the classical (high temperature) limit and the case of system with harmonic potential. Outside these limiting case, precise criteria for comparing different approximate methods are lacking. The discussion of the full extent of simulation methods to compute dynamical properties is outside the scope of this work. Here, we will focus on trajectory-based methods as they provide computationally efficient approximations for treating light nuclei as quantum particle in complex environments.

1.3 Structure of the dissertation

The aim of this work is discussing in details a new quantum Molecular Dynamics (MD) approach, called Quantum Thermal Bath (QTB) [22], which allows to simulate NQEs in real applications. This method is inspired by classical Langevin-based MD methods. We present also the recent refinement of QTB, namely the adaptive

QTB (adQTB) [23], which solves one of the issues of QTB and makes it more reliable, while cost-efficient simulation methods for NQEs in anharmonic systems.

In the first Chapter of the dissertation, we present Langevin equations in detail and the classical theory of stochastic processes linked to this fundamental equation. Moreover, we introduce the definitions of time-correlations functions and the Wigner-Khinchin, which, in the context of this work, are fundamental to the implementation of the quantum MD simulations studied in this work.

The second main chapter is dedicated to the Molecular Dynamics methods that are relevant to the study of NQEs. In particular, the classical Langevin thermostat is discussed in details, since it constitutes the basis for further quantum methods. We describe the Ring-Polymer Molecular Dynamics (RPMD) method, which is one of the main standard MD approach used for quantum systems. After the discussion of its drawbacks, we present in full details the two alternative quantum Langevin-based methods, namely the Quantum Thermal Bath and the Adaptive Quantum Thermal Bath, providing both theoretical explanations and computational details

Finally, a simple model to study the diffusion of hydrogen in solids is introduced and all results from classical and quantum simulations are discussed. A particular attention is dedicated to spectra and diffusion coefficients, with the aim of highlight NQEs and confront the different methods in their strength and drawbacks. Diffusion coefficients, which characterize the hydrogen diffusion process in materials, are computed with different techniques. The major result is the implementation of the innovative adaptation for the QTB, which is a completely new MD technique. Indeed, once the method is assessed and probed for simple systems, it can be actively used as a cost-efficient method to simulate NQEs in complex systems.

Chapter 2

Theoretical Background

In this chapter we present the basic theory and the fundamental equations that we have used all along this master thesis work. In particular, we concentrate on the Langevin equation: we introduce the study of Brownian motion and diffusion. Then we demonstrate how the it is possible to study a vast range of stochastic process with a generalized version of the Langevin equation. Then, we will introduce the study of time-correlation functions, which they will be the main tool to study the diffusion as a dinamical phenomena. The main references are [24, 25, 26, 27].

2.1 Langevin equation

2.1.1 Brownian motion

The Langevin equation was introduced for the first time by the French physicist Paul Langevin [28] as an approach to model Brownian motion. Brownian motion is the random motion of a small particle in a fluid and it was discovered by biologist Robert Brown [29] when he observed the motion of pollen grains and dust particles in a viscous medium. Its experimental results found a first theoretical explanation by Einstein [30], which was later confirmed by Perrin in 1909 [31]. He firstly described the problem in terms of a diffusion equation for the Brownian particle: he considered a one dimensional system, in which he defined a continuous density of the Brownian particles $\rho(x,t)$, function of both the position x and the time t, and he introduced also a diffusion coefficient D_x. Then, Einstein wrote a diffusion equation for the particle's density

$$\boxed{\frac{\partial\rho(x,t)}{\partial t} = D_x \frac{\partial^2\rho(x,t)}{\partial x^2}} \tag{2.1}$$

The formal solution of this equations gives a normal density distribution of the form $\rho(x,t) \propto e^{-\frac{x^2}{4Dt}}$. Hence, the first two moments of the distribution are derived: the mean displacement (first moment) is vanishing, resulting in the absence of a drift in the motion of the Brownian particle; however, the variance (second moment) or mean-squared displacement - defined as (2.3) - is non-vanishing

$$\langle x^2 \rangle \sim 2D_x t \tag{2.2}$$

where we considered the initial position $x(0) = 0$. In all previous formulas we also denoted the diffusion constant with a subscript x to indicate that Einstein's result is valid in the positions' space. Thus, Einstein's main result is that the displacement of Brownian particle is proportional to the squared root of the time. This is truly remarkable result because it means that the Brownian particle follows a random walk in its diffusive motion [24]. Furthermore, Einstein derived an expression for the diffusion coefficient directly from the definition of the mean-squared displacement

$$\boxed{D_x = \lim_{t\to\infty} \frac{1}{2t} \langle (x(t) - x(0))^2 \rangle} \tag{2.3}$$

which is extended in 3D as

$$D_x = \lim_{t\to\infty} \frac{1}{6t} \langle |\vec{x}(t) - \vec{x}(0)|^2 \rangle$$

The average $\langle \dots \rangle$ is taken over the ensemble - in our case, Canonical ensemble - at thermal equilibrium. Thanks to the classical Equipartition theorem 3.2.1, we obtain

$$\boxed{D_x = \frac{k_B T}{m\gamma}} \tag{2.4}$$

The formula (2.4) above, known as **Einstein's relation** for the diffusion coefficient, relates directly the friction parameter of the fluid to the main transport coefficient of diffusion. This result has a more wider meaning, since is part of the Fluctuations-Dissipation Theorem [26]. The theory of Brownian motion is one of the simplest approximate way to treat a non-equilibrium systems in which fluctuations play a major role into the the dynamics. In Section 3.4 this main concept will be explained in a more general way.

2.1.2 Langevin method

For a particle in a conservative force field, we can proceed as follows. Instead of using the Newton's equations of motion, which would conserve the energy, we build a microscopic and stochastic dynamics by the addition of two main terms: a frictional force and a random force. The former models the systematic effect of the viscous medium in which the Brownian particle moves. Therefore, this force has the usual form proportional - with a negative sign - to the velocity of the particle and a friction coefficient γ is introduced as a proportionality constant. The random force aims at modeling the random collisions that the Brownian particle has with the surrounding particles of the medium. Thus, **Langevin equation** has the following form:

$$\boxed{m\frac{d^2x}{dt^2} = -\gamma m\frac{dx}{dt} + F(t) + m\xi(t)} \tag{2.5}$$

which is equivalent to the system of equations

$$\boxed{\begin{cases} v(t) = \frac{dx}{dt} \\ m\frac{dv}{dt} = -\gamma m v(t) + F(t) + m\xi(t) \end{cases}} \tag{2.6}$$

The force $m\xi(t)$ is a random variable, for which the two following properties hold:

- $\langle \xi(t) \rangle = 0$
- $\langle \xi(t_1)\xi(t_2) \rangle = 2D\delta(t_2 - t_1)$

The physical reason behind this stochastic process introduced by Langevin is to model the random collisions in the viscous medium. These collisions result in no net drift for the particle, hence the first property. Moreover, after a punctual collision in time, the second property makes the system lose memory of its condition before the collision, in such way any time correlations vanish.

2.1.3 Diffusion in the velocity space

For simplicity, we consider a 1D particle of mass m with speed $v(t)$. We assume also to be in a pure diffusion regime, i.e. there is no external forces $F(t)$. Therefore, Langevin equation for the velocity (2.6) takes the form

$$\frac{dv}{dt} = -\gamma v(t) + \xi(t) \tag{2.7}$$

If we consider the random variable $d\chi(t) = \xi(t)dt$, it is possible to show, thanks to the Central Limit Theorem [24], that $d\chi(t)$ is a Gaussian random variable and the stochastic process takes the name of Wiener process. We can solve this equation multiplying both sides by $e^{\gamma t}$

$$\frac{d}{dt}\left(e^{\gamma t}v(t)\right) = e^{\gamma t}\xi(t)$$

and integrating both sides from 0 to t, we obtain the solution:

$$v(t) = v(0)e^{-\gamma t} + \int_0^t dt'\xi(t')e^{-\gamma(t-t')} \tag{2.8}$$

Two quantities are relevant in the study of diffusion. The first is the mean velocity

$$\langle v(t)\rangle = v(0)e^{-\gamma t} \tag{2.9}$$

obtained thanks to the property $\langle \xi(t)\rangle = 0$. The second important quantity is the variance σ_v^2. We focus on the quantity

$$v(t_1)v(t_2) = v^2(0)e^{-\gamma(t_1+t_2)} + \int_0^{t_1} dt' \int_0^{t_2} dt'' e^{-\gamma(t_1+t_2-t'-t'')}\xi(t')\xi(t'')$$

We compute the average $\langle \dots \rangle$ exploiting the second property of the random process $\xi(t)$ 2.1.2, in order to obtain

$$\langle v(t_1)v(t_2)\rangle = v^2(0)e^{-\gamma(t_1+t_2)} + \frac{D}{\gamma}e^{-\gamma(t_1+t_2)}\left(e^{-\gamma|t_1-t_2|} - e^{-\gamma(t_1+t_2)}\right)$$

For $t_1 = t_2 = t$, we have

$$\langle v^2(t)\rangle = v^2(0)e^{-2\gamma t} + \frac{D}{\gamma}\left(1 - e^{-2\gamma t}\right)$$

and finally

$$\sigma_v^2 = \langle v^2(t)\rangle - \langle v(t)\rangle^2 = \frac{D}{\gamma}\left(1 - e^{-2\gamma t}\right) \tag{2.10}$$

We have obtained in this way two different diffusion regimes:

- for $t \ll \gamma^{-1}$, the average speed recalls the initial condition $\langle v\rangle \sim v(0)$ and the mean value has a diffusive behaviour $\sigma_v^2 \simeq 2Dt$, independent from the friction;
- for $t \gg \gamma^{-1}$, the average speed tends to 0 for large t, which is the correct pure diffusion behaviour we were expecting for the Brownian particle. Moreover, the variance tends to constant value $\sigma_v^2 \sim \frac{D}{\gamma}$, which is time independent.

The latter result is particularly important because this means that the velocities at large time have a (Gaussian) Maxwell-Boltzmann distribution, of the form:

$$\boxed{P(v,t;v,0) = \sqrt{\frac{1}{2\pi\sigma_v^2}}\, e^{-\frac{(v-v(0)e^{-\gamma t})^2}{2\sigma_v^2}}} \tag{2.11}$$

Furthermore, thanks to the Equipartition theorem 3.2.1, we obtain the following relation between the diffusion constant in the velocity space D and the friction γ

$$\boxed{\frac{D}{\gamma} = \frac{k_B T}{m}} \tag{2.12}$$

2.1.4 Diffusion in the position space

If we consider the first equation in (2.6), we can easily obtain the formal solution for the position of the particle $x(t)$ as

$$x(t) = x(0) + \frac{v(0)}{\gamma}\left(1 - e^{-\gamma t}\right) + \int_0^t dt' \int_0^{t'} dt'' e^{-\gamma(t'-t'')}\xi(t'') \tag{2.13}$$

Again we compute the mean value of the position

$$\langle x(t)\rangle = \frac{v(0)}{\gamma}\left(1 - e^{-\gamma t}\right) \tag{2.14}$$

the mean squared position

$$\langle x^2(t)\rangle = \left(v^2(0) - \frac{D}{\gamma}\right)\left(\frac{e^{-\gamma t} - 1}{\gamma}\right)^2 + \frac{2D}{\gamma^3}\left(\gamma t + e^{-\gamma t} - 1\right)$$

and the variance

$$\sigma_x^2 = \frac{2D}{\gamma^2}t - \frac{D}{\gamma^3}\left(1 - e^{-\gamma t}\right)^2 - \frac{2D}{\gamma^3}\left(1 - e^{-\gamma t}\right) \tag{2.15}$$

We consider these quantities in the two different time regimes. For $t \ll \gamma^{-1}$, the mean value of the position is $x(t) \simeq v(0)t$, as expected. For the variance, we expand all exponential to $\mathcal{O}(t^3)$ in (2.15) and the following expression is obtained:

$$\sigma_x^2 \simeq \frac{2}{3}Dt^3 \to \sigma_x \sim t^{3/2}$$

In the other regime $t \gg \gamma^{-1}$, we obtain instead that the mean value is again a constant, as expected, depending on the friction

$$\langle x \rangle \simeq \frac{v(0)}{\gamma}$$

and the variance from (2.15) takes the form

$$\sigma_x^2 \simeq \frac{2Dt}{\gamma^2}$$

which recovers Einstein's result (2.2). We also notice that, in this regime, we recover Einstein's relation (2.4):

$$D_x \simeq \frac{\sigma_x^2}{2t} = \frac{D}{\gamma^2} = \frac{k_B T}{m\gamma}$$

where we used the relation (2.12) for the diffusion constant in the velocity space.

2.2 Fokker-Plank Equation

In general, we can use Langevin equation to study many different systems, for which the macroscopic behaviour is known and we also assume that fluctuations are present. 'Langevin method' [27] is then a way to describe these fluctuations of the system. It consists in considering the deterministic equations of motion of the system and add a 'Langevin force', given by two contributions, the damping term and the random noise. Therefore, we obtain a stochastic process that can be studied in all generality through the equivalent description of the Fokker-Plank equation, which describes the evolution of the probability density for a stochastic process. In the particular case of the Langevin stochastic dynamics, the Fokker-Plank equation is in fact equivalent to Einstein's diffusion equation (2.1), which allows to link the two different approaches. In the following section we demonstrate this link in full generality and we discover how Langevin equation can be used to study a wide spectrum of stochastic phenomena.

2.2.1 Kramers-Moyal expansion

We consider, for simplicity, the one-dimensional stochastic process $y(t)$, for which the dynamics is expressed by the following general Langevin equation:

$$\boxed{\frac{dy}{dt} = A(y,t) + B(y,t)\xi(t)} \tag{2.16}$$

where A, B are two generic - regular enough - functions and $\xi(t)$ is a stochastic process, that we assume to be Gaussian. We assume also the following properties on ξ:

- $\langle \xi(t) \rangle = 0$
- $\langle \xi(t_1)\xi(t_2) \rangle = 2D\delta(t_2 - t_1)$

These are the properties that Langevin assumed on the random force in his model 2.1.2. From these elements, the Kramers-Moyal coefficient for the Langevin equation can be obtained. Firstly, we consider the integral expression of (2.16), with y as initial condition at t and a finite increment Δt

$$y(t+\Delta t) - y = \int_t^{t+\Delta t} \left[A(y(t'),t') + B(y(t'),t')\xi(t')\right] dt'$$

and we expand the coefficients around the initial y to the first order in $y(t)$, obtaining

$$\begin{aligned} y(t+\Delta t) - y = \int_t^{t+\Delta t} &\left[A(y,t') + \frac{\partial A(y,t')}{\partial y}(y(t') - y)\right] + \\ &\left[B(y(t'),t')\xi(t') + \frac{\partial B(y,t')}{\partial y}(y(t') - y)\xi(t') + ...\right] dt' \end{aligned}$$

where $\ldots$ indicates the presence of higher orders terms, which are neglected in the expansion. Iterating for $y(t') - y$, we obtain

$$\begin{aligned} y(t+\Delta t) - y \simeq &\int_t^{t+\Delta t} \left[A(y,t') + B(y(t'),t')\xi(t')\right] dt' + \\ &\int_t^{t+\Delta t} A(y,t') \left\{ \int_t^{t'} \left[A(y,t'') + B(y(t''),t'')\xi(t') + ...\right] dt'' \right\} dt' + \\ &\int_t^{t+\Delta t} B(y(t'),t') \left\{ \int_t^{t''} \left[A(y,t'') + B(y(t''),t'')\xi(t'') + ...\right] dt'' \right\} \xi(t') dt' \end{aligned}$$

Then, we consider the average $\langle ... \rangle$ over many realizations of the stochastic process and exploit the properties of $\xi(t)$. All terms with $\langle \xi(t) \rangle$ vanish and we use the property $\langle \xi(t)\xi(t') \rangle = 2D\delta(t' - t)$ to further simplify the expression, hence obtaining

$$\begin{aligned} y(t+\Delta t) - y \simeq &\int_t^{t+\Delta t} A(y,t') dt' + \\ &\int_t^{t+\Delta t} A(y,t') \left[\int_t^{t'} A(y,t'') dt''\right] dt' + D \int_t^{t+\Delta t} B(y(t'),t')^2 dt' \end{aligned}$$

Finally, dividing by Δt and taking the limit for small Δt, we obtain the series of **Kramers-Moyal coefficients**

$$\boxed{\begin{array}{rcl} a^{(1)}(y,t) & = & A(y,t) + DB(y,t)\frac{\partial B(y,t)}{\partial y} \\ a^{(2)}(y,t) & = & 2DB^2(y,t) \\ a^{(n)}(y,t) & = & 0, n \geq 3 \end{array}} \tag{2.17}$$

2.2.2 Fokker-Plank equation

The general form of the Fokker-Plank equation involves only the first two Kramers-Moyal coefficients

$$\frac{\partial P(y,t)}{\partial t} = -\frac{\partial}{\partial y}\left[a^{(1)}(y,t)P(y,t)\right] + \frac{1}{2}\frac{\partial^2}{\partial y^2}\left[a^{(2)}(y,t)P(y,t)\right] \tag{2.18}$$

Substituting (2.17) into (2.18), we obtain the **Fokker-Plank equation**, completely equivalent to the general Langevin equation (2.16)

$$\boxed{\frac{\partial P(y,t)}{\partial t} = -\frac{\partial}{\partial y}\left[\left(A(y,t) + DB(y,t)\frac{\partial B(y,t)}{\partial y}\right)P(y,t)\right] + D\frac{\partial^2\left[B^2(y,t)P(y,t)\right]}{\partial y^2}} \tag{2.19}$$

2.2.3 Multivariate Fokker-Plank equation

For a multivariate stochastic process $\vec{y} = (y_1, ..., y_N)$, there is a set of generalized Langevin equations of the form

$$\frac{dy_i}{dt} = A_i(\vec{y},t) + \sum_k B_{ik}(\vec{y},t)\xi_k(t) \quad \forall i = 1, ...N \tag{2.20}$$

where for each $\xi_k(t)$ properties 2.1.2 hold. For each of these equations, Kramers-Moyal coefficients and the Fokker-Plank equations can be derived following the same computation as before:

$$\begin{array}{rcl} a_i^{(1)}(\vec{y},t) & = & A_i(\vec{y},t) + D\sum_{j,k} B_{jk}(\vec{y},t)\frac{\partial B_{jk}(\vec{y},t)}{\partial y_j} \\ a_i^{(2)}(\vec{y},t) & = & 2D\sum_k B_{ik}(\vec{y},t)B_{jk}(\vec{y},t) \\ a_{j1,\ldots jm}^{(n)}(\vec{y},t) & = & 0, n \geq 3 \end{array} \tag{2.21}$$

$$\begin{aligned}\frac{\partial P(\vec{y},t)}{\partial t} = -\sum_i \frac{\partial}{\partial y_i}\left[A_i(\vec{y},t)P(\vec{y},t) + D\sum_{j,k} B_{jk}(\vec{y},t)\frac{\partial B_{jk}}{\partial y_j}P(y,t)\right] \\ + D\sum_{i,j}\frac{\partial^2}{\partial y_i \partial y_j}\left[\sum_k B_{ik}(\vec{y},t)B_{jk}(\vec{y},t))P(\vec{y},t)\right] \qquad (2.22)\end{aligned}$$

2.2.4 Klein-Kramers equation for diffusion

We consider, for simplicity, a one dimensional particle of coordinate $x(t)$ and mass m in an external potential $U = U(x)$, which obeys to the following Langevin equation

$$\boxed{m\frac{d^2x}{dt^2} = -m\gamma\frac{dx}{dt} - \frac{dU}{dx} + m\xi(t)} \qquad (2.23)$$

which is equivalent to the following system of Langevin equations

$$\begin{cases} v = \frac{dx}{dt} \\ \frac{dv}{dt} = -\gamma v - \frac{1}{m}\frac{dU}{dx} + \xi(t) \end{cases}$$

From this system of equations we can derive the bi-variate Kramers-Moyal coefficients

$$\begin{array}{rcl} a_x^{(1)}(v,x,t) & = & v \\ a_x^{(2)}(v,x,t) & = & 0 \\ a_v^{(1)}(v,x,t) & = & -\gamma v - \frac{1}{m}\frac{dU}{dx} \\ a_v^{(2)}(v,x,t) & = & 2D \end{array}$$

and the bi-variate Fokker-Plank equation

$$\frac{\partial P(v,x,t)}{\partial t} = -\frac{\partial\left[vP(v,x,t)\right]}{\partial x} + \frac{\partial}{\partial v}\left[\left(\gamma v + \frac{1}{m}\frac{dU}{dx}\right)P(v,x,t)\right] + D\frac{\partial^2 P(v,x,t)}{\partial v^2} \qquad (2.24)$$

If we consider by hypothesis that the stationary distribution is the Boltzman distribution $P_0 \propto e^{-(\frac{1}{2}mv^2+U(x))/k_BT}$, we can insert it into the stationary condition of (2.24), i.e.

$$v\frac{\partial P}{\partial x} - \gamma\left[P(v,x,t) + v\frac{\partial P}{\partial v}\right] - \frac{1}{m}\frac{dU}{dx}\frac{\partial P}{\partial v} = D\frac{\partial^2 P}{\partial v^2}$$

and obtain the following relation between the γ and D

$$\boxed{\frac{D}{\gamma} = \frac{k_B T}{m}} \tag{2.25}$$

This is exactly the same relation that we obtained with the Langevin method in the velocity space (2.12). Using this relation into (2.24), we obtain, after few algebraic passages, the **Klein-Kramers equation**

$$\boxed{\frac{\partial P}{\partial t} = -v\frac{\partial P}{\partial x} + \frac{1}{m}\frac{dU}{dx}\frac{\partial P}{\partial v} + \gamma\left[\frac{\partial(vP(v,x,t))}{\partial v} + \frac{k_B T}{m}\frac{\partial^2 P}{\partial v^2}\right]} \tag{2.26}$$

2.2.5 Free particle case: Ornstein-Uhlembeck process

In the case of $U(x) = 0$, we obtain a simplified version of equation (2.26).

$$\frac{\partial P}{\partial t} = -v\frac{\partial P}{\partial x} + \gamma\left[\frac{\partial(vP(v,x,t))}{\partial v} + \frac{k_B T}{m}\frac{\partial^2 P}{\partial v^2}\right] \tag{2.27}$$

The general solution of this equation is obtained by applying the Fourier transform of $P(v,t)$ and then using the method of characteristics. It reads

$$\boxed{P(v,t;v,0) = \sqrt{\frac{\gamma}{2\pi D\left(1-e^{-2\gamma t}\right)}}\, e^{-\frac{\gamma\left(v-v(0)e^{-\gamma t}\right)^2}{2D\left(1-e^{-2\gamma t}\right)}}} \tag{2.28}$$

This stochastic process with this Gaussian distribution takes the name of Ornstein-Uhlembeck process. We notice that we have recovered the exact results - (2.9) and (2.10) - obtained from Langevin equation in the velocities' space for $t \gg \gamma^{-1}$. Indeed, the average value of the speed from (2.28) is

$$\langle v(t)\rangle = v(0)e^{-\gamma t}$$

and the variance is

$$\sigma_v^2 = \frac{D}{\gamma}\left(1 - e^{-2\gamma t}\right)$$

This is the formal derivation stating that the stochastic process of Langevin equation in the velocity space is a Ornstein-Uhlembeck process.

2.2.6 Overdamped-Smoluchowski equation

We consider equation (2.23) in the overdamped regime i.e. when $\frac{d^2x}{dt^2} = 0$ and the force is proportional to the speed of the particle

$$\frac{dx}{dt} = v = -\frac{1}{m\gamma}\frac{dU}{dx} + \frac{\xi(t)}{\gamma} \tag{2.29}$$

Another way to express this regime - more convenient from a computational point of view - is to have the friction much grater than the integration time-step i.e. $\gamma \gg \Delta t$. This is a one variable differential equation, so it is possible to find the uni-variate Fokker-Plank's equation form the Kramers-Moyal coefficients

$$\begin{aligned} a_x^{(1)}(v,x,t) &= -\tfrac{1}{m\gamma}\tfrac{dU}{dx} \\ a_x^{(2)}(v,x,t) &= \tfrac{2D}{\gamma^2} \end{aligned}$$

$$\frac{\partial P(x,t)}{\partial t} = -\frac{\partial}{\partial x}\left[\left(-\frac{1}{m\gamma}\frac{dU}{dx}\right)P(x,t)\right] + \frac{D}{\gamma^2}\frac{\partial^2 P(x,t)}{\partial x^2} \tag{2.30}$$

If we consider as stationary distribution the Boltzmann's distribution $P_0 \propto e^{-(U(x))/k_BT}$, again the relation (2.12) is obtained and, by substituting it into (2.30), the **Smoluchowski equation** is obtained.

$$\boxed{\frac{\partial P(x,t)}{\partial t} = \frac{1}{m\gamma}\frac{\partial}{\partial x}\left[\frac{dU}{dx}P(x,t)\right] + \frac{k_BT}{m\gamma}\frac{\partial^2 P(x,t)}{\partial x^2}} \tag{2.31}$$

Free particle: pure diffusion equation

An important sub-case of (2.31) is the free particle case i.e. $U(x) = 0$. Then, Smoluchowski equation reduces to the **diffusion equation**

$$\boxed{\frac{\partial P(x,t)}{\partial t} = \frac{k_BT}{m\gamma}\frac{\partial^2 P(x,t)}{\partial x^2}} \tag{2.32}$$

The solution of this equation is found with the Fourier transform method. Using the initial condition $P(x,t=0) = \delta(x)$, the solution is an Orstein-Uhlembeck process in the positions' space

$$\boxed{P(x,t) = \sqrt{\frac{\gamma}{4\pi Dt}}\,e^{-\frac{\gamma}{4Dt}x^2}} \tag{2.33}$$

We obtain the same relations for the diffusion constant in the position space (2.4)

$$\frac{D}{\gamma} = \frac{k_B T}{m}$$

2.3 Time correlation functions

Time-correlation functions (TCFs) have the same role in non-equilibrium statistical mechanics as the partition functions have in equilibrium statistical mechanics. Many transport coefficients, which are associated and characterize each non-equilibrium or transport property of the system under study, can be expressed in terms of TCFs [32]. Furthermore, they can be also related to many experimental techniques, such as spectroscopy and measurements of rate constants.

In general, any TCF is given by the average in some equilibrium ensemble of two time-dependent quantities $A(t)$ and $B(t')$, where $t \neq t'$ are the times at which they are evaluated. It is worth noticing that there exists many types of TCFs because there are many possible non-equilibrium states, while from the sole equilibrium partition function is possible to derive all static properties.

2.3.1 Classical TCFs

Consider a system of N, one-dimensional (for simplicity) particles of positions and momenta $\{x_i(t), p_i(t)\}, \forall i = 1, \ldots, N$. They form a time dependent trajectory $(\vec{x}(t), \vec{p}(t))$ in the phase space, which evolves according to Hamilton's equations, starting from the initial point $(\vec{x}(0), \vec{p}(0))$. The ensemble is assumed to be Canonical, with the equilibrium phase space distribution function given by the Boltzmann distribution and Canonical partition function. We define the **classical time correlation function** [33] of A and B as

$$\boxed{C_{AB}(t) = \langle A(0)B(t)\rangle = \frac{1}{Z}\int d\vec{x}\int d\vec{p} A(x(\vec{0}), p(\vec{0}))B(x(\vec{t}), p(\vec{t}))e^{-\beta H(\vec{x}(t),\vec{p}(t))}} \tag{2.34}$$

The time auto-correlation function is defined as $C_{AA}(t)$. The detailed balance condition is given by $C_{AB}(t) = C_{BA}(-t)$. We define also the Fourier transform of C_{AB} as

$$C_{AB}(\omega) = \mathcal{F}\{C_{AB}(t)\}(\omega) = \frac{1}{2\pi}\int dt C_{AB}(t)e^{-\imath\omega t} \tag{2.35}$$

2.3.2 Application to classical diffusion

The classical study of a diffusion process uses TCFs to express the diffusion constant in the positions' space D_x (2.4), and in the velocities' space D (2.12), which are the main transport coefficients involved in this problem. As already stated by Einstein, diffusion coefficient in the positions' space is given by the mean squared displacement (2.3). It is easy to show that the diffusion coefficient can be written in terms of the **velocity-velocity TCF**. Indeed, we know that

$$x(t) - x(0) = \int_0^t v(t)dt$$

Substituting this into (2.3), we obtain

$$\boxed{D_x = \lim_{t\to\infty} \frac{1}{2t} \int_0^t dt_1 \int_0^t dt_2 \langle v(t_1)v(t_2)\rangle = \int_0^\infty dt\ \langle v(0)v(t)\rangle = \lim_{t\to\infty} C_{vv}(t)} \tag{2.36}$$

The full derivation of this result can be found in the Linear Response Theory [25], which is not reported in this work. An analogous relation is true for the diffusion coefficient in the velocity space:

$$D = \frac{1}{m}\int_0^\infty \langle R(0)R(t)\rangle = \lim_{t\to\infty} C_{RR}(t) \tag{2.37}$$

where $R(t) = m\xi(t)$ is the random force in the Langevin equation (2.5).

2.3.3 Quantum TCFs

Quantum TCFs are given in different forms [33, 34], which are all related to the classical TCFs in the limit of high temperature. Given two observables with operators $\hat{A}$ and $\hat{B}$, we define then the **standard form of the quantum TCFs** as

$$C_{AB}(t) = Tr[\hat{\rho}\hat{A}e^{\imath\hat{H}t/\hbar}\hat{B}e^{-\imath\hat{H}t/\hbar}] \tag{2.38}$$

where $e^{\imath\hat{H}t/\hbar}$ and $e^{-\imath\hat{H}t/\hbar}$ are the forward and backward time propagator respectively and $\hat{B}_t = e^{\imath\hat{H}t/\hbar}\hat{B}e^{\imath\hat{H}t/\hbar}$ is the time propagated operator in the Heisenberg picture. C_{AB} is a complex quantity and the equivalent detailed balance condition is $C_{AB}(t) = C^*_{BA}(-t)$.

Another common form of the quantum TCF is the **Kubo-transformed time correlation function** [26], defined as

$$K_{AB}(t) = \frac{1}{\beta\mathcal{Z}}\int_0^\beta d\lambda Tr[e^{-(\beta-\lambda)\hat{H}}\hat{A}e^{-\lambda\hat{H}}e^{\imath\hat{H}t/\hbar}\hat{B}e^{-\imath\hat{H}t/\hbar}] \tag{2.39}$$

This version seems more complicated but it is real and the detailed balance condition is simply $K_{AB}(t) = K_{BA}(-t)$. It is related to the standard TCF using the relation:

$$\mathcal{F}\{C_{AB}(t)\}(\omega) = \frac{\beta\hbar\omega}{1 - e^{-\beta\hbar\omega}} \mathcal{F}\{K_{AB}(t)\}(\omega) \tag{2.40}$$

2.4 Harmonic Analysis of Stationary Stochastic Processes

In this Section, we introduce some basic concepts which are fundamental for the theoretical explanation of Langevin-based algorithms in Section 3.2, 3.4 and 3.5. For this part we refer to [35].

2.4.1 Spectral Density

Let us suppose $s(t)$ is a stationary stochastic process i.e. its probability distribution does not change in time.

For any signal $s(t)$ in a limited temporal window, it is possible to compute its **energy spectral density** and the **power spectral density** i.e. the energy spectral density per unit time. The spectrum of a physical phenomena contains interesting information about its properties and it is particularly useful in the study of stochastic processes. Consider a signal $s(t)$, its total energy E is given by

$$E = \int_{-\infty}^{+\infty} dt\ |s(t)|^2 \tag{2.41}$$

for which we can define the **energy spectral density** (ESD) as

$$\boxed{\hat{S}(\lambda) = |s(\lambda)|^2} \tag{2.42}$$

where we defined $s(\omega)$ as the Fourier transform $\mathcal{F}\{s(t)\}$ in the following way:

$$s(\lambda) = \int_{-\infty}^{+\infty} dt\ s(t) e^{-2\pi\imath\lambda t}$$

The same definitions are valid in the case of the total power of a signal:

$$P = \lim_{T\to\infty} \frac{1}{T} \int_{0}^{T} dt\ |s(t)|^2 \tag{2.43}$$

The Fourier transform of $s(t)$ now is defined as

$$s(\omega) = \frac{1}{T}\int_0^T dt\ s(t)e^{-\imath\omega t}$$

and the **power spectral density** (PSD) as

$$\hat{S}(\omega) = \lim_{T\to\infty} \mathbb{E}\left[|s(\omega)|^2\right] \tag{2.44}$$

where $\mathbb{E}$ is the expected value, which can be written explicitly in the following way, for $s(t)$ complex in general:

$$\begin{aligned}\mathbb{E}\left[|s(\omega)|^2\right] = \mathbb{E}\left[\frac{1}{T}\int_0^T dt\ s^*(t)e^{\imath\omega t}\int_0^T dt'\ s(t')e^{-\imath\omega t'}\right] = \\ \frac{1}{T}\int_0^T dt\ \frac{1}{T}\int_0^T dt'\ \mathbb{E}\left[s^*(t)s(t')\right]e^{\imath\omega(t-t')}\end{aligned} \tag{2.45}$$

2.4.2 Wiener–Khinchin theorem

We consider the definition of the PSD (2.44) and we take the limit with $T \to \infty$. In this way, we obtain is the **Wiener–Khinchin theorem**

Theorem 2.4.1 (Wiener–Khinchin) *For an absolutely integrable $C_{ss}(t)$, the PSD is given by:*

$$\boxed{\hat{S}(\omega) = \int_{-\infty}^{+\infty} C_{ss}(t)e^{-\imath\omega t}dt = C_{ss}(\omega) = \mathcal{F}\{C_{ss}(t)\}} \tag{2.46}$$

where the expected value $\mathbb{E}\left[s^*(t)s(t')\right]$ is expressed as a TCF with $\Delta t = (t - t')$:

$$\mathbb{E}\left[s^*(t)s(t')\right] = \langle s^*(t)s(t+\Delta t)\rangle = C_{ss}(\Delta t)$$

Application to diffusion

Wiener-Khinchin theorem has a fundamental role in the implementation of both classical and quantum Langevin-based simulation methods. In particular, we will use the following form of the theorem:

$$\boxed{C_{RR}(\tau) = \langle R(t)R(t+\tau)\rangle = \int_{-\infty}^{+\infty}\frac{d\omega}{2\pi}C_{RR}(\omega)e^{\imath\omega\tau}} \tag{2.47}$$

where $R(t)$ will be a stationary stochastic process that plays the role of the random force in a generalized Langevin equation. Therefore this formula gives a general procedure to obtain, for example, the main property 2.1.2 from the assumption of a power spectral density suitable for the problem under study. In Section 3.2, this concept is used to generalize the classical approach of Langevin thermostat. Furthermore, in Section 3.4 and 3.5, this result becomes very useful to develop the new MD approaches to quantum systems.

2.5 Feynman's Path Integrals

The most reliable MD methods used to simulate real systems in which NQEs are present is based on the Feynman's formalism of Path Integrals [36]. This is a framework of Quantum Mechanics (QM) alternative to Schrödinger's wave mechanics and Dirac's theory.

Feynman's theory is closer to the Classical picture and it is very useful for MD techniques because it preserves the concept of trajectories of the particles. For the following exposition, we refer to [25].

2.5.1 Heuristic picture

Let us consider a quantum particle with position operator $\hat{x}$ which evolves in time thanks to the propagator operator $\hat{U}(t) = e^{-\frac{\imath \hat{H} t}{\hbar}}$. The particle starts in position x and we perform a measure in position x'. The Hamiltonian operator is defined as:

$$\hat{H} = \frac{\hat{p}}{2m} + \hat{V}(\hat{x})$$

Until a measure is performed, we are completely ignorant on the possible path the quantum particle is following, accordingly to the laws of QM. Therefore, instead of introducing a probability distribution for the particle's position, we state Feynman's hypothesis: the quantum particle follows an infinite number of paths from the starting point x to the point in which its position is measured x'.

The link with the probabilistic picture is given by the measured amplitude $A(x', x)$: the probability distribution for the position of the particle when it is measured is given by $|A(x', x)|^2$. This amplitude has the contributions of all possible paths followed by the quantum particle going from x to x', so the probability reads to find in x' the particle starting in x :

$$\boxed{P(x', x) = \left| \sum_{paths} A_{path}(x', x) \right|^2}$$

2.5.2 Time evolution operator and density matrix

We consider for simplicity one particle in a 1D system, prepared initially in state $|x\rangle$, which evolves with the time evolution operator $\hat{U}(t) = e^{-\frac{\imath \hat{H} t}{\hbar}}$ until state $|x'\rangle$. We define the amplitude as the **time propagator's coordinate-space matrix** as

$$\boxed{\hat{U}(x, x', t) = \langle x'| \, e^{-\frac{\imath \hat{H} t}{\hbar}} \, |x\rangle} \tag{2.48}$$

There is an analogy between this operator and the density matrix of the system $\hat{\rho}(\beta) = e^{-\beta \hat{H}}$ in the following way:

$$\hat{\rho}(\beta) = e^{-\beta \hat{H}} = \hat{U}(-\imath \beta \hbar) \tag{2.49}$$

which is equivalent to

$$\hat{U}(t) = e^{-\frac{\imath \hat{H} t}{\hbar}} = \hat{\rho}(\frac{\imath t}{\hbar}) \tag{2.50}$$

This means that we have two times in our system:

- the density matrix $\hat{\rho}$ corresponds to the imaginary time propagator, where we defined the imaginary time as $\Im[\theta] = -\imath \beta \hbar$;
- the real time propagator $\hat{U}(t)$, which can be obtained from $\hat{\rho}$ by defining the imaginary inverse temperature $\beta = \frac{\imath t}{\hbar}$.

Therefore, if $\hat{U}(t)$ is the quantum real-time propagator, the operator $\hat{\rho}(\beta) = e^{-\beta \hat{H}}$ is also called the quantum imaginary-time propagator. The precise mathematical relation between $U(t)$ and $\hat{\rho}(\beta)$ is given by a Wick rotation [37]. The density matrix is defined by an analytical continuation of its argument in the complex plane. Here, we do not go through the mathematical theorems about the Wick's transformation, rather we stress that in quantum statistical mechanics, PI do not have the same meaning This use of PI was also introduced by Feynman, even though later they refer to systems at thermal equilibrium, not to the real system dynamics.

2.5.3 Quantum Canonical partition function

The **density matrix in coordinates' space** is in general given by

$$\hat{\rho}(x, x', \beta) = \langle x'| \, e^{-\beta \hat{H}} \, |x\rangle \tag{2.51}$$

In order to compute the explicit expression of the density matrix, the Baker-Campbell-Hausdorff formula [38] is used, with a splitting in N steps, as in (3.8). For the full derivations, we refer to [25]. The final expression reads

$$\hat{\rho}(x,x',\beta) = \lim_{N\to\infty}\left(\frac{mN}{2\pi\beta\hbar^2}\right)^{N/2}\int_{x=x_1}^{x'=x_{N+1}} dx_2\dots dx_N \\ \exp\left[-\frac{1}{\hbar}\sum_{k=1}^{N}\left(\frac{mN}{2\beta\hbar}(x_{k+1}-x_k)^2+\frac{\beta\hbar}{2N}(V(x_{k+1})-V(x_k)\right)\right] \quad (2.52)$$

where the index N discretizes the path into $N \to \infty$ intermediate positions, the integration is over all these intermediate positions and there is a resulting term of harmonic nearest-neighbours coupling between the intermediates points of the path. The only fixed point are the start x and the end x'.

The most important result obtainable from the density matrix $\hat{\rho}$ is the **quantum Canonical partition function** (QCPF), as

$$\mathcal{Z}(L,T) = \lim_{N\to\infty}\left(\frac{mN}{2\pi\beta\hbar^2}\right)^{N/2}\int dx_1\dots dx_N \\ \exp\left[-\frac{1}{\hbar}\sum_{k=1}^{N}\left(\frac{mN}{2\beta\hbar}(x_{k+1}-x_k)^2+\frac{\beta\hbar}{2N}V(x_k)\right)\right] \quad (2.53)$$

where we used the periodic boundary conditions (PBC) $x_1 = x_{N+1}$ and we integrate on the whole spatial domain. Once the QCPF is know, the whole quantum Canonical thermodynamics can be found, using the following definition for the ensemble average of an operator $\hat{O}$:

$$\langle\hat{O}\rangle = \frac{1}{\mathcal{Z}}Tr\left[\hat{O}\hat{\rho}\right]$$

In Section 3.3 we will explain how it is possible to use the fundamental expression of the QCPF (2.53) in Molecular Dynamics simulations for quantum systems via the so-called Path-Integral Molecular Dynamics method. In particular, we will explain the classical isomophism between (2.53) and the classical partition function of a ring-polymer with N harmoically interacting beads.

We note that, using the equivalence (2.50), we can find the expression for the time propagator

$$\hat{U}(x,x',t) = \lim_{N\to\infty} \left(\frac{mN}{2\pi\imath\hbar t}\right)^{N/2} \int_{x=x_1}^{x'=x_{N+1}} dx_2 \dots dx_N$$
$$\exp\left[-\frac{\imath}{\hbar}\sum_{k=1}^{N}\left(\frac{mN}{2t}(x_{k+1}-x_k)^2 - \frac{t}{2N}(V(x_{k+1})-V(x_k)\right)\right] \quad (2.54)$$

Although this formula is very useful conceptually and for the development of perturbation and exact theories, this expression is not practical for numerical computations because of the phase term $e^{\imath}$ which oundergoes strong oscillations and is very difficult to converge (contrary to the case of imaginary time PI where the factor in the exponential is real). This is the so-called sign problem [39].

2.6 Rate processes

We introduce briefly the classical Arrhenius law, which will be an important tool for the analysis of the diffusion coefficient in Section 4.2. We refer for this part to [20].

2.6.1 Arrhenius law

As already mentioned in the Introduction, all chemical reactions can be studied from a kinetic point of view. The main quantities involved are the chemical reaction constants, which determine the direction of the reactions (from reactants to products), and reaction rates, which quantify the speed at which reactants are converted to products.

Let us consider a general reaction, which involves reactant and products. From a physical point of view, the reactants are particles, atoms or molecules, which can collide and give rise to the products. Therefore, we are in the general context of a collision theory, which aims of explaining the kinetics of a reaction. We introduce the reaction rates k, depending in general on many quantities, such as the concentration of reactants, the pressure of the system or the surface area of contact between the reactants. It has been observed that k is a generally function of the temperature, following a specific law

$$log(k) = log(C) - \frac{E}{k_B T}$$

where C is defined as the collision number or frequency factor - giving then the frequency/probability of collision between reacting molecules - and E is the activation energy of the reaction. Thus, we obtain the so-called Arrhenius law

$$\boxed{k(T) = Ae^{-E/k_BT}} \tag{2.55}$$

where e^{-E/k_BT} can be seen as the probability of occurrence of the reaction or equivalently the fraction of molecules that possess the required activation energy. It is clear from this simple arguments that the computation of reaction rates involves the computation of two main quantities: the activation energy E and the frequency factor A.

In general, A is obtained by the kinetic theory of gasses or other more complicated theories. Instead, the activation energy involves a study of the potential energy or free energy surface according to the Eyring-Polanyi semi-empirical method, which is in general a very complex problem.

The simplest possible description of this problem is a two states model, as the one used in [21]. Let us consider a two state reactions, where A is the state of the reactants and B is the state of the products. As an example, on Figure 2.1 we illustrate the double-well potential appearing in the hydrogen diffusion model that we study in Section 4.1.2 (it will reproduce this situation in the case of the problem of hydrogen's diffusion). As function of a given reaction coordinate ξ, the two states are separated by a free energy barrier. The height of this barrier is the activation energy i.e. the energy needed by the reactants to overcome the barrier and pass to the state of the products. The reaction rates is then the probability to overcome the barrier, express as a frequency of the passage from A to B.

We can state the Eyring-Polanyi equations for a two states system

$$k(T) = \frac{2\pi k_BT}{\hbar} e^{-\frac{\Delta F}{k_BT}} \tag{2.56}$$

where ΔF is the free-energy of activation. The most important point of this new equation is the use of the free energy, instead of the activation energy E, which is a much more general quantity and takes into account the complex thermodynamic aspects of the kinetic problem. We comment also that ΔF does not depends on the mass of the particles of the system. On the other hand, the prefactor of Eyring-Polanyi law can have a strong dependence on the mass.

2.6.2 Transition State Theory

Equation (2.56) is the starting point of the so-called Transition State Theory (TST), which is the general theory that aims to compute chemical reactions rates between two or more chemical states in a reaction. In particular, it focuses on the computation of the free-energy barrier ΔF in Eyring-Polanyi equation. The Quantum TST is an extension of the classical theory, for which the goal is

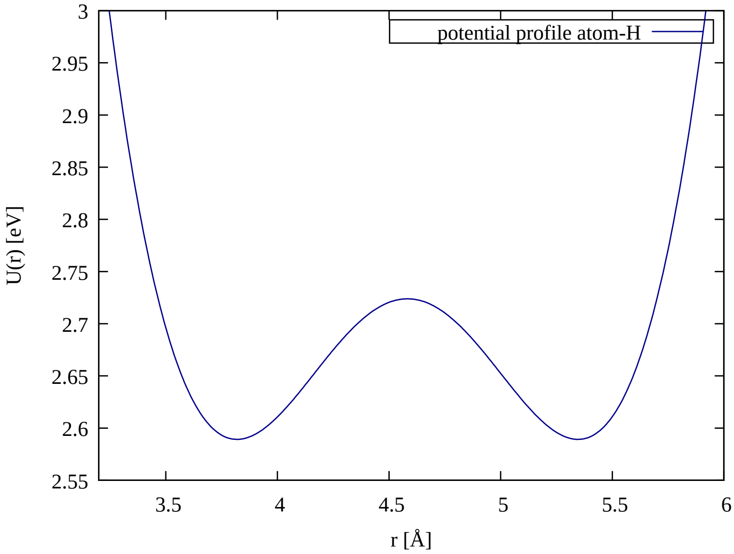

Figure 2.1: Model system: double-well potential between two lattice cells (zoom of Figure 4.5, reported in Section 4.1.2).

to compute reaction rates in processes dominated by quantum effects, such as tunneling and zero-point energy.

Time-correlation functions play a major role in both classical and quantum TST. This is because the reaction rates can be expressed mainly by the so-called Flux-Side Time Correlation Function. The computation of this TCF cannot be done exactly for many systems, hence the need of approximated method and low-cost simulation techniques. Molecular Dynamics methods are particularly useful to study the dynamics of this systems in terms of trajectories crossing the free energy barrier.

Chapter 3

Methods

The core of this work is a study of different methods of simulation of a simple system both in a classical and a quantum picture. The physical problem is the diffusion of a single hydrogen atom in a solid lattice. As already explained, hydrogen has a light nucleus, which makes imperative considering its quantum nature because of the presence of NQEs. In order to study this problem from a computational point of view, most methods are based on **Molecular Dynamics** (MD) techniques. These methods have become a useful numerical tool to investigate physical, chemical and biophysical systems at molecular and atomic scale [40]. Classical MD consists in the simulation of the trajectories of the atomic nuclei, within the Born-Oppenheimer approximation, by numerically solving their newtonian equations of motion. This provides a clear classical picture of the properties of the system and, relying on the Ergodic hypothesis (3.4), which ensures the equivalence with the ensamble's formalism, allows to compute both static and dynamic properties of the system.

On the other hand, considering the nuclei as quantum objects is way more complex. Solving numerically Schrodinger's evolution equation for the nuclei wave-function is impossible for realistic condensed matter system, as it scales exponentially with the number of atoms involved. For static properties at thermal equilibrium, reliable results can be obtained within Feynman's Path Integral (PI) formalism of Quantum Mechanics. Although these methods are very computationally demanding and cannot be used safely for quantum dynamics. Therefore, the study of dynamical properties in quantum system remains a theoretical opened challenge for which different approximations have been proposed but none of them is fully general and reliable for all real systems. Some of these approaches are based on PI formalism and take the name of Ring Polymer Molecular Dynamics (RPMD) [34, 41, 42] and Centroid Molecular Dynamics (CMD) [43]. However, they rely on approximations with accuracy not always accessible [44] and they are particularly heavy. We discuss briefly RPMD in Section 3.3.

In this work, we present a different approach based on a generalized Langevin equation and called Quantum Thermal Bath (QTB) and its refinement, the adaptive QTB. This is an approximated method which is able to access directly dynamic properties and to reproduce NQEs with a computational cost of the same order of standard classical MD. These new methods are shown to give exact results for harmonic systems and approximated results for anharmonic systems, which is satisfactory for some cases [45].

3.1 Classical Molecular Dynamics

3.1.1 Integration of Newton's second law

MD consists in integrating directly the equations of motion of the nuclei in order to have a full knowledge of the trajectory of the system in the phase space. This is particularly useful to study non-equilibrium time-dependent properties, which are not always linked to an equilibrium ensemble. MD is then preferred to Monte Carlo techniques, that are largely used to study static properties [46].

Let us consider a general system of N classical particles, in a 1D space for simplicity. The extension to 2D or 3D is straightforward. For each particle i of mass m_i and position x_i, $i = 1, \dots, N$, Newton's second law states its dynamics:

$$\boxed{m_i \frac{d^2 x_i}{dt^2} = f_i} \tag{3.1}$$

where the force $f_i = f(x_1, \dots, x_N)_i$ acting on the particle i, which depends in general by the positions of all particles of the system. Newton's law for the particle i is equivalent to Hamilton's equations of motion, where we introduced $p_i = m_i \frac{dx_i}{dt}$ as the momentum of particle i and $H(\vec{x}, \vec{p})$ is the Hamiltonian of the system, which depends in general on all momenta and positions and it physical correspondence is the total energy of the system. In particular, we assume that the Hamiltonian has the form

$$H(\vec{x}, \vec{p}) = \sum_{n=1}^{N} \frac{p_i^2}{2m_i} + U(\vec{x})$$

where the $U = U(\vec{x})$ is the potential energy of the system and its first derivative with respect to particle i gives the force $f_i = -\frac{\partial U(\vec{x})}{\partial x_i}$. The resulting Hamilton's equations are:

$$\boxed{\begin{cases} \frac{dx_i}{dt} = \frac{\partial H(\vec{x},\vec{p})}{\partial p_i} = \frac{p_i}{m_i} \\ \frac{dp_i}{dt} = -\frac{\partial H(\vec{x},\vec{p})}{\partial x_i} = f(x_1, \dots, x_N)_i \end{cases}} \tag{3.2}$$

These equations describe the evolution of the system, drawing a trajectory $(\vec{x}(t), \vec{p}(t))$ in the phase space. They have two major properties:

- **conservation of energy**: $\frac{dH}{dt} = 0$
- **time reversibility** under the change: $x' = x(-t), p' = -p(-t)$

Conservation of energy is particularly relevant, because it means that, no matter how long the total time of the evolution of the system, the points explored by the trajectory in the phase space are always on a iso-energetic (hyper-)surface. In a statistical mechanics contexts, this means we are in the Microcanonical ensemble (N, V, E), with fixed energy $H = E$ constant in time.

The MD starting point is the integration of Hamilton equations or Newton's second law, for example via the **Verlet algorithm** [47]. Starting from an initial point $(\vec{x}_0, \vec{p}_0)$, for each discrete time step Δt, we compute the forces acting on the system and update positions and momenta iteratively, until we reach the final point.

3.1.2 Ergodic hypothesis

The main goal of MD is to compute the values of macroscopic observables from the evolution of the microscopic particles of the system. Consider a general observable $O = O(\vec{x}, \vec{p}, t)$ which depends explicitly on the system's trajectory in the phase space. We define the **time average** of O as

$$\bar{O} = \lim_{T \to \infty} \frac{1}{T} \int_0^T O(\vec{x}, \vec{p}, t) dt \tag{3.3}$$

MD simulations which aim at studying equilibrium properties are usually based on the following assumption, namely the Ergodic hypothesis:

$$\boxed{\langle O \rangle = \bar{O}} \tag{3.4}$$

The Ergodic hypothesis is true in the case of Hamilton's equations in the thermodynamic limit, i.e for very large number of particles at fixed density. Indeed, sampling from the (N, V, E) ensemble is perfectly equivalent to the exploration of the (hyper-)surface at constant energy in the phase space, if the total time of the simulation is long enough to allow the system to explore all possible states.

3.1.3 Liouville's operator formalism

Given the generalized positions $\vec{q} = (\vec{x}(t), \vec{p}(t))$ in phase space, we can introduce the generalized density $\rho(\vec{q}(t), t)$. Therefore, the evolution of the system is given by the time evolution of the generalized density

$$\frac{d\rho}{dt} = \frac{\partial \rho}{\partial t} + \sum_{i=1}^{N} \left[\frac{\partial \rho}{\partial p_i} \frac{dp_i}{dt} + \frac{\partial \rho}{\partial x_i} \frac{dx_i}{dt} \right]$$

Theorem 3.1.1 (Liouville's theorem) *Under Hamilton's equations,*

$$\frac{d\rho}{dt} = 0$$

Another way to express Liouville's theorem is to state the incompressibility of the flux in the phase space i.e. the volume occupied by the system in the phase space does not change in time. Therefore, we can write **Liouville's equation**

$$\boxed{\frac{\partial \rho}{\partial t} = -\imath \hat{\mathscr{L}} \rho} \tag{3.5}$$

where $\hat{\mathscr{L}}$ is **Liouville's operator**, defined as follows:

$$\imath \hat{\mathscr{L}} = \sum_{i=1}^{N} \left[\frac{\partial H}{\partial p_i} \frac{\partial}{\partial x_i} - \frac{\partial H}{\partial x_i} \frac{\partial}{\partial p_i} \right] \tag{3.6}$$

Hence, the solution of the (3.5) for a small time interval Δt

$$\boxed{\rho(t + \Delta t) = e^{-\imath \hat{\mathscr{L}} \Delta t} \rho(t)} \tag{3.7}$$

We can also write Liouville's operator in the following way, in order to highlight explicitly the contribution coming from the positions and the contribution of the momenta

$$\imath \hat{\mathscr{L}} = \imath (\hat{\mathscr{L}}_x + \hat{\mathscr{L}}_p) = \sum_{i=1}^{N} \left[\frac{p_i}{m_i} \frac{\partial}{\partial x_i} + f_i \frac{\partial}{\partial p_i} \right]$$

The effects of the two contributions on the density of the system during the integration are the following

- $\hat{\mathscr{L}}_x$: if $f_i = 0, \forall i$, we obtain $\rho(t + \Delta t) = \rho(\vec{p}, \vec{x} + \frac{\vec{m}}{m} \Delta t, t)$, which is a general translation of all positions;
- $\hat{\mathscr{L}}_p$: if $f_i = 0, \forall i$, we obtain $\rho(t + \Delta t) = \rho(\vec{p} + \vec{f} \Delta t, \vec{x}, t)$, which is a general translation of all momenta.

However, the combined effect is not trivial and we need to rely on an approximation to split the two contribution and integrate separately positions and momenta. We consider the general operators/matrices $n \times n$ A, B and a real parameter λ. We state the **Lie-Trotter product formula** [48]

$$\boxed{e^{\lambda(A+B)} = \lim_{N\to\infty} \left(e^{\lambda A/N} e^{\lambda B/N}\right)^N} \tag{3.8}$$

This formula is generalized by the Baker–Campbell–Hausdorff formula for non commutative operators [38]. Then, if we consider the following splitting:

$$e^{\lambda(A+B)} \simeq e^{\lambda A} e^{\lambda B}$$

it is easy to demonstrate that it would lead to an error $\mathcal{O}(\lambda^2)$ i.e. of the second order in λ. In order to obtain an error $\mathcal{O}(\lambda^3)$, we use the following symmetric splitting:

$$e^{\lambda(A+B)} \simeq e^{\lambda B/2} e^{\lambda A} e^{\lambda B/2}$$

which in terms of Liouville's operator becomes

$$\boxed{e^{\imath \hat{\mathscr{L}} \Delta t} \simeq e^{\imath \hat{\mathscr{L}}_B \Delta t/2} e^{\imath \hat{\mathscr{L}}_A \Delta t} e^{\imath \hat{\mathscr{L}}_B \Delta t/2}} \tag{3.9}$$

Therefore, it is possible to integrate the equations of motion with an error of the order of Δt^3, which is negligible if the integration time step is small enough. The latter integration scheme that is applied is the **Velocity-Verlet algorithm** [49]. The formalism of Liouville's operator is particularly elegant to evaluate the different integration steps and it is widely used in MD techniques.

3.2 Classical Langevin Thermostat

3.2.1 Sampling the Canonical ensemble

As we mentioned in the previous section, simply integrating Hamilton's equations leads to the exploration of the isoenergetic surface $H(\{x_i, p_i\}) = E$. A more realistic situation is a system with a variable total energy and at fixed temperature. These conditions are expressed by the Canonical ensemble (N,V,T). Here, the system is in contact with an infinite thermal source, called thermostat or bath. Energy is not conserved, but it is possible to show that, in the thermodynamic limit i.e. if the number of particles $N \to \infty$ at constant density, relative fluctuations tend to vanish.

As explained in the previous section, if we simply integrate Hamilton's equations of motion, all time averages of macroscopic observables are equivalent to ensemble averages, where the understood ensemble is the (N, V, E). In order to sample from the (N, V, T) ensemble instead, various MD methods are used, both deterministic [50, 51, 52] and stochastic [53, 54]. Usually, they are based on a rescaling of the velocities of the system via a thermostat. This rescaling is implemented thanks to the knowledge of the Equipartition Theorem, which imposes a constraint on the kinetic energy of a system of N classical particles in the Canonical ensemble, following the Maxwell-Boltzmann distribution, at thermal equilibrium.

Theorem 3.2.1 (Equipartition Theorem) *For a particle of mass m in a 3D space at thermal equilibrium with a bath at temperature T, then:*

$$\langle \frac{1}{2} m v^2 \rangle = \frac{3}{2} k_B T \tag{3.10}$$

Each velocity degrees of freedom contributes to the total kinetic energy proportionally to the temperature T. Deterministic algorithms, such as Berendsen's [50] and Nose-Hoover's [55, 51], usually obtain the correct rescaling of velocities in terms of a variable γ, which gives the coupling between Hamilton's equations and the thermal bath, by integrating a new equation of motion for the γ to make the rescaling smoother.

3.2.2 Langevin thermostat

Langevin equation (2.5) offers a simple and efficient way to couple the equations of motion with a thermostat which gives the correct classical energy distribution [56, 57, 58]. The main idea is always a form of velocity rescaling, obtained with the two contributions of the Langevin equation, explained in Section 2.1: a friction parameter γ and a stochastic process that allows to randomize the velocities imposing the correct Canonical energy distribution.

For simplicity, we consider the 1D problem and recall the Langevin equation (2.5). Then, the equations of motion of the particle i are:

$$\begin{cases} \frac{dx_i}{dt} = \frac{p_i}{m_i} \\ \frac{dp_i}{dt} = -\gamma p_i + f_i + R(t) \end{cases} \tag{3.11}$$

The term $-\gamma p_i$ is the damping force acting on the particle i, $f_i = -\frac{\partial U}{\partial x_i}$ is an external force given by the presence of an external potential $U = U(x_1, \ldots, x_N)$. Finally, the random force $R(t)$ is assumed to be a stationary random process - for which is valid the Wiener-Khinchin theorem 2.4.1 - and it needs to have $\langle R(t) \rangle = 0$ and the following property:

$$\langle R(t) R(t+\tau) \rangle = 2 m_i \gamma k_B T \delta(\tau) \tag{3.12}$$

From Klein-Kramers equation for diffusion (2.26), it is possible to show that these equations of motion ensure that the system reaches the equilibrium with the proper Boltzmann distribution and the proper classical energy density such that the Equipartition theorem 3.2.1 is recovered.

Note that Langevin equation was originally introduced to model an actual physical process - the Brownian motion, as explained in Section 2.1 - whereas in the MD algorithm it is a simulation tool to ensure the sampling from the (N, V, T) ensemble, instead from the (N, V, E) ensemble of standard, non-thermostated MD.

In order to better express this result, which is central also in Langevin-based quantum methods exposed in Sections 3.4 and 3.5, we state the generalized Langevin equation as:

$$\boxed{\begin{cases} \frac{dx_i}{dt} = \frac{p_i(t)}{m_i} \\ \frac{dp_i}{dt} = -\frac{\partial U}{\partial x_i} - \int_0^\infty \Gamma(\tau)\; p_i(t-\tau)\; d\tau + R(t) \end{cases}} \tag{3.13}$$

where the momentum p_i is convoluted with the memory function $\Gamma(t)$, used to obtain a generalized friction force $\int_0^\infty \Gamma(\tau) p_i(t-\tau)\; d\tau$. The stochastic process $R(t)$ has $\langle R(t) \rangle = 0$ and power spectral density given by Wiener-Khinchin's formula (2.47) in terms of the time auto-correlation function

$$\boxed{C_{RR}(\omega) = \int_{-\infty}^{+\infty} \langle R(t)R(t+\tau)\rangle e^{-\imath\omega\tau} d\tau = 2m_i k_B T \gamma(\omega)} \tag{3.14}$$

where we defined $\gamma(\omega)$ as the Fourier transform $\mathcal{F}\{\Gamma(t)\}(\omega)$ of the memory function. The memory kernel $\Gamma(t)$ can be chosen arbitrarily; the standard choice is

$$\Gamma(t) = \gamma\delta(t) \tag{3.15}$$

where $\delta(t)$ is the Dirac delta function. This means that the stochastic process loses memory immediately of itself i.e. we recover condition (3.12), exactly as it was supposed in the Brownian motion for the random collisions with the fluid's particles. In this way, we obtain $R(t)$ to be a white noise, with constant PSD

$$\boxed{C_{RR}(\omega) = \int_{-\infty}^{+\infty} \langle R(t)R(t+\tau)\rangle e^{-\imath\omega\tau} d\tau = 2m_i \gamma k_B T} \tag{3.16}$$

In order to integrate the equations of motions, we use Liouville's operator formalism and we apply the so called BAOAB integration scheme [58], which has been shown to optimally perform with respect of other possible integration schemes of Langevin equation. The integration of position and momentum of each particle

i is split in the following steps, each of them corresponding to a specific Liouville's operator:

- **step B**: momenta are updated with the forces computed in the positions $\vec{x}(t)$ of an half-step Δt, as:

  $$p_i(t + \Delta t/2) = p(t) + \frac{f_i(\vec{x}(t))}{m_i}\Delta t/2$$

  The extension to more dimensions is straightforward;

- **step A**: the positions are updated with the momenta of a half-step Δt. Explicitly, this is:

  $$x_i(t + \Delta t/2) = x_i(t) + \frac{p_i(t)}{m_i}\Delta t/2$$

  As shown in (3.9), steps A and B symmetrically split integrates Hamilton's equations of motion with an error of $\mathcal{O}(\Delta t^3)$;

- **step O**: the core of the Langevin thermostat is the rescaling of the velocities, which is obtained by two terms, the friction and the ramdom force, depending explicitly on the integration step Δt. A full step integration of the momenta by the Langevin thermostat states:

  $$\boxed{p_i(t + \Delta t) = p_i(t)e^{-\gamma\Delta t} + \sqrt{(1 - e^{-2\gamma\Delta t})\, m_i k_B T}\,\mathbf{g}} \tag{3.17}$$

  where $\mathbf{g}$ is a Gaussian random number, sampled independently at every step Δt from a normal distribution with zero mean and unitary variance i.e. $\mathbf{g} \sim \mathcal{N}(0,1)$. This expression is obtained from the solution of the following differential equation:

  $$\frac{dp(t)}{dt} = -\gamma p(t) + R(t)$$

  where we dropped the index i for simplicity. By multiplying both sides by $e^{\gamma t}$, we obtain:

  $$\frac{d}{dt}\left(e^{\gamma t}p(t)\right) = e^{\gamma t}R(t)$$

  Then, integrating both sides from t to $t+\Delta t$, we obtain the following expression:

  $$p(t + \Delta t) = p(t)e^{-\gamma\Delta t} + e^{-\gamma\Delta t}\int_t^{\Delta t} dt' R(t')e^{\gamma t'}$$

We consider then the second term, that we denote as $N(t)$, and we compute:

$$\langle N(t)^2\rangle = e^{-2\gamma\Delta t}\int_t^{\Delta t} dt' \int_{t'}^{\Delta t} dt'' \langle R(t')R(t'')\rangle e^{\gamma(t'-t'')} \tag{3.18}$$

Using the property of $R(t)$ (3.12) and the property of the Dirac delta, the following expression is derived, with the final integral taken between 0 and Δt:

$$\langle N(t)^2\rangle = mk_BT\left(1 - e^{-2\gamma\Delta t}\right)$$

which leads to the integration step O.

The symmetric decomposition of Liouville's operator for the scheme BAOAB is then:

$$e^{\imath\hat{\mathscr{L}}\Delta t} = e^{\imath\hat{\mathscr{L}}_B\Delta t/2} e^{\imath\hat{\mathscr{L}}_A\Delta t/2} e^{\imath\hat{\mathscr{L}}_O\Delta t} e^{\imath\hat{\mathscr{L}}_A\Delta t/2} e^{\imath\hat{\mathscr{L}}_B\Delta t/2}$$

which has an overall error $\mathcal{O}(\Delta t^3)$, which is negligible for a small integration step Δt. It is worth noticing that the shorter the time step, the longer the total simulation time becomes. However, too large Δt would alter the phase-space distribution that would not correspond to Boltzmann distribution anymore. A qualitative criteria to choose the integration step is to compare it with the largest vibrational frequency of the system, or the shortest period. Therefore, the integration step is chosen as $\Delta t \ll 1/\nu_{max}$.

Particular attention must be given to the friction parameter γ. Indeed, it is also the strength of the coupling of equations of motion with the thermal bath. This means that the higher the value of γ, the stronger the damping term and the influence on the dynamics. The effect of γ can be clearly seen in the shape of the spectra shown in Section 4.2, where they appear to broaden as the friction increase. To explain this effect, let us consider the case of a damped harmonic oscillator of frequency ω. The effect of the damping term result in an exponential decrease of the amplitude of oscillations. In the frequency domain, this means that the spectra is not anymore a $\delta(\omega)$, but the spectral profile is given by a Lorentzian distribution. As long as the damping term is kept in a small range of values, the broadening of the spectra has no serious consequence on the dynamics. However, for large values of γ compared to the typical frequencies of the system, we fall in the overdamped regime 2.2.6 and the dynamics is compromised.

Figure 3.1 shows the pseudo-code of Langevin thermostat coupled to Hamilton's equations. For simplicity, momenta and positions are one-dimensional, since the generalization to more dimensions is straightforward. The vector sign indicates that we are dealing with many particles with index $i = 1, \dots, N$.

In our work, Langevin thermostat is implemented with a slight optimization change, namely the Leapfrog Velocity-Verlet, which allow to compute only once

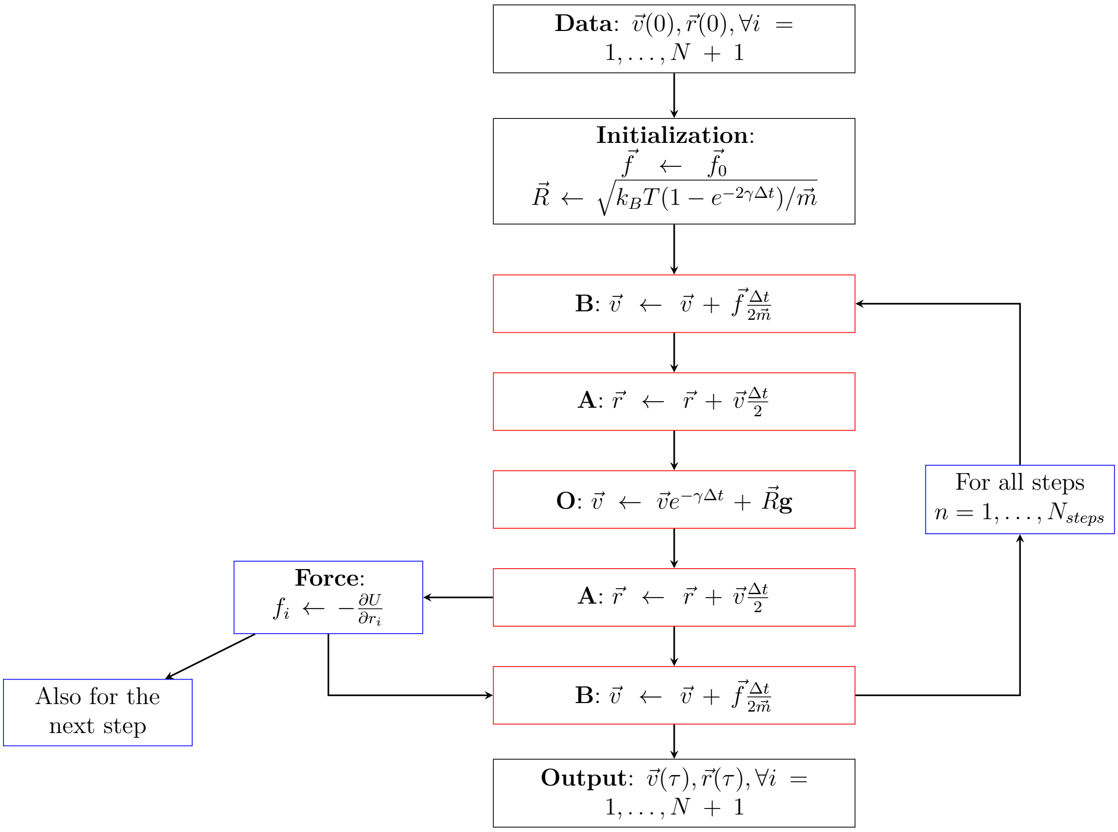

Figure 3.1: Flowchart of the Langevin thermostat with BAOAB integration scheme, where $\mathbf{g} \sim \mathcal{N}(0,1)$

the forces - usually the most time-demanding computation in a MD algorithm - and update the momenta with $\vec{f}$ of a full step Δt, instead of $\Delta t/2$ twice.

3.2.3 Computation of TCFs

Using MD algorithms, it is possible to access the full trajectory of the system in the phase space i.e. all positions and momenta are know at each time-step $n\Delta t$, where the index $n = 1, \ldots, N_{steps}$. We consider two general (classical) observables A and B and their TCFs, given by the definition (2.34). For simplicity, we consider a system of N, 1D particles with trajectory $(\vec{x}(t), \vec{p}(t))$ in the phase space. For this computational part, we refer mainly to [25].

Direct method

The direct method to compute the $C_{AB}(n\Delta t)$ involves an average over many trajectories, which means many MD simulation of the same system, and the direct evaluation of A at the time $t = 0$ and B at time $t = n\Delta t$. For k trajectories, we have

$$C_{AB}(n\Delta t) = \frac{1}{k}\sum_{j=1}^{k} A(\vec{x}_j(0), \vec{p}_j(0))B(\vec{x}_j(n\Delta t), \vec{p}_j(n\Delta t)) \tag{3.19}$$

The direct method is simple because involves only the definition of TCF, but it is really inefficient because usually requires many trajectories' evaluation.

Single trajectory methods

Another possible direct method, which leads to a more efficient computation of TCFs, involves the evaluation of only one, very long trajectory, which is divided in segments of k steps. To exploit this method the following assumptions must be valid:

- the system is large enough such that the thermodynamic limit is valid and Microcanonical and Canonical ensembles are equivalent;
- the system is ergodic, such that the Boltzmann distribution can be obtained by the trajectory - solution of the Hamilton's equations - itself.

Therefore, it is possible to exploit the Ergodic hypothesis (3.4) and define the TCFs as

$$C_{AB}(t) = \langle A(0)B(t)\rangle = \lim_{T\to\infty}\frac{1}{T}\int_0^T dt A(x(\vec{0}), p(\vec{0}))B(\vec{x}(t), \vec{p}(t)) \tag{3.20}$$

Under the assumptions above - which are true for the Langevin thermostat - correlations are local in time i.e. the system has a finite correlation time. After a period longer than the correlation time, the system loses memory of the initial condition and TCFs decay to zero. Hence, each segment can be considered as an independent replica of system. The computation of TCFs is then completely equivalent to the direct method and simplified as

$$C_{AB}(n\Delta t) = \frac{1}{N_{steps} - n}\sum_{j=1}^{N_{steps}-n} A(\vec{x}(j\Delta t), \vec{p}(j\Delta t))B(\vec{x}((j+n)\Delta t), \vec{p}((j+n)\Delta t)) \tag{3.21}$$

where $n = 1, \ldots, k$ and k is the total number of time-steps of each segment.

Fast Fourier Transform method

A more efficient method to compute TCFs is based on the spectral analysis of the observables involved and on the general method to compute Fourier transforms in a time $\mathcal{O}(N\log(N))$, where N is the number of data [59]. Note that the direct computation via equation (3.19) is $\mathcal{O}(N \times N_{max}$, where $N_{max}\Delta t$ is longest coherence time in the TCF. We consider (3.20) and we introduce the Fourier coefficients

$$\begin{aligned} a(\omega) &= \tfrac{1}{2\pi}\int_{-\infty}^{+\infty} dt\ A(\vec{y}(t))e^{-\imath\omega t} \\ b(\omega) &= \tfrac{1}{2\pi}\int_{-\infty}^{+\infty} dt\ B(\vec{y}(t))e^{-\imath\omega t} \end{aligned} \tag{3.22}$$

where we denoted $\vec{y}(t) = (\vec{x}(t), \vec{p}(t))$ for simplicity. It is easy to show that

$$\int_{-\infty}^{+\infty} d\omega\ a^*(\omega)b(\omega)e^{\imath\omega\tau} = \int_{-\infty}^{+\infty} dt\ A(\vec{y}(t))B(\vec{y}(t+\tau))$$

and finally obtain, for very large T, a good approximation of the TCF in terms of the Fourier coefficients (3.22)

$$C_{AB}(t) = \frac{1}{T}\int_{-\infty}^{+\infty} d\omega\ a^*(\omega)b(\omega)e^{\imath\omega t} \tag{3.23}$$

This expression is an extension of Wiener-Khinchin theorem 2.4.1. For the actual computation, we have a discrete time step Δt. So we define the discrete Fourier coefficients

$$\begin{aligned} a_k &= \textstyle\sum_{j=0}^{N_{steps}-1} A(\vec{y}(j\Delta t))e^{-\frac{2\pi\imath kj}{N_{steps}}} \\ b_k &= \textstyle\sum_{j=0}^{N_{steps}-1} B(\vec{y}(j\Delta t))e^{-\frac{2\pi\imath kj}{N_{steps}}} \end{aligned} \tag{3.24}$$

where $\omega_k = 2\pi k/N_{steps}\Delta t$ are the discrete frequencies and $t_j = j\Delta t$ are the discrete time points. We can compute then the TCF as

$$C_{AB}(n\Delta t) = \frac{1}{N_{steps}}\sum_{k=0}^{N_{steps}-1} a^*(\omega_k)b(\omega_k)e^{\imath\omega_k t_j} \tag{3.25}$$

With this method two FFT operations are required to compute the TCFs. Moreover, in order to compute the spectra, only (3.23) is required, allowing the use of FFT only once for A and once for B.

3.2.4 Application to diffusion

The diffusion coefficient is related to the velocity-velocity TCF (2.36), as shown in Section 2.4.2. We define the discrete time version of the velocity-velocity TCF as:

$$C_{vv}(n\Delta t) = \frac{1}{N_{steps}}\sum_{j=0}^{N_{steps}-1} v(j\Delta t)v((j+n)\Delta t) \tag{3.26}$$

The discrete Fourier transform of the velocity is:

$$\hat{v}(k\Delta\omega) = \frac{1}{\sqrt{N_{steps}}} \sum_{j=0}^{N_{steps}-1} v(j\Delta t) e^{-\imath k\Delta\omega j} \tag{3.27}$$

where $\Delta\omega = 2\pi / N_{steps}\Delta t$. With this definition, we can compute the velocity-velocity TCF, using the FFT method, substituting (3.27) into (3.26):

$$C_{vv}(n\Delta t) = \frac{1}{N_{steps}} \sum_{k=0}^{N_{steps}-1} |\hat{v}(k\Delta\omega)|^2 e^{\imath k\Delta\omega n} \tag{3.28}$$

where we used the following property, given the Kronecker delta $\delta_{ij} = 1$ if $i = j$ and 0 otherwise:

$$\sum_{jk} e^{\frac{2\pi\imath jk}{N_{steps}}} = N_{steps}\delta_{0k}$$

There is a subtlety about the periodicity of the Fourier transform of the $C_{vv}(\omega)$. Indeed, when computing a discrete Fourier transform, the function is made periodic in time and unphysical time correlations can appear into the correlation function due to periodicity of the function over the total time of the simulation $N_{steps}\Delta t$. In order to eliminate these time correlations, a number of N_{steps} zeros is added to the vector containing the discrete components of the C_{vv}.

The same method can be used to compute the C_{RR} and all other correlations function that are needed. We note that the velocity-velocity TCF, as well as the (random-)force-velocity TCF C_{vR}, acquires a fundamental importance in the methods based on quantum baths that are described in Section 3.4 and 3.5.

3.3 Path Integral Molecular Dynamics

3.3.1 Classical isomorphism

Path-Integrals Molecular Dynamics (PIMD), based on Feynman's Path Integral formalism explained in Section 2.5, is a reliable method to compute quantum static properties usign the imaginary-time propagator $\hat{\rho}(\beta) = e^{-\beta\hat{H}}$ (2.52). The main idea of PIMD is to exploit the so-called **classical isomorphism**, which is derived naturally from the expression of the quantum Canonical partition function (QCPF) (2.53). This isomorphism allows to introduce a MD scheme with classical Hamiltonian and classical equations of motion right at the core of the quantum problem.

We have written the discrete QCPF (2.53) in the following way:

$$\mathcal{Z}(L,T) = \lim_{N\to\infty}\left(\frac{mN}{2\pi\beta\hbar^2}\right)^{N/2}\int_{D(L)} dx_1\dots dx_N$$
$$\exp\left[-\frac{1}{\hbar}\sum_{k=1}^{N}\left(\frac{mN}{2\beta\hbar}(x_{k+1}-x_k)^2+\frac{\beta\hbar}{2N}V(x_k)\right)\right]$$

The QCPF can be also seen as the classical partition function of a **ring-polymer** with N beads moving in a classical potential (see Figure 3.2)

$$Z_{RP}^{(N)}(L,T) = \int dp_1\dots dp_N\int dx_1\dots dx_N$$
$$\exp\left[-\beta_N\sum_{k=1}^{N}\left(\frac{p_k^2}{2m}+\frac{1}{2}m\omega_N^2(x_{k+1}-x_k)^2+V(x_k)\right)\right] \tag{3.29}$$

where we defined $\beta_N = \frac{\beta}{N}$, $\omega_N = \frac{1}{\beta_N\hbar}$ as chain frequency of the coupled beads in the ring-polymer and we applied PBC $x_1 = x_{N+1}$. Hence, $\{x_k, p_k\}$ are the positions and momenta of the $k = 1,\dots,N$ beads. This corresponds to a classical Hamiltonian for the ring-polymer of the following form:

$$H_{cl}^{(N)}(\{x_k,p_k\}) = \sum_{k=1}^{N}\left(\frac{p_k^2}{2m}+\frac{1}{2}m\omega_N^2(x_{k+1}-x_k)^2+V(x_k)\right) \tag{3.30}$$

Thus, the classical equations of motion of the ring-polymer are written as

$$\begin{cases}\frac{dx_k}{dt} &= \frac{p_k(t)}{m}\\ \frac{dp_k}{dt} &= -\frac{\partial V}{\partial x_k} - m\omega_N^2(2x_k - x_{k+1} - x_{k-1})\end{cases} \tag{3.31}$$

The classical isomorphism is exact in the limit of infinite number of beads, i.e.

$$\boxed{\mathcal{Z}(L,T) = \lim_{N\to\infty} Z_{RP}^{(N)}(L,T)} \tag{3.32}$$

For a real computation with a finite number of beads N, the error given by the splitting in deriving (2.52) is of $\mathcal{O}(\frac{1}{N^3})$ for each bead, which means a total error of $\mathcal{O}(\frac{1}{N^2})$. If we couple the equations of motion (3.31) with Langevin thermostat, we can sample from the Canonical distribution as shown in Section 3.2.

3.3.2 Ring-Polymer Molecular Dynamics

Path-Integrals Molecular Dynamics (PIMD) is an important computational tool for quantum static properties but it does not allow in general to compute dynamical

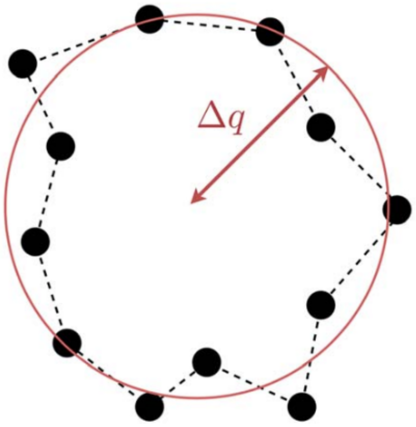

Figure 3.2: Schematic representation of the ring-polymer for a free quantum particle with gyration radius given by (3.34) (from [41])

properties that involve real time quantum propagation. Therefore, numerous approximated theories had been proposed to compute dynamical properties in terms of time correlation functions, such as Kubo's (2.39). In this section, we consider a particular approximation, the **Ring Polymer Molecular Dynamics** (RPMD) [34, 41, 42] which is able to compute approximate (Kubo-transformed) TCFs from the dynamics of imaginary-time path integrals.

Considering the dynamics of a ring polymer path integral, RPMD obtains the following definition of the Kubo-transformed time correlation function [33] of two observables A and B is the following:

$$\langle A(0)B(t)\rangle = \frac{1}{Z^{(N)}(2\pi\hbar)^N}\int dx_1\ldots d_N\int dp_1 dp_N$$
$$e^{-\beta H_{cl}^{(N)}(x_k,p_k)}A^{(N)}(0)B^{(N)}(t) \quad (3.33)$$

where $A^{(N)}(0) = \frac{1}{N}\sum_{k=1}^{N} A(x_k(0), p_k(0))$ and $B^{(N)}(t) = \frac{1}{N}\sum_{k=1}^{N} B(x_k(t), p_k(t))$ and $Z^{(N)}$ given by (3.29).

In general, the RPMD Kubo-transformed TCF is a refinement of Matsubara dynamics, which relies on delicate approximations. The full derivation of this expression and the analysis of the approximations are discussed in detail in [60].

3.3.3 NQEs in RPMD

The main point of the ring-polymer description is that the swelling of the quantum particle due to the combination of thermal and quantum fluctuations is reproduced by the interacting chain [41]. Indeed, we can define the gyration radius of the ring-polymer of a free particle

$$\Delta q = \sqrt{\langle \frac{1}{N} \sum_{k=1}^{N} (x_k - \bar{q})^2 \rangle} \tag{3.34}$$

where

$$\bar{q} = \frac{1}{N} \sum_{k=1}^{N} x_k$$

is the position of the centroid of the polymer. For $N \to \infty$, the gyration radius has the following limit for a free particle:

$$\Delta q = \sqrt{\frac{\beta \hbar^2}{12m} \left(1 - \frac{1}{N^2}\right)} \to \frac{\hbar}{\sqrt{12 m k_B T}} \tag{3.35}$$

In Figure 3.2 a schematic representation is shown, taken from [41].

Therefore, the smaller the mass and the lower the temperature, the more pronounced is the swelling of the polymer and the quantum distribution of the particle is recovered. With this picture, it is possible to include naturally into a MD method the NQEs due to the quantum delocalization of the particle.

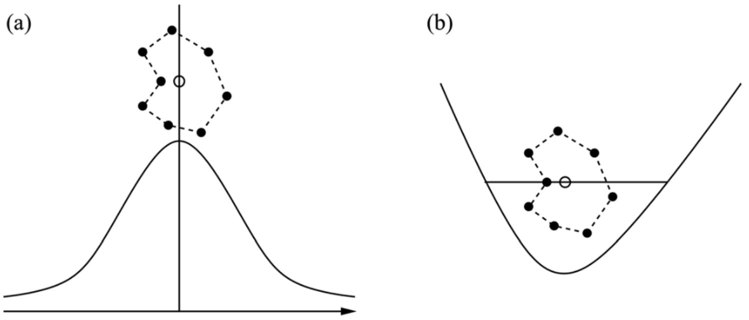

Figure 3.3: Qualitative representation of the tunneling (a) and zero-point energy (b) in the RPMD method (from [41])

Zero-point Energy

A classical particle, with initial position at the bottom of a well, has no zero-point potential energy. For a quantum, particle instead, the energy has a non-zero distribution. The same happens in a system at $T = 0K$: the classical particle is completely frozen, while a quantum particle still has some zero-point quantum fluctuations. The RPMD picture captures the qualitative aspect of the zero-point energy thanks to the dispersion of the beads, which are not experiencing all the same zero-point potential at the bottom of the well, and the QCPF reduces to $e^{-\beta E_0}$ in the limit of low temperature, where E_0 is the ground state of the system. In Figure 3.3 a schematic representation is shown, taken from [41].

Tunneling

If we are in presence of a potential barrier, a classical particle cannot overcome it unless it has an energy equal or higher than the top of the barrier V_{max}. The Canonical probability to find the classical particle at the top of the barrier is $e^{-\beta V_{max}}$. Instead, a quantum particle can tunnel through a potential barrier with exponentially low but finite probability depending on the width of the potential. A ring-polymer reproduces qualitatively this quantum effect. Indeed, the beads are not feeling all the potential V_{max} but some potential $V(x_k) \leq V_{max}$. For the probabilities, this means that $e^{-\beta V(x_k)} \geq e^{-\beta V_{max}}$. Therefore, the polymer can cross the barrier even if the mean energy (averaged over the different beads) is lower than the barrier height. In Figure 3.3 a schematic representation is shown, taken from [41].

3.3.4 Problems with PIMD

As already mentioned, PIMD allows to compute exactly quantum static properties but it cannot provide a unified and exact theory for quantum dynamics.

RPMD has some drawbacks due to the fact that it is based on the imaginary time representation of the density matrix in Feynman's picture. First of all, we have to deal with an imaginary time, due to the Feynman's picture explained in Section 2.5, and not on real time dynamics. Therefore, for the Kubo-transformed TCF, there is no actual rigorous derivation to prove this result. Moreover, RPMD simulations involve a significant increase of the computational cost (equal to the number N of beads) for each quantum particle with respect to a classical MD simulation, although the computation could be parallelized on many processors. Finally, there are problems in which interference between the intrinsic chain frequencies of the ring-polymer with physical frequencies of the system can be observed causing spurious resonances [44].

Apart RPMD, other PIMD methods exists, such as Linearized Semi-Classical Initial Value Representation (LSC-IVR) [61] and Centroid Molecular Dynamics, which is the mean-field version of Matsubara dynamics [60]. These methods linked to the PI framework have to rely on approximations, which are not always valid for every quantum system. Moreover, real-time path integral formulations, in principle, would allow the computation of dynamical properties, but it suffers of the so-called sign problem, which derives from the oscillations of the phase factor when very large number of paths are summed (as qualitatively explained in Section 2.5). For these reasons, even if PIMD remains the favourite tool to deal with NQEs, alternative approaches are needed.

3.4 Quantum Thermal Bath

The drawbacks of PIMD require to find a suitable alternative to simulate dynamical properties of quantum systems in which are present NQEs. One promising quantum MD alternative method is the **Quantum Thermal Bath** [22]; a similar algorithm, called Quantum thermostat, have been implemented by several groups and all of them are based on Langevin equations [62, 63].

The main idea of the QTB is similar to the classical case and consists in mimicking the quantum delocalization of a light nucleus with a stochastic process. As for the classical Langevin thermostat, two contributions are added to the Hamilton's equation of motions: a frictional force with parameter γ and a random force which makes explicit the quantum nature of the particle via its power spectral density. Indeed, the bath now is a quantum version of the Langevin thermal bath and it is given by the quantum Fluctuation-Dissipation theorem (3.38). The random force is therefore not a white noise, but a coloured 'quantum' noise. The main advantages of the QTB are the reduced computational costs compared to PIMD methods and the use of a clear classical picture, in which the concept of particle's trajectories in real time is well defined and can be easily simulated with well known MD techniques.

QTB method is based on the Langevin equation of the form of (2.5). We recall also the generalized Langevin equation (3.13). For simplicity, we consider a 1D system, which can be easily generalized to more dimensions and more particles as shown below. The main difference from the classical case is the implementation of the random force $R(t)$, which now is a random process with $\langle R(t)\rangle = 0$ and the force-force TCF $C_{RR}(\tau)$ by defining the following power spectral density for the quantum problem

$$\boxed{C_{RR}(\omega) = 2m\gamma\theta(\omega, T)} \tag{3.36}$$

and relating to $C_{RR}(\tau)$ via the Wiener-Khinchin theorem (2.47). Here, we assume the quantum energy density function $\theta(\omega, T)$ is given by the following formula:

$$\boxed{\theta(\omega, T) = \hbar\omega\left(\frac{1}{2} + \frac{1}{e^{\frac{\hbar\omega}{k_B T}} - 1}\right) = \frac{\hbar\omega}{2}\frac{1}{tanh\left(\frac{\hbar\omega}{k_B T}\right)}} \tag{3.37}$$

This expression correspond to the average energy of an harmonic oscillator of frequency ω at thermal equilibrium. The idea of the QTB is therefore to thermalize each vibration mode of the quantum system, not with the classical distribution of energy - given by the Equipartition theorem 3.2.1 - but with the quantum energy distribution $\theta(\omega, T)$. In particular, the first term $\frac{\hbar\omega}{2}$ corresponds to the zero-point energy and ensures that, even when $T = 0K$, the system does not freeze but insead continues to fluctuate with an average probability distribution that mimics the delocalization of the quantum ground state.

For a many particles and more (2 or 3) dimensions, the power spectral density takes the form of:

$$C_{R_{i\alpha}R_{j\beta}}(\omega) = 2m\gamma\theta(\omega, T)\delta_{ij}\delta_{\alpha\beta}$$

for $\alpha, \beta = 1, 2, 3, \dots$ and $i, j = 1, \dots, N$.

3.4.1 Fluctuation-Dissipation Theorem

The relation between the frictional force and the random force in Langevin equation - expressed by Wiener-Khinchin's formula (3.14) - is related a much more general result [26], which takes the name of **Fluctuation-Dissipation therorem** (FDT). It sates that the response of a system to an external disturbance is related to the internal fluctuations of the system in absence of the disturbance. Time-correlation functions can express and characterize internal fluctuations - or their fluctuations spectra - and they are linked in general to quantities such as admittance or impedence. Knowing one side of the theorem allows to know also the other in full generality. The expression of (3.37) is then derived by using the quantum version of the Fluctuation-Dissipation theorem in [64] and it is not reported in this work.

A condensed way to express the FDT is the following:

$$\boxed{\frac{1}{2}mC_{vv}(\omega) = \Re\left[\widetilde{\chi}_{vx}(\omega)\right] k_B T \kappa(\omega, T)} \tag{3.38}$$

where C_{vv} is the FT of the velocity-velocity TCF (2.36), the function $\kappa(\omega, T)$ is a spectral 'thermal energy distribution function' which can be specified for the problem under study. Finally, the $\widetilde{\chi}_{vx}(\omega)$ is the linear generalized susceptibility - defined in full generality in [26] - which, in this case, characterize the velocity response $\Delta v(\omega)$ to a small perturbative force in the frequency domain

$$\Delta v(\omega) = \widetilde{\chi}_{vx}(\omega)\Delta F(\omega)$$

What is most important is the interpretation of the (3.38) and its use in the context of Langevin methods presented in this work. First of all, let us consider the classical case in which the function $\kappa(\omega, T) = 1$. What we obtain is the classical Equipartition theorem (3.10), in which every mode posses the same energy. Therefore, the quantity $2\Re\left[\widetilde{\chi}_{vx}(\omega)\right]$ can be seen also as the vibrational density of state of an harmonic system.

For the quantum case, $\kappa(\omega, T) = \frac{\theta(\omega,T)}{k_B T}$. Then, from the FDT (3.38) we recover exactly the distribution of energy of the QTB (3.37), and the new quantum density distribution is inserted into the system by the random force $R(t)$.

For a full derivation of the Linear Response Theory we refer to [25] and to a general discussion of the generalized susceptibility and the FDT we refer to [64] and [23].

3.4.2 Integration of Equations of Motion with QTB

Again, the QTB algorithm integrates the equations of motion with the BAOAB scheme already employed for classical Langevin thermostat. The only difference is in the step O of the velocity rescaling (3.17) and in particular in the expression of the random noise coefficient (3.18), which is now correlated in time. Hence we want to compute

$$\langle N(t)N(t')\rangle = \langle N(0)N(\tau)\rangle$$

where $\tau = N_{steps}\Delta t$. We have then

$$\langle N(0)N(\tau)\rangle = e^{-2\gamma\Delta t}\int_0^{\Delta t} dt' \int_0^{\Delta t} dt'' e^{\gamma(t'+t'')}\langle R(t+t')R(t+t'')\rangle$$

Using the definition of $C_{RR}(\tau)$ given by (3.36), we have

$$\langle N(0)N(\tau)\rangle = e^{-2\gamma\Delta t}\int_0^{\Delta t} dt' \int_0^{\Delta t} dt''\ e^{\gamma(t'+t'')}\int_{-\infty}^{+\infty}\frac{d\omega}{2\pi}\ e^{\imath\omega(t'-t'')}\ 2m\gamma\ \theta(\omega, T)$$

which can be rearranged into

$$\langle N(0)N(\tau)\rangle = e^{-2\gamma\Delta t}2m\gamma\int_{-\infty}^{+\infty}\frac{d\omega}{2\pi}\ \theta(\omega, T)e^{\imath\omega t}\int_0^{\Delta t} dt' \int_0^{\Delta t} dt''\ e^{(\imath\omega+\gamma)t'}e^{(-\imath\omega+\gamma)t''}$$

Integrating over t' and t'' and rearranging the expression, we obtain the final shape of the coefficient we need to apply in order to rescale the momenta

$$\langle N(0)N(\tau)\rangle = 2m\gamma\int_{-\infty}^{+\infty}\frac{d\omega}{2\pi}\left[\frac{1 - 2cos(\omega\Delta t)e^{-\gamma\Delta t} + e^{-2\gamma\Delta t}}{\omega^2+\gamma^2}\right]\theta(\omega, T)e^{\imath\omega t}$$

To simplify the notation, we call the factor between $[\dots] = \phi(\omega, \gamma, \Delta t)$. Then, finally, we obtain the following integration step O of the BAOAB integration scheme:

$$\boxed{p_i(t+\Delta t) = p_i(t)e^{-\gamma\Delta t} + \sqrt{2m\gamma \int_{-\infty}^{+\infty} \frac{d\omega}{2\pi}\phi(\omega,\gamma,\Delta t)\theta(\omega,T)\mathbf{g}(\Delta t)e^{\imath\omega t}}} \tag{3.39}$$

where $\mathbf{g}$ is a Gaussian random number sampled from a normal distribution with zero mean and unitary variance i.e. $\mathbf{g}(t) \sim \mathcal{N}(0,1)$. The steps A and B remain unchanged.

Three important subtleties must be discussed. First of all, since the random noise is now correlated in time, we need to compute it all before the integration. Therefore, it is necessary to divide the full integration time τ in segments of length $N_{steps}\Delta t$. Hence, the total time of the simulation is $\tau = N_{seg} \times N_{steps}\Delta t$. This segmentation here it is only a computational trick to not have to save too long vectors in the memory, but it will have a important role in the implementation of the Adaptive QTB (see Section 3.5).

The second subtlety is the need of a cut-off frequency ω_{cut} [65]. Indeed, the spectral energy density (3.37) diverges proportionally to ω at high frequencies. Thus, the QTB includes fluctuations at arbitrary high frequencies, most of which are not physical. We introduce then a cutoff function of the form:

$$f_{cut}(\omega;\omega_{cut},\omega_{smear}) = \frac{1}{e^{\frac{(\omega-\omega_{cut})}{\omega_{smear}}}+1} \tag{3.40}$$

The parameter ω_{cut} gives the maximal frequency, few times higher than the physical maximal frequency ω_{max} observed in the spectrum. The parameter ω_{smear} makes the cutoff smoother. The final version of the O step becomes

$$p_i(t+\Delta t) = p_i(t)e^{-\gamma\Delta t} + \sqrt{2m\gamma \int_{-\infty}^{+\infty} \frac{d\omega}{2\pi}\kappa(\omega,\gamma,\Delta t)\theta(\omega,T)\mathbf{g}f_{cut}(\omega)e^{\imath\omega t}}$$

The other important parameter that must be chosen wisely is again the 'friction' γ. As in the classical case described in Section 3.2, it cannot be too small if we want to keep the simulation total time to a accessible order but it must be smaller than a typical frequencies of the system. However, γ gives also the strength of the coupling between the quantum thermostat and the equations of motion. This means that its value must be large enough to have the correct quantum energy distribution given by (3.37).

Figure 3.4 is the pseudo-code of the QTB algorithm. The routine **QTB-noise** generates the quantum noise for the whole sequence of N_{steps} before each segment of the simulation, exactly as described by (3.39). The total time of the simulation is $\tau = N_{seg} \times N_{steps}\Delta t$.

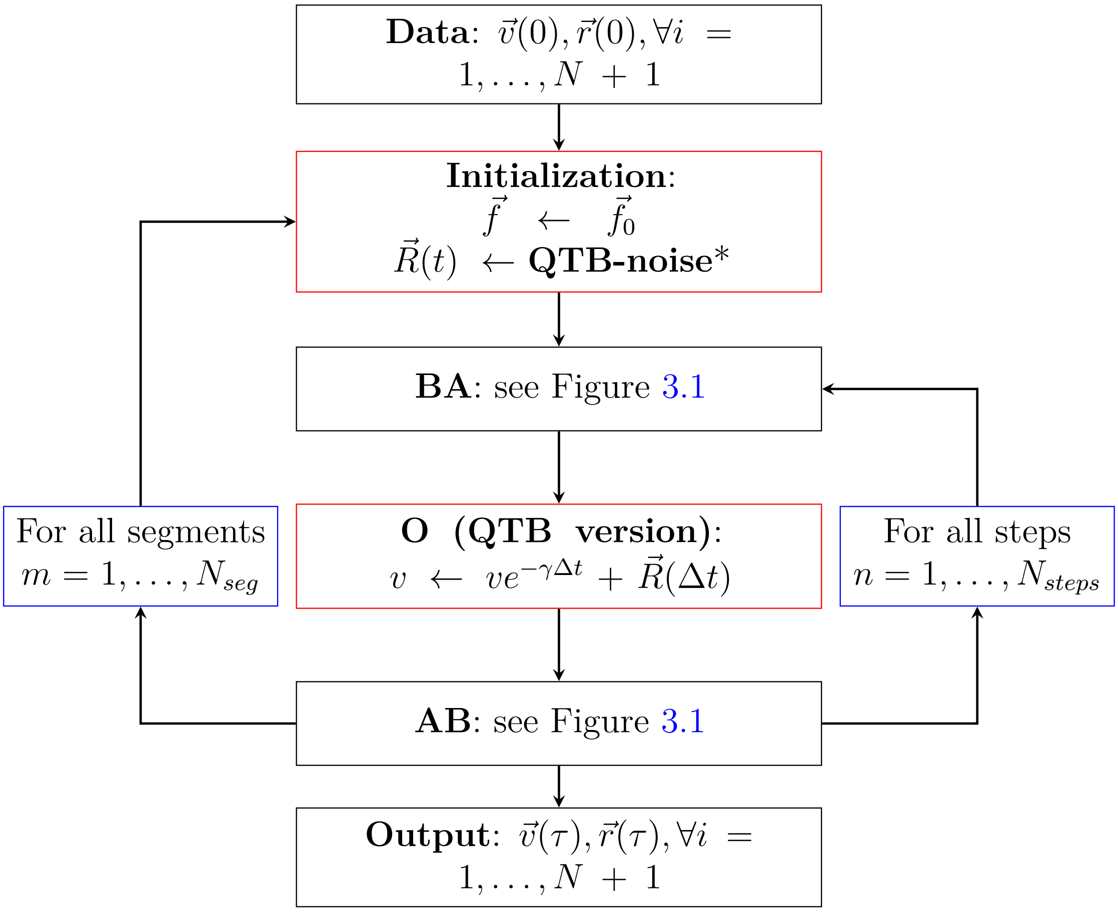

Figure 3.4: Flowchart of the QTB thermostat

3.4.3 Zero-Point Energy Leakage

Although the QTB gives exact results in the simulation of NQEs in harmonic systems [16, 2, 5] in presence of anharmonicity it fails, due to the so-called **Zero-Point Energy Leakage** (ZPEL) [45].

In the QTB method, the quantum bath given by the stochastic process $R(t)$ is coupled with Hamilton's equations via the parameter γ. The higher the value of γ, the stronger the coupling and thus the effect of the bath on the dynamics. As a general rule of thumb, the friction should be chosen small enough to avoid to fall in the overdamped regime and completely modify the dynamical properties of the system. The quantum bath thermalizes each vibrational mode of the quantum system at the correct energy density $\theta(\omega, T)$, given by (3.37).

However, the presence of classical external forces $-\frac{\partial U(\vec{x})}{\partial x_i}$ which couple the modes (creating anharmonicity) leads to the ZPEL. The energy of high frequency modes is transfered to the low frequency ones, because classical equations of motions enforces the Equipartition theorem (3.10). As a results, the effective energy density distribution will be lower than $\theta(\omega, T)$ for high ωs and higher than $\theta(\omega, T)$ for low ωs.

The first approach to solve the ZPEL is to use higher values of the friction, which has been shown to reduce - but not eliminate - the drawback, at the cost of a stronger influence on the dynamics by the bath [45]. Indeed, as already explained in Section 3.2, the friction γ is the strength of the coupling between the quantum bath and the equations of motion. By increasing γ, the system is forced to thermalize with the quantum distribution, even though the spectra may significantly change due to the damping term in Langevin equation. The best compromise between these two aspects must be found to ensure correct dynamical results.

A second, more sophisticate and precise method used to correct the ZPEL takes the name of **adaptive** QTB and is described in the following section.

3.5 Adaptive Quantum Thermal Bath

3.5.1 Diagnosis of the ZPEL

The main idea to quantify the error given by the ZPEL is to measure the violation of the quantum Fluctuation Dissipation Theorem involved in the Langevin-based process of QTB [23].

We recall the FDT (3.38) in terms of the generalized susceptibility $\Re\left[\widetilde{\chi}_{vx}(\omega)\right]$. From the Linear Response Theory, we have the following result for the position and velocity operators $\hat{x}$ and $\hat{v}$:

$$\boxed{\Re\left[\widetilde{\chi}_{vx}(\omega)\right] = \frac{\omega}{2\imath\theta(\omega, T)} \int_{-\infty}^{+\infty} \langle \hat{x}(0)\hat{v}(t)\rangle e^{-\imath\omega t} dt = \frac{C_{vv}(\omega)}{2\theta(\omega, T)}} \tag{3.41}$$

This result is valid for every frequency and it is exact for quantum operators which evolves with the correct quantum dynamics. However, in the QTB we are using classical equations of motion and classical variables as observable. Thus, this relation is not exact anymore and we can measure the difference of the two quantities in order to correct the ZPEL.

The velocity-velocity TCF can be computed in QTB in the way described by (3.19). This is not the case for the generalized susceptibility, which in general cannot be computed analitically and must be integrated with numerical methods. Therefore, we look for an expression of (3.41) in terms of TCFs. We consider the following property for the spectral component of the random force $R(t)$:

$$\langle \widetilde{R}(\omega)\widetilde{R}(\omega')\rangle = 0, \forall\omega \neq \omega'$$

Based on the fact that the forces at distinct frequencies are not correlated, the quantum Fluctuation-Dissipation theorem is fulfilled for each frequency (for details, see [23]). This is also true for simulations, provided $\Delta\omega = \frac{2\pi}{N_{steps}\Delta t}$ be small i.e. for long enough simulations. Therefore, we have the following relation for the generalized susceptibility:

$$\Re\left[\widetilde{\chi}_{vx}(\omega)\right] \simeq \frac{\Re\left[C_{vR}(\omega)\right]}{C_{RR}(\omega)} \tag{3.42}$$

This relation can be rewritten using (3.41) and (3.36) in the following way:

$$\boxed{m\gamma C_{vv}(\omega) = \Re\left[C_{vR}(\omega)\right]} \tag{3.43}$$

The interpretation of this formula is the equivalence between the spectrum of the power injected in the system by the random force C_{vR} and the spectrum of the power dissipated by the frictional force $m\gamma C_{vv}$. Any deviation from the quantum FDT in (3.43) is due to the energy that is transferred from a frequency to another one. Therefore, equation (3.43) provides a measure of the ZPEL. The velocity-(random) force TCF can be computed in the same way of the C_{vv}.

3.5.2 Cure of the ZPEL

The main idea of the adQTB is to use a frictional coefficient that is a function of the frequencies $\gamma(\omega)$ and adapt on the fly the dynamics in such way that it compensate the error given by the ZPEL on the energy distribution, using (3.43). We define then a new power spectral density

$$\boxed{C_{RR}(\omega) = 2m\gamma(\omega)\theta(\omega, T)} \tag{3.44}$$

such that (3.43) takes the form:

$$C_{vR}(\omega) = m\gamma(\omega)C_{vv}(\omega) \tag{3.45}$$

and we can compute the difference

$$\boxed{\Delta_{FDT}(\omega) = \Re\left[C_{vR}(\omega)\right] - m\gamma(\omega)C_{vv}(\omega)} \tag{3.46}$$

From this quantity we have a estimation of the ZPEL for each frequency, hence we can correct it by adapting the $\gamma(\omega)$ in a way such that it increases at high ωs and decreases at low ωs. Another possible method could be to adapt the memory function $\Gamma(\tau)$ [23] - or rather its spectral component $\Gamma(\omega)$ - but this method has not been used in this work.

3.5.3 Adaptation of the friction

Once C_{vv}, C_{vR} and the difference (3.46) are computed, the main goal is to adapt $\gamma(\omega)$ such that $\Delta_{FDT} \simeq 0, \forall\omega < \omega_{cut}$. We have therefore an equation for the friction function for every frequency:

$$\boxed{\frac{d\gamma(\omega)}{dt} = \gamma A_\gamma \frac{\Delta_{FDT}(\omega)}{||\Delta_{FDT}(\omega)||}} \tag{3.47}$$

where γ is the friction parameter, A_γ is the velocity of adaptation and $||\Delta_{FDT}(\omega)||$ is the norm

$$||\Delta_{FDT}(\omega)|| = \sqrt{\sum_{\omega<\omega_{cut}} \Delta^2_{FDT}(\omega)} \tag{3.48}$$

The integration of the adaptive $\gamma(\omega)$ is not done over a single time step Δt but over a full segment $N_{steps}\Delta t$, where the total time of the simulation is $\tau = N_{seg} \times N_{steps}\Delta t$ (see Section 3.4 for the explanation). We obtain therefore

$$\gamma^{(n+1)}(\omega) = \gamma^{(n)}(\omega) + \gamma A_\gamma \frac{\Delta_{FDT}(\omega)}{||\Delta_{FDT}(\omega)||} N_{steps}\Delta t \tag{3.49}$$

where the index n indicates the segment of the simulation ($n = 1, \ldots, N_{seg}$). We note that a large value of the A_γ, compared to the friction parameter, leads to a fast convergence. However, the faster the adaptation process, the larger are the fluctuations, which can have repercussions on the dynamics. Figure 3.5 shows the implementation of the adQTB, following the implementation of the QTB in Figure 3.4.

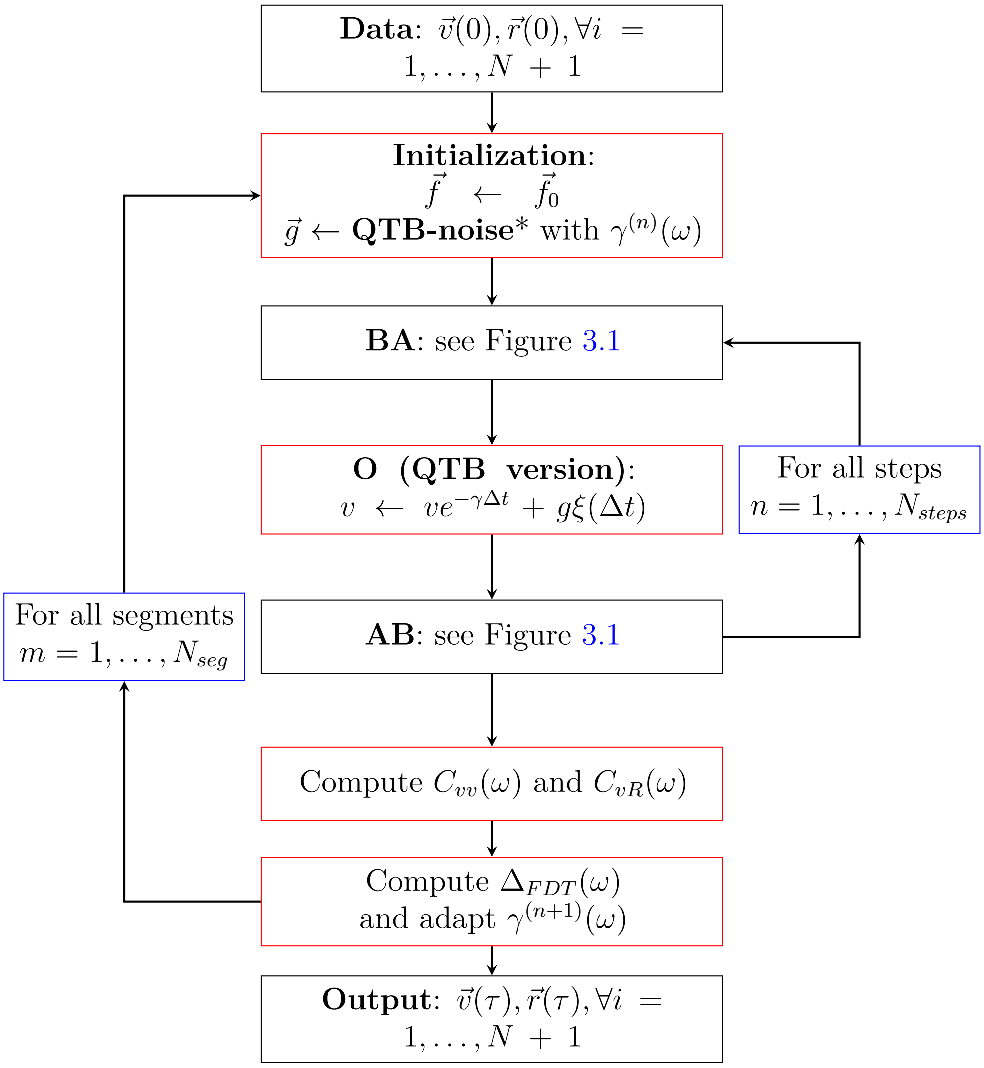

Figure 3.5: Flowchart of the adQTB thermostat

Chapter 4

Results

In this Chapter the main results of classical and quantum MD simulations are discussed. First, we describe the simple model for hydrogen's diffusion. This model is created in such a way it has physical properties of a quantum diffusion problem but it is simple enough to be easily tested with different methods. Then, this model was studied with the classical Langevin thermostat described in Section 3.2, characterize the classical diffusion effect and its temperature dependence. Then, both QTB and adQTB - described in Section 3.4 and 3.5 respectively - were tested on the same system, and their results are evaluated. We show that even in this simplified model, complex physical behaviors can arise, in particular, we evidence the effect of phonon-assisted hopping on diffusion and its interplay with NQEs, such as zero-point motion.

A FORTRAN molecular dynamic code was developed from scratch in order to easily test all tree main MD methods - Langevin thermostat, QTB and adQTB, presented in Section 3.2, 3.4 and 3.5 respectively - and their assumptions. All problems due to convergence and numerical evaluations, some of which are discussed in Chapter 3, were solved for this simple system. This code can be easily extended to incorporate other MD methods (such as RPMD, see Section 3.3) and more sophisticated problems in the future.

4.1 System description

The goal of this work is to study the diffusion of an hydrogen atom in a solid material, in order to highlight the capacity of Langevin-based methods, both classical and quantum to simulate such phenomenon.

The system is then composed by a 2D triangular lattice of 'heavy atoms', named in this way because their mass is many times heavier than the hydrogen atomic mass, which is $m_H = 1{,}00784u = 1836$ in atomic units ($a.u.$). We recall that atomic units means $\hbar = e = m_e = 1 = 4\pi\epsilon_0$. The two elementary direction's vectors are:

- $\vec{a}_1 = (1{,}0)a$;
- $\vec{a}_2 = (\frac{1}{2}, \frac{\sqrt{3}}{2})a$;

where a is the distance between two lattice atoms in $a.u.$. The two principal diagonals of the system are a linear combination of the elementary vectors:

- principal diagonal: $\vec{d}_1 = (\frac{\sqrt{3}}{2}, \frac{1}{2})a = \frac{1}{\sqrt{3}}(\vec{a}_1 + \vec{a}_2)$;
- normal diagonal: $\vec{d}_2 = (-\frac{1}{2}, \frac{\sqrt{3}}{2})a = (\vec{a}_2 - \vec{a}_1)$;

where all distances are in $a.u.$ We preferred a 2D version of the problem to better picture the system and have a better idea of the qualitative diffusion of the hydrogen. Moreover, the triangular shape is preferred to other geometries, such as a squared lattice, because we want to avoid instabilities with respect to shearing.

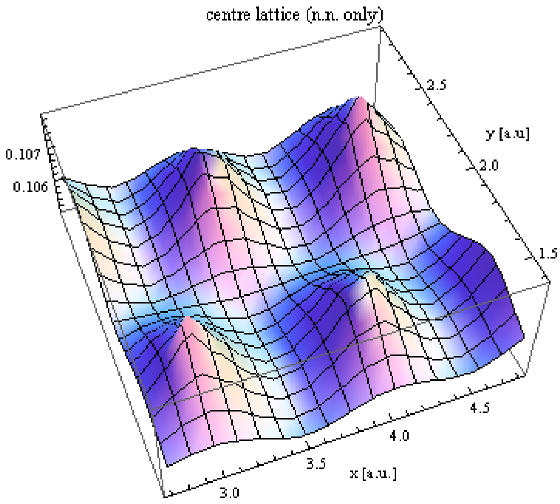

Figure 4.1: Model system: 3D representation of the elementary triangular lattice cell. On the z-axis the interaction potential U(r) between heavy atoms and the hydrogen (4.2) is shown in a.u.

A 3D representation of two nearest neighbours elementary lattice cells is shown in Figure 4.1. We can have then a qualitative picture of the interaction potential (4.2) seen by the hydrogen in its diffusion: the highest peak of the lattice are the heavy atoms of the lattice, whereas the hydrogen equilibrium position is likely to be the bottom of a potential well in the middle of a elementary triangular cell.

In Figure 4.2 the same potential is shown as a 2D map, on which the two main directions of the lattice $\vec{d}_1$ and $\vec{d}_2$ are drawn. The main feature of interest is at the center of this image, along direction $\vec{d}_1$: the saddle point between two elementary cell.

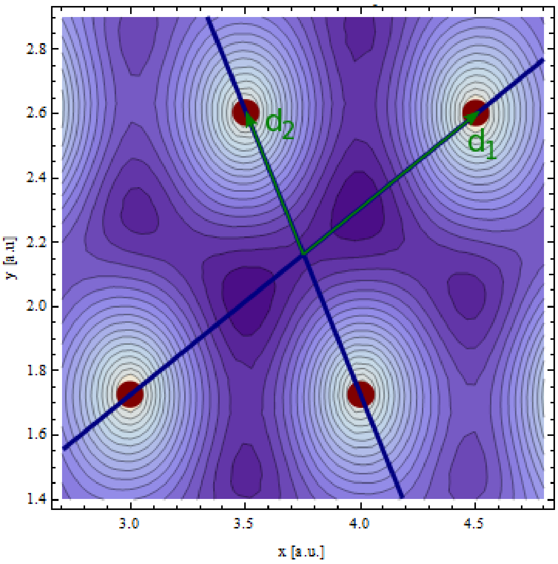

Figure 4.2: Model system: 2D map of the interaction potential U(r) (4.2) for two elementary triangular lattice cells, shown in a.u., with the main direction vectors $\vec{d}_1$ and $\vec{d}_2$.

It is worth noticing that the images show only a portion of the full system because periodic boundary conditions (PBC) are applied in order to recover the thermodynamic limit i.e. very large number of particles.

4.1.1 Interaction potential

The main computation effort of a MD simulation is usually the computation of the forces acting on each particle. We decided to use an empirical force field in order to have few parameters under control, which can be tuned to obtain the different conditions for the diffusion problem. In particular, the height of the potential barrier between two adjacent cell is the most important parameter of the system. Indeed, a very high barrier can suppress diffusion even up to the melting temperature, loosing any possibility of simulation of diffusion in a solid. On the other hand, a very low barrier allows a classical particle to hop between the cells even at low temperature, making it impossible to distinguish evident NQEs such as zero-point motion.

The interaction potential of the 'heavy atoms' between themselves is a Morse

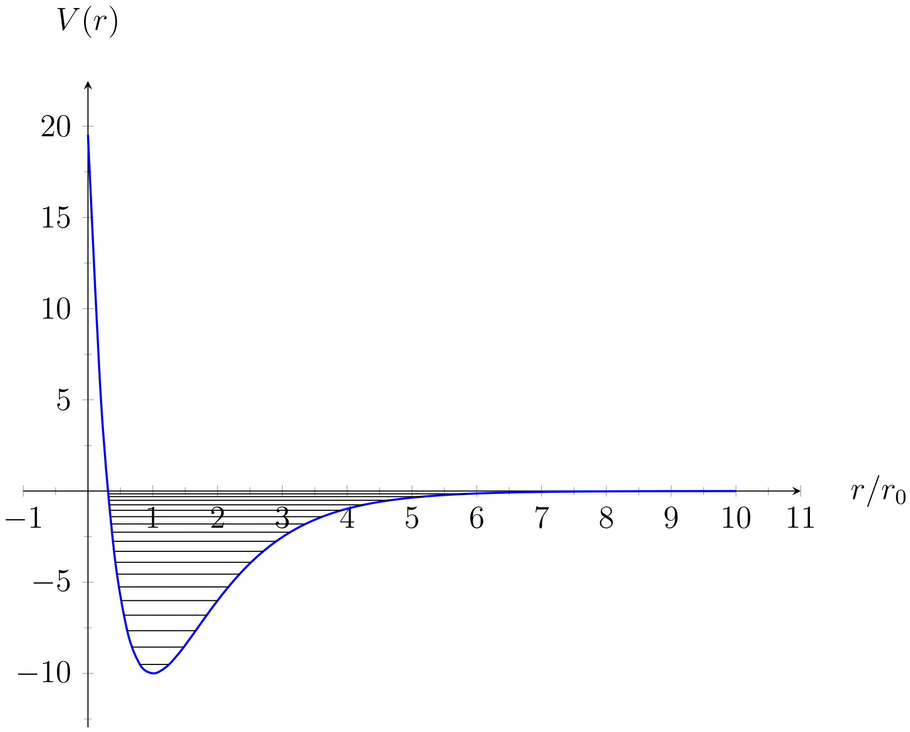

Figure 4.3: Example of Morse potential $V(r)$ (4.1)

potential [66] of the form

$$\boxed{V(r) = V_0 \left[\left(1 - e^{-\lambda (r-r_0)^2} \right) - 1 \right]} \tag{4.1}$$

where $r = |\vec{r}|$ is the distance between the heavy atom nuclei, r_0 is the equilibrium distance, V_0 is a parameter that gives the depth of the potential well and $\lambda = 1/\alpha$ set the width of the potential well.

Figure 4.3 provides a representation of the empirical potential that is felt by a hydrogen on the scale of the unit 2D cell of the system. In general, the full interaction potential depends on the positions of all the atoms in the system. Therefore, the calculation of the forces acting on an atom would include a sum over all neighbors, whatever the distance, which would diverge in the thermodynamic limit. Instead, we adopt a cutoff in the real space: for all neighbors with a distance bigger than the cutoff radius r_{cut}, their contribution is neglected. r_{cut} is chosen in such a way that the residual potential energy, would give a small contribution to the total energy: $\int_{r_{cut}}^{\infty} 4\pi \, r^2 \, dr \, |V(r)| \ll \int_0^{r_{cut}} 4\pi \, r^2 \, dr \, |V(r)|$.

The interaction potential between the heavy atoms and the hydrogen that we

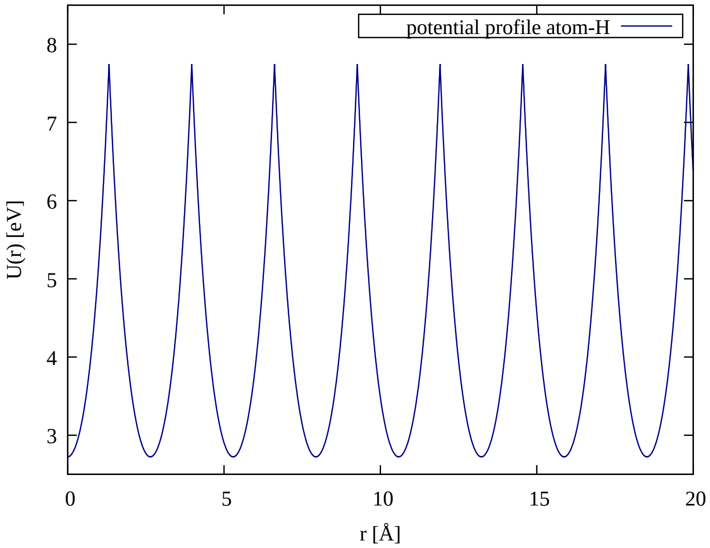

Figure 4.4: Model system: interaction potential $U(\vec{r})$ (4.2) between the hydrogen and the lattice along direction $\vec{d_2}$.

chose is simple repulsive potential

$$\boxed{U(r) = U_0 e^{-r/\alpha}} \tag{4.2}$$

where the parameters U_0 and α are chosen carefully, together with the parameters of the Morse potential, in order to obtain physically relevant properties, first of all to allow the diffusion and to avoid the melting of the lattice at room temperature. Furthermore, we are interested to create a system in which the hydrogen has higher typical frequencies than the vibration frequencies of the lattice, as is generally the case in actual materials. Once all parameters are fixed, we will vary only the masses of the heavy atoms, in order to understand the possible effects on hydrogen diffusion. Table 4.1 summarizes the values of the parameters used in our code.

In Table 4.2, we report also the main values of the physical units, derived from the use of $[a.u.]$

In Figure 4.4 the profile of the interaction potential between the hydrogen and the lattice is shown along $\vec{d_2}$, i.e. from one heavy atom to the next. This is also depicted in a different way by Figure 4.1 and 4.2. We can see that along d_2 there is quite a large barrier, of about $6eV$, in correspondence of the position of the heavy atoms of the lattice. This barrier is huge compared to the thermal energy at the ambient conditions, which amounts to about $25meV$. We can thus anticipate that hydrogen diffusion would be negligible in any direction that links two main heavy

Parameters	values $[a.u.]$
r_{cut}	25.0
r_0	5.0
V_0	0.05
α	1.0
U_0	0.25
λ	1.3

Table 4.1: Values of the parameters of the Morse potential (4.1) and the hydrogen-heavy atom interaction potential (4.2) used in the simulations.

Physical quantity	unit
distances	0.520Å
times	$2.41 \times 10^{-5} ps$
energies	$27.2 eV$
temperatures	$3.158 \times 10^5 K$

Table 4.2: Units of measured converted from the $[a.u.]$.

atoms, like $\vec{d_2}$.

This fact restricts drastically the possible direction of diffusion. Indeed, as shown in Figure 4.5 along direction given by the diagonal $\vec{d_1}$ i.e. from one minimum to the next, it is present the potential barrier - which become a saddle point in 3D space, as shown in Figure 4.2 - through which is most likely the hydrogen hops from one cell to another.

Note that the description of the hydrogen diffusion problem in terms of a 1D double-well allows to state the physical problem in very simple terms, but it has applications also in real systems. Indeed, in the Introduction, we explained briefly the quantum phase transition between ice phases VII and X, where the oxygen-oxygen distance was the order parameter [2]. Also in that system, using as main spatial coordinate the distance between two oxygen atom, a double-well potential was considered and the quantum dynamics of proton was studied.

4.1.2 Static estimation of the free energy barrier

Once all parameters of the interactions potentials (4.1) and (4.2) are fixed, it is possible to estimate the height of the potential barrier of the double-well shown in Figure 2.1. This will be useful later as a comparison with the dynamical measure of the diffusion coefficient and the assessment of the classical Langevin thermostat via the Arrhenius law (4.3), which is expected to hold for the simple system in the classical (high temperature) regime.

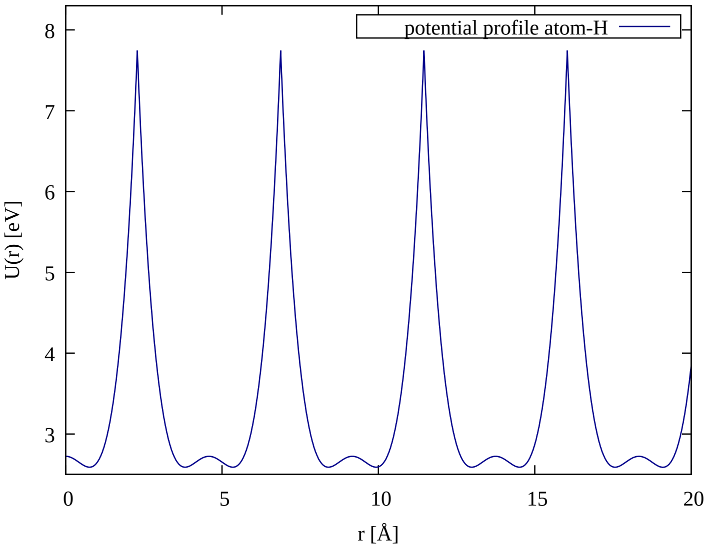

Figure 4.5: Model system: interaction potential $U(\vec{r})$ (4.2) between the hydrogen and the lattice along direction $\vec{d}_1$.

Figure 4.6 gives the static estimation of $\Delta U = 135meV$, which will be compared in the next section with the values of the free energy barrier ΔF extracted by the dynamical measure of the diffusion coefficient.

Finally, we show a simplified picture of the full system in Figure 4.7. This picture gives a qualitative idea of the classical dynamics of the system, integrated with the classical Langevin thermostat. In this specific case, we plot the positions that have been visited by the hydrogen along $10ps$ Langevin dynamics at ambient temperature $(300K)$. The heavy atoms are only represented at their equilibrium position.

Although the hydrogen spends much of the simulation time around the equilibrium position, it is clear that, at room temperature, the hydrogen atom has enough thermal energy to hop from the equilibrium position of a cell to another through the saddle point. When the temperature decreases, the hopping becomes a rare event and requires longer simulations to be studied.

4.2 Classical results

In this Section, we present the results of the classical Langevin simulation, emphasizing some important points:

- the influence of the friction coefficient on the computed diffusion coefficients as shown in Section 3.2, the presence of a thermostat (in our case, the Langevin

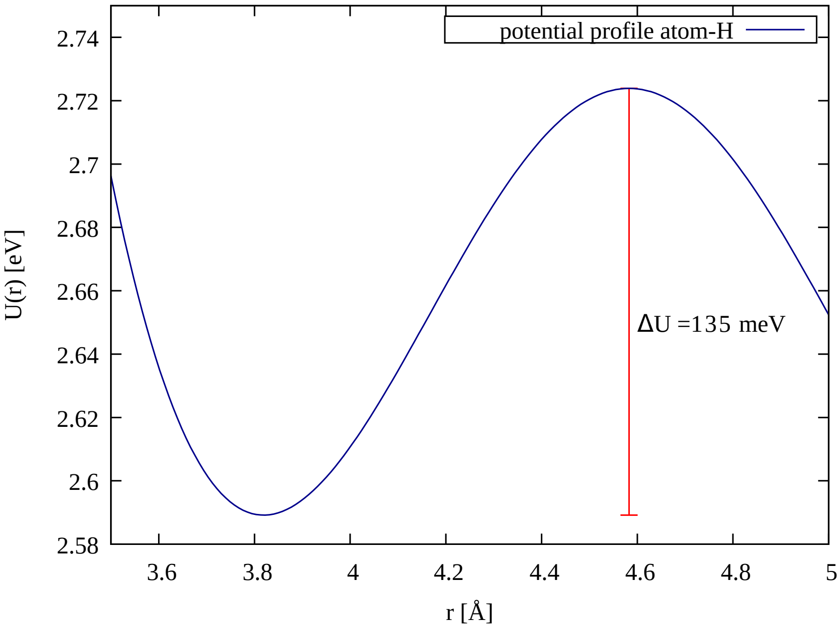

Figure 4.6: Model system: static estimation of the potential barrier (zoom from Figure 4.5).

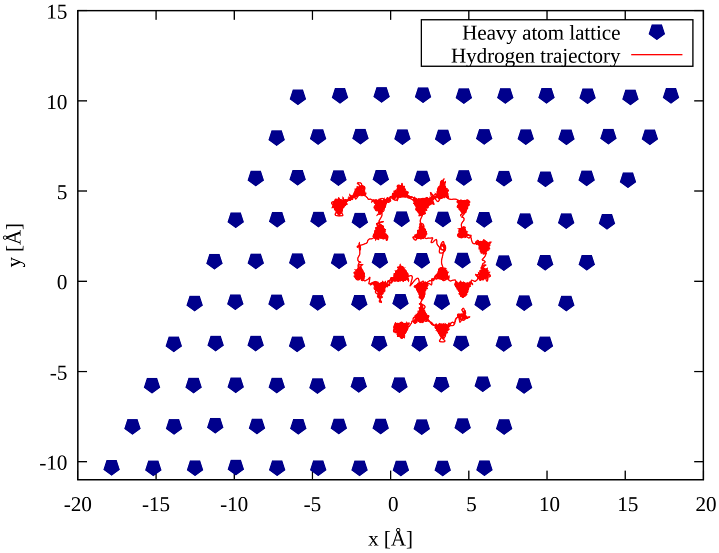

Figure 4.7: Model system: 'heavy atoms' lattice (blue points in their equilibrium positions) with a single hydrogen atom diffusing, for $t = 10ps$ and a $T = 300K$ (red trajectory)

thermostat) can influence the results obtained for dynamical observables such as time-correlation functions (TCFs) and diffusion rates. It is therefore important to ensure that, for the Langevin's parameters that we use in this study, the diffusion coefficient is not strongly altered with respect to the one that would be obtained from non-thermostated (NVE) simulations;

- the diffusion of light particles can in some systems be activated by the motion of the heavier particles. In this case, one speaks of Phonon-Assisted Hopping (PAH) [**...**]. We will assess the importance of this effect by studying the influence of the heavy atom mass on the hydrogen diffusion.

Therefore, for all results, we consider three different types of lattice:

- oxygen lattice: $m_O = 29376 a.u. = 16 m_H$. We expect the spectra of the hydrogen and the oxygen lattice to be so close that the specific modes of the two elements cannot be decoupled, and correlations will play a role in the dynamics;
- niobium (Nb) lattice: $m_{Nb} = 150552 a.u. = 82 m_H$. We chose this element in order to have an intermediate situation between the two extremes of oxygen and lead;
- lead (Pb) lattice: $m_{Pb} = 301104 a.u. = 164 m_H$. The difference of masses is huge, so we expect the spectrum of the hydrogen to be very well separated from the one of the Pb lattice. Therefore we assume that is possible to decouple the two elements and observe their quasi-pure spectral modes.

In the following spectral analysis, the importance of using different masses is explained.

4.2.1 Classical spectral analysis

The first main goal of the analysis of the performance of classical Langevin thermostat is the evaluation of the effect of the mass and the friction γ on the dynamical properties of the system. In order to accomplish the first goal, the vibration spectra of the lattice and the hydrogen are computed after the integration of the equations of motions, by saving the velocities and the random forces on the fly along the trajectory. All spectra are then averaged over many trajectories: $\mathcal{O}(10^2)$. The spectral analysis gives important insight on the physical properties of the system and it is of crucial importance for the implementation and evaluation of the quantum Langevin-based MD techniques.

The spectra are obtained from the computation of the TCFs C_{vv} (3.26) and C_{vR} with the Fast Fourier method (3.25). We spend few words about the computation.

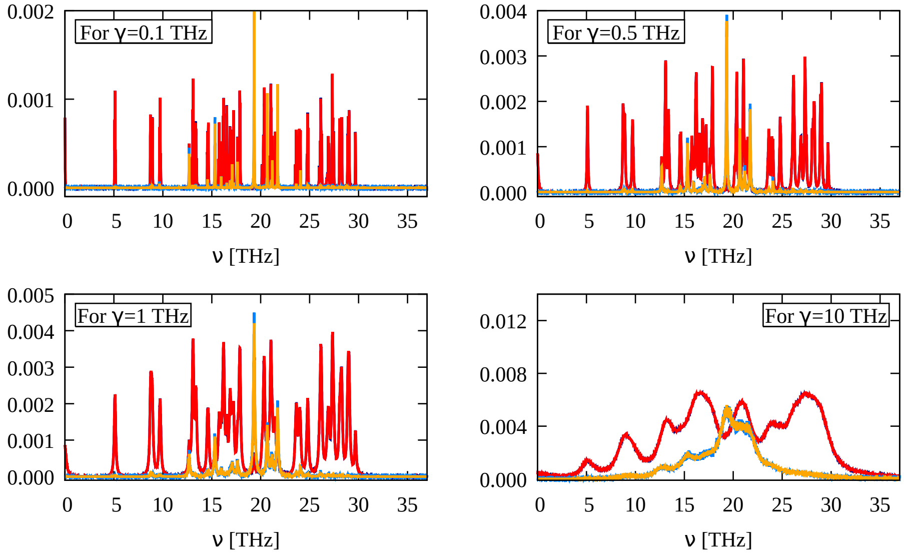

Figure 4.8: Spectra of oxygen lattice (darker colours) and hydrogen (lighter colours) for different values of γ at $T = 16K$.

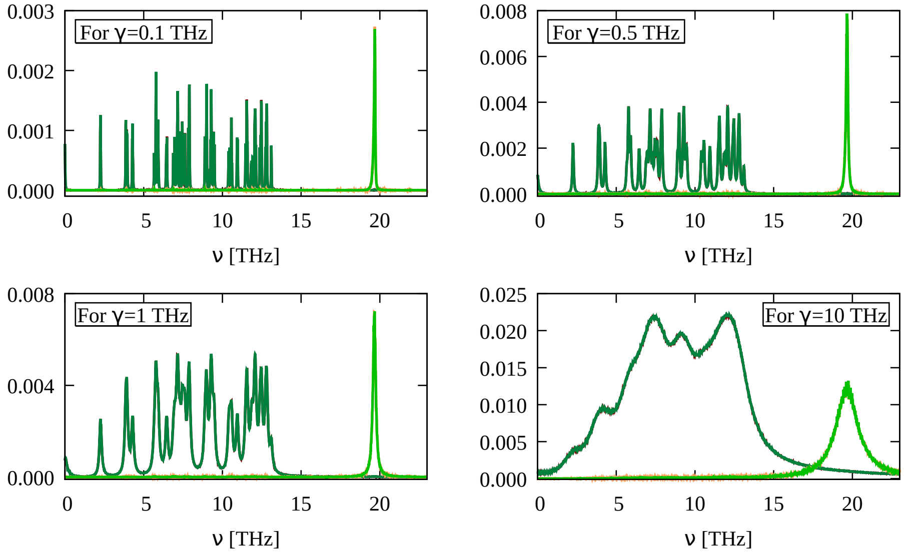

Figure 4.9: Spectra of Nb lattice (darker colours) and hydrogen (lighter colours) for different values of γ at $T = 16K$

During each integration step, the $v(\Delta t)$ and the forces $R(\Delta t)$ are saved for each atom of the system. Then, the two correlation functions are computed for both the hydrogen atom and the lattice atoms, using their velocities $v(t)$ and random force $R(t)$ respectively (the formulas are reported in 1D but in the simulation two dimensional quantities are computed). For example, for the hydrogen atom, referring to formula (3.28), we have

$$C^H_{vv}(n\Delta t) = \frac{1}{N_{steps}} \sum_{k=0}^{N_{steps}-1} |\hat{v}_H(k\Delta\omega)|^2 e^{\imath k\Delta\omega n}$$

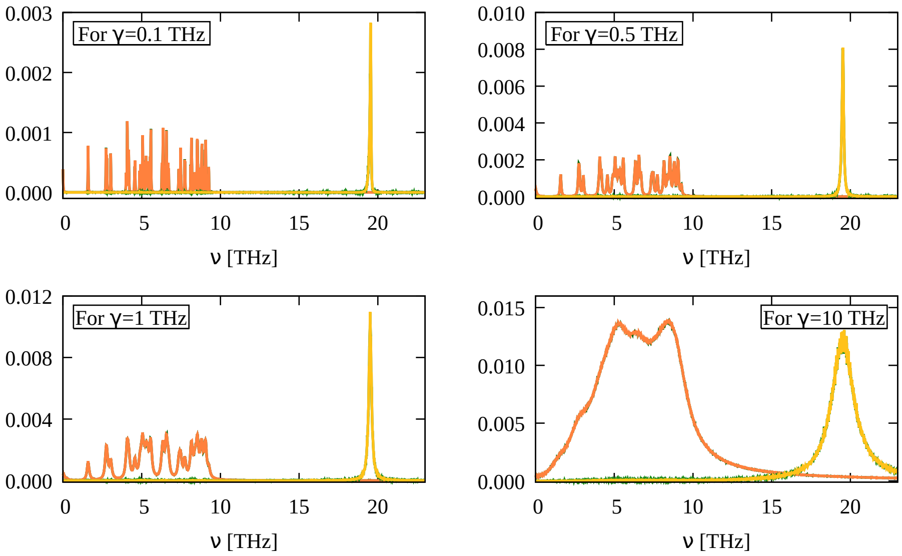

Figure 4.10: Spectra of Pb lattice (darker colours) and hydrogen (lighter colours) for different values of γ at $T = 16K$

The same computation is done for the atoms of the lattice. Notice that the lattice spectra are obtained by averaging on the number of particles of the lattice, in order to reduce the noise. Moreover, we consider a very low temperature ($T = 16K$). Indeed, at this low temperature, the vibrations are essentially harmonic whereas anharmonicity becomes more apparent at higher temperatures and causes a broadening of the spectral peaks.

Figures 4.8, 4.9 and 4.10 shows the spectra obtained from the C_{vv} and C_{vR} using the classical Langevin thermostat. The difference between the two TCFs will be analyzed later and it will be of fundamental importance for QTB and adQTB methods, as explained in Sections 3.4 and 3.5. We use the following colours convention:

- darker colours for lattice spectra;
- lighter colours for hydrogen spectra.

We use also three different chromatic scales for the three different lattice types, to facilitate the confront between different methods.

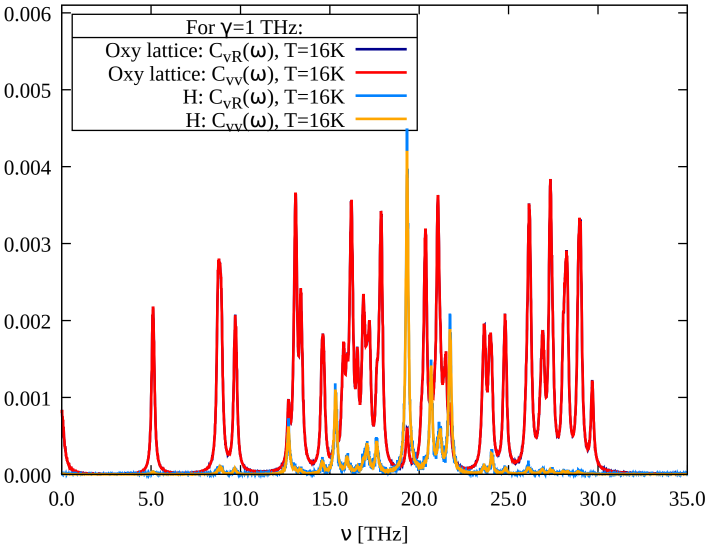

Figure 4.11: Spectra of oxygen lattice (darker colours) and hydrogen (lighter colours) at $T = 16K$, for $\gamma = 1THz$. No separation between the two elements' spectra.

The first thing we can deduce by the spectra in Figure 4.8, 4.9 and 4.10, is the effect of the damping term. Clearly, for values of γ of the same order of the typical frequencies of the system, the spectra are significantly broadened. Indeed, as explained in Section 3.2, higher values of the friction have stronger effect on the dynamics. The ideal classical limit can be found for $\gamma \to 0$, when we recover exactly Hamilton's equations. Later in this Section we analyze the dependence of the diffusion rate on the friction coefficient γ. This is the main effect of the friction on classical Langevin thermostat.

We note that, for very small values of γ, the thermalization time increases and longer simulations are needed before it is possible to compute physical properties safely. A way to understand how much time is required for the system to thermalize is computing on the fly the kinetic energy of the system. Once it reaches an average value given by the Equipartition theorem 3.2.1, i.e. $\langle K \rangle \simeq Nk_BT$, where N is the number of particles, then it means the Canonical distribution is reached thanks to the action of Langevin thermostat. Although a thermalization period is always necessary, a simple trick to reduce its time is to use a larger value of γ at the beginning of the simulation and after the system is thermalized, decrease the value of γ to have a gentle effect of the damping term on the dynamics.

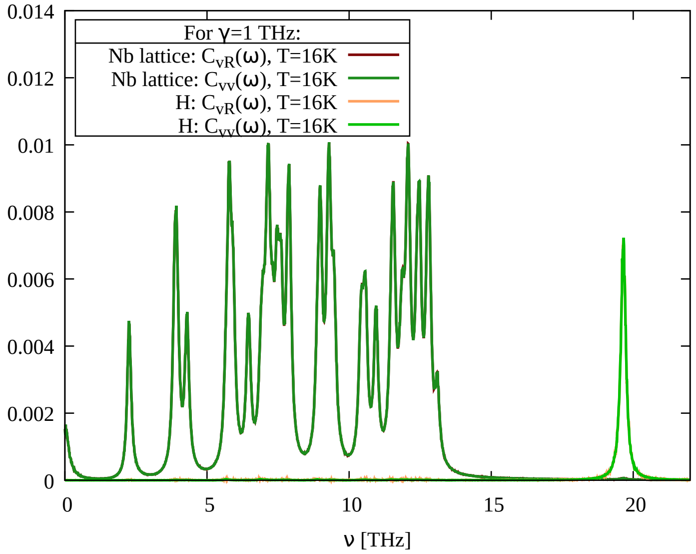

Figure 4.12: Spectra of Nb lattice (darker colours) and hydrogen (lighter colours) at $T = 16K$, for $\gamma = 1THz$. The two spectra are mostly well separated.

4.2.2 Coupling of spectra

From Figures 4.8, 4.9 and 4.10 it is also possible to see clearly how the spectrum of the hydrogen can be superposed to the spectrum of the lattice, depending on the mass of the different elements. Before considering the three cases more in details, we make the following clarification: the distinction between the hydrogen and the lattice spectra is due to the fact we are computing the TCFs for the two different degrees of freedom. The system has a unique coupled spectrum and this coupling can be more or less pronounced according to the mass of the lattice.

In Figure 4.11, the spectra are clearly on top of the other, which means that we cannot decorrelate the modes of the two elements and we expect the coupling have stronger anharmonic effects.

In Figure 4.12, the two spectra are better separated, but still a small coupling for the high frequencies of the lattice is present.

Finally, in Figure 4.13, the modes are well separated due to the huge difference between the masses. In this case, we can approximately distinguish between hydrogen and lattice modes.

To conclude, let us consider also the following Figure 4.14 and 4.15 for the Nb lattice. Together with the spectrum, also the difference Δ_{FDT} between the C_{vv} and C_{vR} is shown, with reference to Formula (3.46).

It is clear that the difference is extremely small and it is appreciable only in the case of the hydrogen 4.15. However, it does not show a clear trend (as the

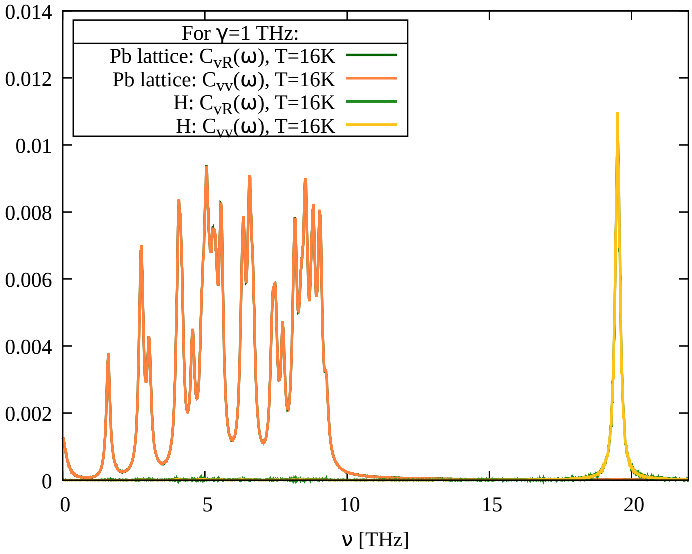

Figure 4.13: Spectra of Pb lattice (darker colours) and hydrogen (lighter colours) at $T = 16K$, for $\gamma = 1THz$. Full separation of the two elements' spectra.

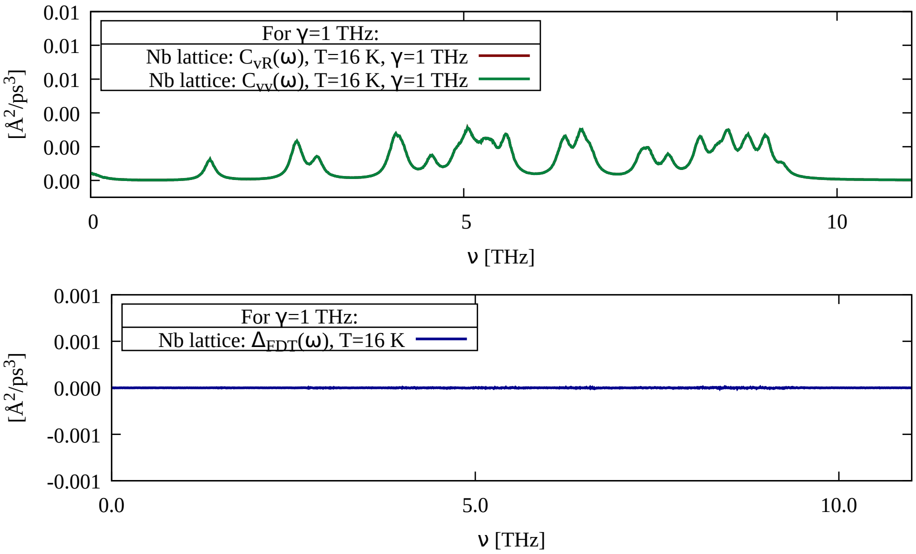

Figure 4.14: Spectra of Nb lattice and difference between the two TCFs

one expected from the ZPEL described in Section 4.3 below) and it disappears when a larger statistic is considered, as in 4.14, where the spectra is obtained also averaging on the number of particles of the lattice. This is perfectly expected, because, in the classical Langevin thermostat, the (classical) fluctuation-dissipation

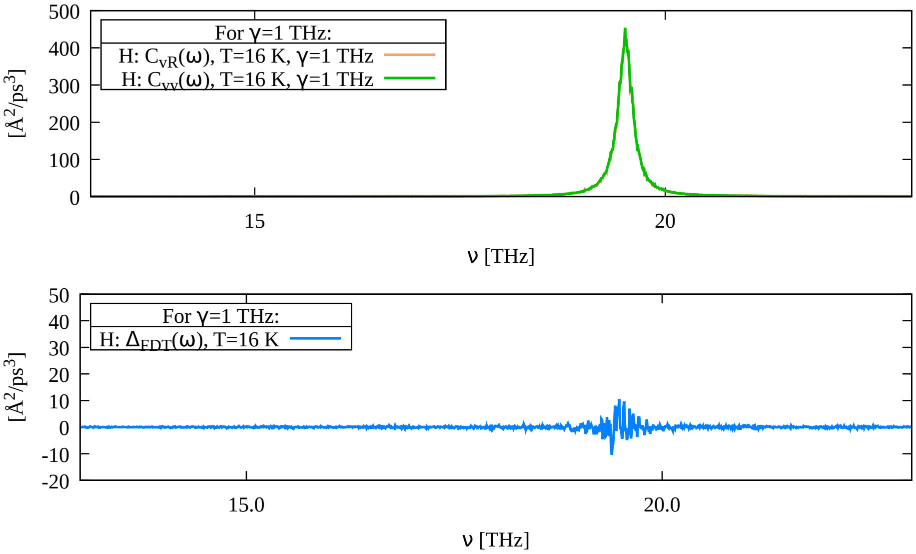

Figure 4.15: Spectra of hydrogen in the case of Nb lattice and difference between the two TCFs

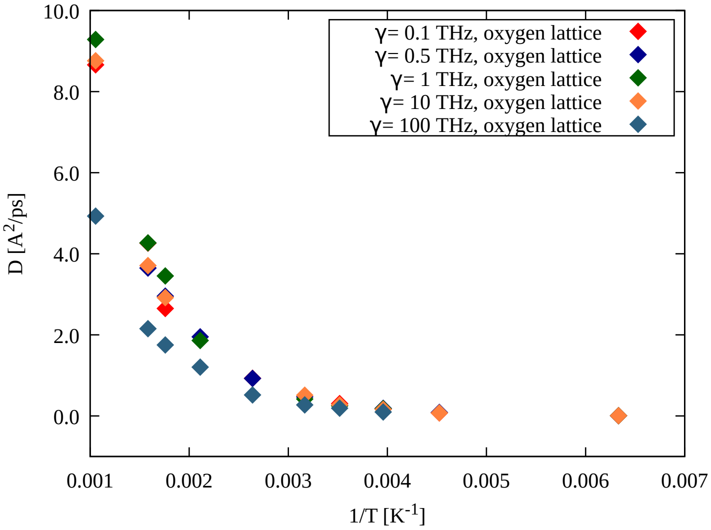

Figure 4.16: Oxygen lattice: Diffusion coefficient as a function of the inverse temperature for different values of γ.

theorem is naturally enforced so that the two spectra are always superimposed.

4.2.3 Diffusion coefficient

The diffusion coefficient is computed in two main ways:

- as the direct evaluation of the mean squared displacement, following Einstein's formula (2.3). Even if this is not an efficient way, the system is simple enough to use this direct method and it allows to have a rough estimation of the diffusion constant D_x;
- with the use of the velocity time autocorrelation function (2.36). This is a much more efficient way to compute the diffusion coefficient and it has a direct link with the spectral analysis explained in previous Section. Indeed, the long time limit of formula (2.36) can also be seen as

  $$D_x = \lim_{\omega \to 0} C_{vv}(\omega)$$

  In this way, from the values of $C_{vv}(0)$ obtained in the spectra, it also possible to compute the main dynamical coefficient of diffusion.

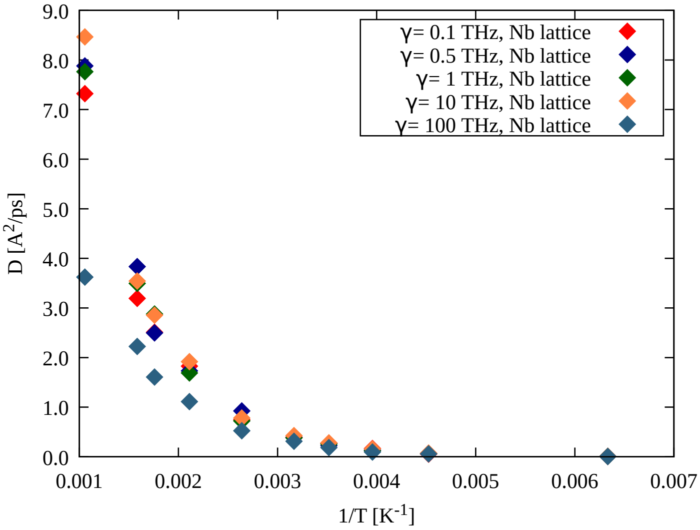

Figure 4.17: Nb lattice: Diffusion coefficient as a function of the inverse temperature for different values of γ.

Figure 4.16, 4.17 and 4.18 report the diffusion constant D_x as a function of the inverse temperature $\frac{1}{T}$. At low temperature, diffusion is suppressed because hydrogen does not posses enough energy to overcome the free energy barrier 4.6 and to hop between to adjacent cells. Therefore, the hydrogen atom remains confined inside the elementary cell where it was originally placed and even for simulation of $\mathcal{O}(10^2)ps$, no or very few hopping are observed. Hence, diffusion coefficient values are saturating to zero for $T \to 0$, as expected in a classical system where no zero-point energy is present. We will see how this result remarkably changes in Section 4.3, when the quantum nature of the nuclei is implemented by QTB.

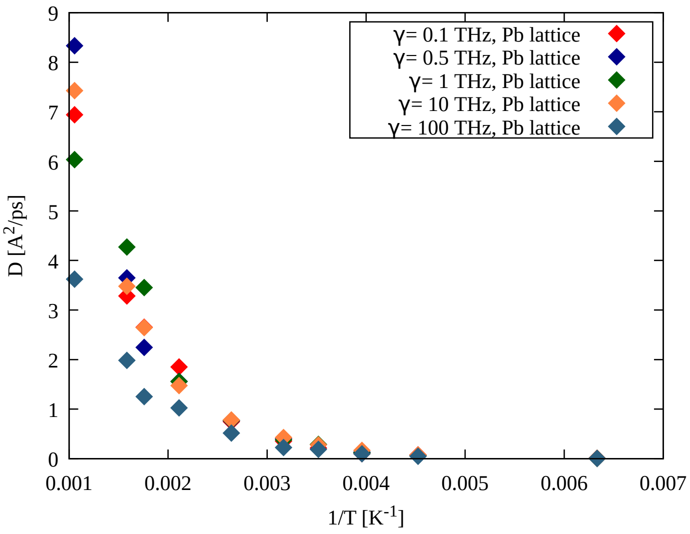

Figure 4.18: Pb lattice: Diffusion coefficient as a function of the inverse temperature for different values of γ.

As temperature increases, diffusion starts to appear but is still rare and requires long simulation to be studied. Here, the hydrogen spends most of its movement oscillating around the equilibrium position. Finally, on the opposite side of the graph, in the highest temperature's regime, hydrogen can easily diffuse due to the fact that it has higher thermal energy than the potential barrier 4.6. This is the regime depicted in Figure 4.7 and it remains unchanged until temperature is so high that the lattice melts. At that point, after a brief transition period in which it moves near the melted lattice, hydrogen behaves as a free particle, due to the cutoff r_{cut}.

4.2.4 Arrhenius law

In Figure 4.19, 4.20 and 4.21 the relation between the diffusion coefficient and the inverse of the temperature is shown in logaritmic scale. Those graphs allow to obtain a rough estimate of the influence of the friction coefficient γ on the diffusion.

This is the usual way to report these data in a chemical contest, when transition rates are studied. We recall the Arrhenius law (2.56) for a 1D diffusion process in a double-well potential of the form of 2.1:

$$\boxed{D \propto e^{-\Delta F/k_B T}} \tag{4.3}$$

where ΔF is in general the free energy barrier between the equilibrium state at the bottom of the well and the saddle point (saddle point in 3D space). We used a linear function with two parameters: $f(x) = ax + b$ to fit the data of D_x vs $1/T$. From the values of the parameter a, it is possible to find the free energy barrier ΔF. The values of the diffusion coefficients are reported in Table 4.3.

Free-energy barrier			
γ [THz]	ΔF Oxy lattice [eV]	ΔF Nb lattice [eV]	ΔF Pb lattice [eV]
0.1	115	111	113
0.5	111	115	116
1.0	118	111	116
10.0	114	113	110
100.0	114	107	109

Table 4.3: Classical values of the free energy barrier obtained from the dynamic measure of D, using the Arrhenius law

Now, we can compare the dynamical measure of the height of the barrier with the static estimation, which is $\Delta U = 135meV$. In general, the dynamical values are all lower than the static estimation. In Section 4.2.6 we explain the possible physical explanation to this result.

4.2.5 The role of the friction

Once the integration time-step is chosen as $\Delta t < 1/\nu_{max}$, only the friction γ remains as a main free parameter of the Langevin thermostat that needs to be chosen carefully. Indeed, it must be small enough to limit the thermostat effect on the dynamics and not to fall into the overdamped regime given by equation (2.29), but also large enough not to have to wait a long time before the convergence to the equilibrium Boltzmann's distribution. We have also discussed previously the role of the damping term in the broadening of the spectra.

Furthermore, dynamical observables can be functions of γ. In Figure 4.19, 4.20 and 4.21, classical Arrhenius law is shown for different values of the friction γ. This allows to show the dependence $D(\gamma)$ and select a 'safe' windows of values of γ such that the dynamical properties are not much affected by the choice of this parameter.

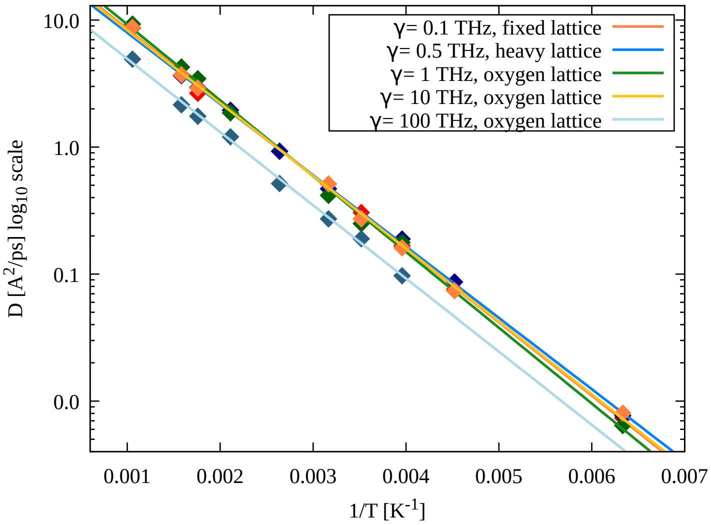

Figure 4.19: Oxygen lattice case: Arrhenius plot of the hydrogen diffusion coefficient for different values of γ.

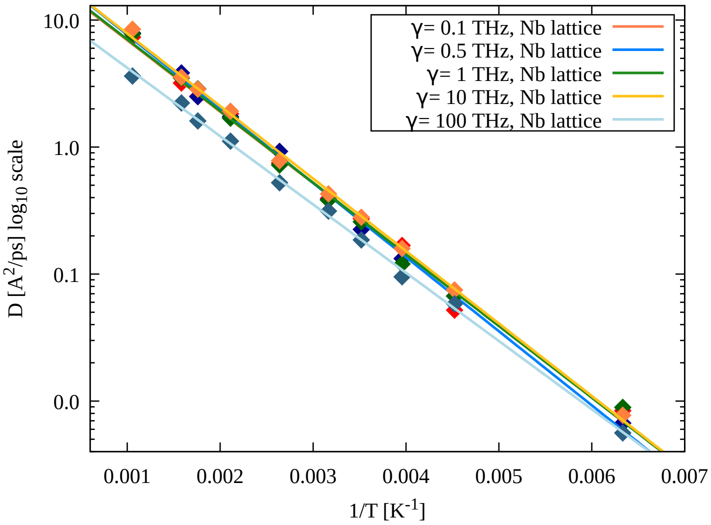

Figure 4.20: Nb lattice case: Arrhenius plot of the hydrogen diffusion coefficient for different values of γ.

It is clear that when $\gamma = 100THz$, much larger than the highest frequency of the system - typically the hydrogen frequency - the system is in the overdamped regime and diffusion is strongly hindered. However, for all the other values of gamma used in this study, the values obtained for D are equivalent within the statistical error,

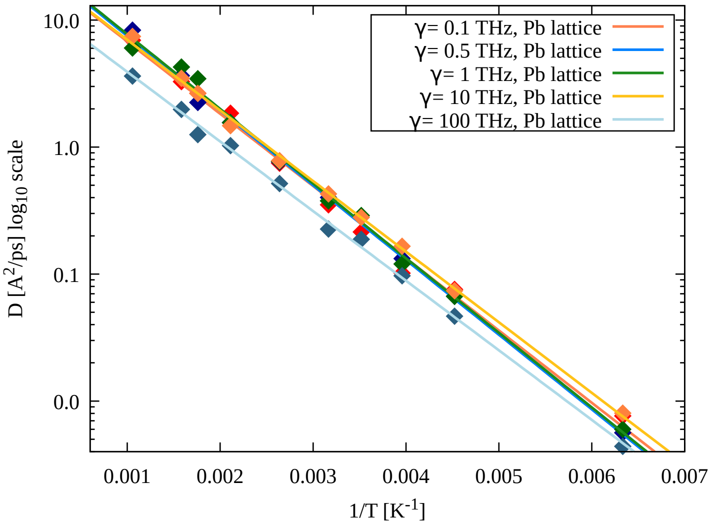

Figure 4.21: Pb lattice case: Arrhenius plot of the hydrogen diffusion coefficient for different values of γ.

which seems to indicate that γ has little impact on the diffusion (at least up to 10THz).

4.2.6 Phonon assisted hopping

In condensed matter, atoms vibrate around their equilibrium positions at much lower temperatures than the melting temperature. In the classical picture , vibrations are due to thermal excitations. The simplest way to model this phenomenon is to consider a lattice as a chain of springs. Their motion can be studied via the Fourier analysis, which allows to study the modes distribution. Therefore, it is possible to describe this phenomenon with a discretized description, introducing the quasi-particles called phonons with energy modes given by the vibrations of the lattice.

In our system, phonons can have a impact on the diffusion coefficient. In particular, we are interested in the coupling of the hydrogen atom hopping with lattice vibrations of the heavier atoms. Indeed, the vibration of the lattice can modify the potential barrier - which now is a function of time - and allow the hydrogen to hop easily from one cell to the other. The variation of the potential will lead to a modification of the free energy barrier ΔF, which is part of the Eyring-Polanyi law (2.56), here applied to diffusion. This effect is called **Phonon assisted hopping** (PAH). We notice that we expect the presence of phonons will enhance the diffusion because even a small modification of the potential barrier leads to a exponential change in the probability factor in Arrhenius law (4.3).

In order to probe the presence of the PAH, we consider other two other 'types' of lattice:

- 'heavy' lattice, with a mass 10 times heavier than the mass of lead atom;
- 'fixed' lattice: all atoms of the lattice are fixed in their equilibrium positions and they cannot move, removing, in theory, completely the effect of PAH.

What we observe in Figure 4.22 is that the values of the diffusion coefficient in the fixed lattice are significantly lower with respect to the other lattices in which phonons are present. Thus, we have a direct observation of the PAH in our system, which can enhance the diffusion of the hydrogen. We highlight that it is extremely interesting that even in our simple model for diffusion such complex physical properties can be observed and characterized at least qualitatively.

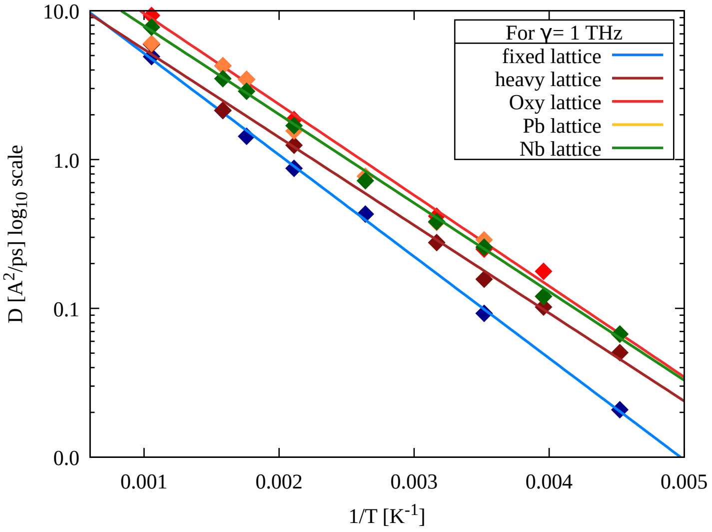

Figure 4.22: Phonons assisted hopping for $\gamma = 1THz$

Another important feature of the model can be derived from the study of PAH. In Tables 4.4 the values of the free-energy barrier - computed from the dynamical measure of the diffusion coefficient - are compared.

In particular, we observe that the values of the energy barrier in the case of the fixed lattice are higher than the dynamical values obtained with a moving lattice. Moreover, as expected, we have an agreement on the dynamical measure of free-energy barrier, which is now a pure potential energy, with the static estimation presented in Section 4.1.2. Both measures give an average $\Delta U = 135meV$. Therefore, we have the direct observation of how the change from a static to a

Phonon assisted hopping					
γ [THz]	ΔF fixed lattice [eV]	ΔF 'heavy' lattice[eV]	ΔF Oxy lattice [eV]	ΔF Nb lattice [eV]	ΔF Pb lattice [eV]
0.1	135	117	115	111	113
0.5	147	111	111	115	116
1.0	135	117	118	111	116

Table 4.4: Classical values of the free energy barrier obtained from the dynamic measure of D, using the Arrhenius law, with the intent of highlight PAH, with $\gamma = 1THz$

moving lattice changes the nature of the activation energy (2.55) to a free-energy barrier, as stated by the Eyring-Polanyi law (2.56), explained in Section 2.6.

On the other hand, when the lattice is not static, we observe very small changes in the diffusive behaviour (see Figure 4.22) and no significantly changes in the free energy barrier values. This was expected, as already explained in Section 2.6. Indeed, according to Eyring-Polanyi law, the slope of the plot ΔF which is independent on the atomic masses (it is by definition a static quantity, that can be computed from the Boltzmann probability density, and which therefore depends on the form of the potential only and not on the mass). On the other hand, the prefactor in front of the exponential in the Eyring-Polanyi law depends on the heavy atom mass and light atoms seem to favor diffusion, which is a further indication of the importance of the coupling between the hydrogen and the lattice dynamics, i.e. PAH, in this system.

4.3 Quantum Thermal Bath results

In this Section, we present the results obtained with the QTB method discussed in Section 3.4. In particular, the aim is to obtain the measurements of quantum diffusion coefficients, in order to compare them with the classical results and have a qualitative but direct observation of the NQEs. In our system, two types of NQEs can impact the diffusion coefficient: zero-point motion - which we expect to be well captured by QTB, at least in its adaptive version -, and tunnelling - which we do not expect to be determinant in this case but if present - it is not captured by QTB (only RPMD or other more sophisticated methods could give us an indication).

Moreover, we want to observe and characterize the Zero-Point Energy Leakage, described in Section 3.4.3, through the quantitative measure of the difference $\Delta_{FDT}(\omega)$ (3.46) between the injected power and the dissipated power. We then implement the Adaptive QTB (see. Section 3.5 for the theoretical discussion and Section 4.4 for the adQTB results).

In Table 4.5 we report the main parameters used for the QTB simulations

Parameters	values $[a.u.]$
ω_{cut}	0.007
ω_{smear}	0.0006
N_{seg}	20
t	10^6

Table 4.5: Values of the parameters for the QTB used in the simulations.

4.3.1 Quantum spectra

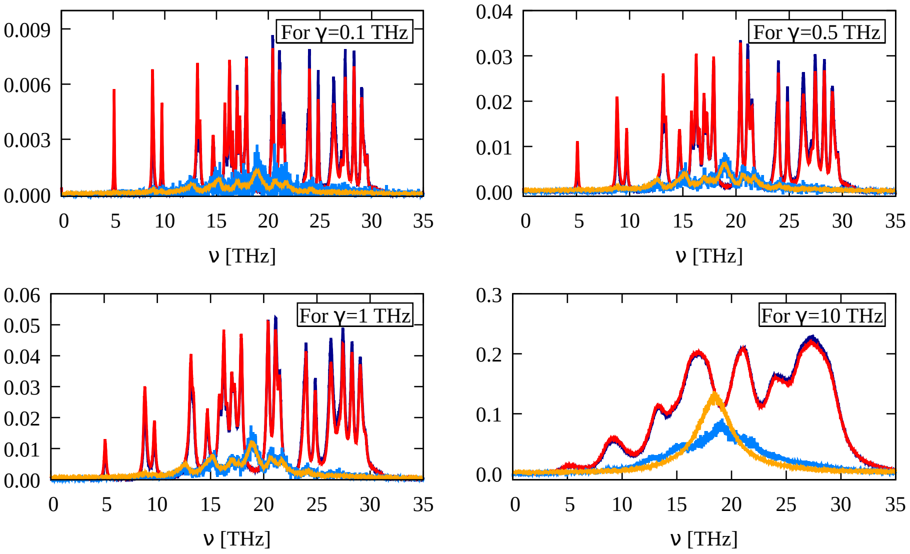

Figure 4.23: QTB spectra of Oxy lattice (darker colours) and hydrogen (lighter colours) for different values of γ

Using the QTB method, we have studied three main cases of different masses: oxygen, naiobium and lead. This is done because it is crucial to see whether, in the quantum case, the zero-point energy leakage, that is, the irreversible transfer from high-frequency to low-energy modes, occurs and quantify it. We compute the spectra for the different lattices and different values of γ. The spectra of the hydrogen into a oxygen, Nb and Pb lattice respectively. Both C_{vv} and C_{vR} functions are shown, with the same colours convention as before, to help the confront. We consider very low temperature - $T = 16K$ - as in the classical case (see Section 4.2).

The spectra of oxygen, Nb and Pb lattices, and the corresponding hydrogen results are reported in Figure 4.23, 4.24 and 4.25. The effect of the damping term is once again clearly evident, making the broadening of the spectra more pronounced

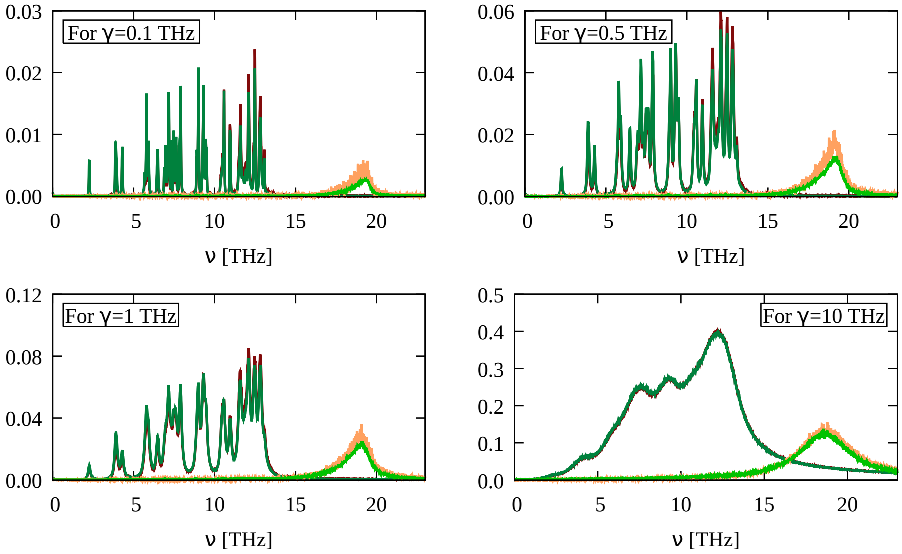

Figure 4.24: QTB spectra of Nb lattice (darker colours) and hydrogen (lighter colours) for different values of γ

as the γ increases. This means that, even in a simple system, the idea of increasing the coupling strength γ between the the quantum bath and the equations of motion, as explained in Section 3.4.3, must be considered with particular care. We notice also that the broadening of the spectra is more pronounced than the respective classical cases, even for small values of γ. This is a first remarkable hint of the presence of the zero-point energy of the proton.

In these pictures we are not focusing on the difference between C_{vv} and C_{vR}. However, it is already possible to see the effect of the ZPEL, explained in Section 3.4.3, in particular in the hydrogen spectra, due to larger fluctuations. Let us consider the Nb as main example to highlight this important effect which is remarkably well depicted even by the simple model of diffusion we are considering.

4.3.2 Zero-Point Energy Lekeage

Let us now concentrate on the ZPEL with more attention. We consider the case of Nb as main illustrative example.

For the lattice spectra of Figure 4.27, it is possible to see that the C_{vR} is lower than C_{vv} at low frequencies and becomes grater than C_{vv} at higher frequency. In order to show the net effect of ZPEL, for both the hydrogen and the Nb lattice the difference Δ_{FDT} (3.46) is plotted in Figure 4.27 and 4.29. Here, the ZPEL trend is clearly apparent.

Let us consider the case of the Nb lattice spectra in Figure 4.27. At low

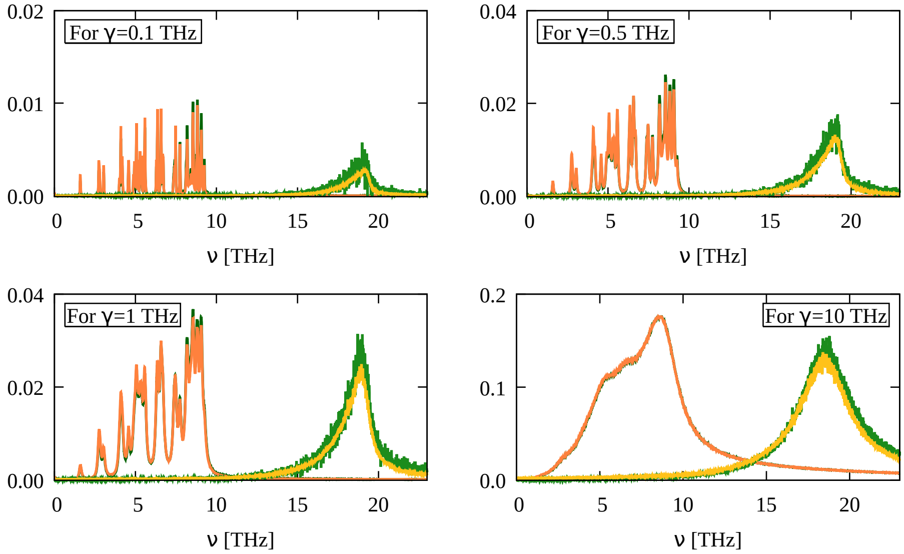

Figure 4.25: QTB spectra of Pb lattice (darker colours) and hydrogen (lighter colours) for different values of γ

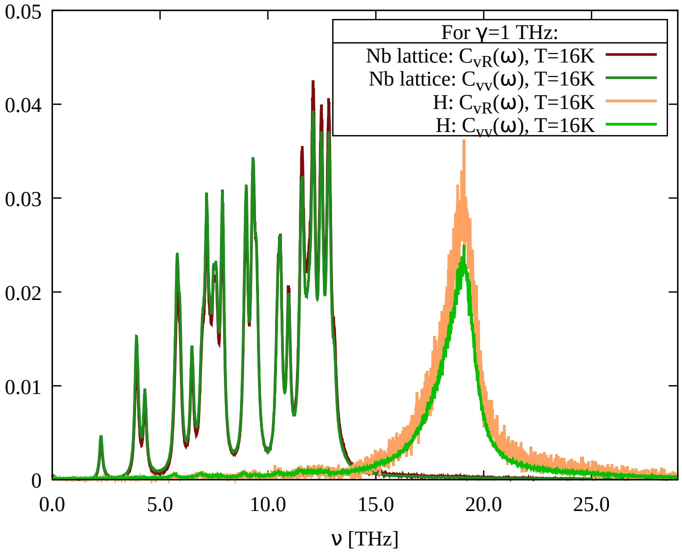

Figure 4.26: Comparison of the spectra of the hydrogen (lighter colours) in the Nb lattice (darker colours) (in arbitrary units). Clear sight on the difference between the C_{vv} and the C_{vR} spectra, which is the sign of the ZPEL (see Section 3.4.3)

frequency, the difference $\Delta_{FDT} = \Re\left[C_{vR}\right] - m\gamma C_{vv}$ (3.46) is negative. This means that the spectral power dissipated by the frictional force is greater than the spectral

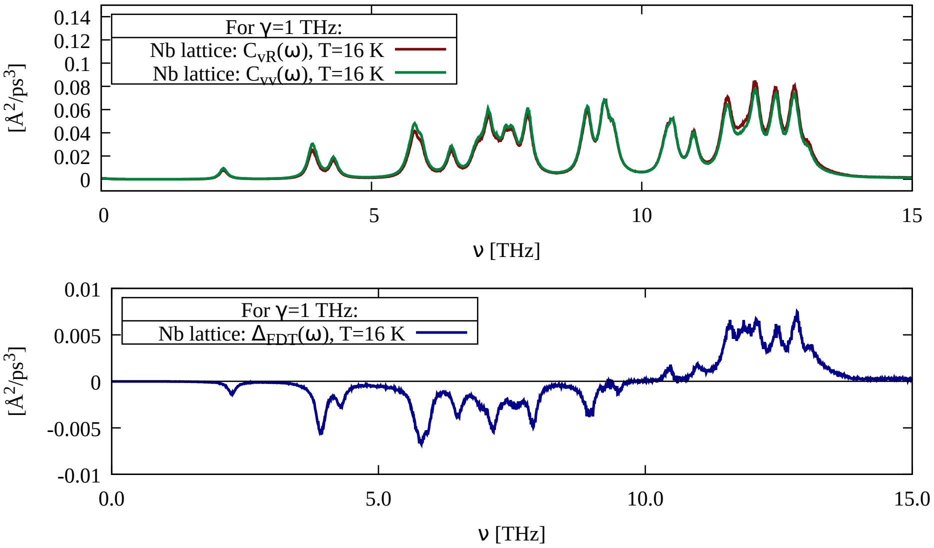

Figure 4.27: Spectra of the Nb lattice and the corresponding difference between C_{vv} and C_{vR}

power pumped to the system via the random force. On the other hand, at high-frequencies, the spectral dissipated power is lower than the spectral power injected by the quantum bath. This reveals the presence of an energy leakage from the high-frequency modes to the low-frequency modes.

4.3.3 Effect of γ on the leakage

Another important result that we can deduce from the spectral analysis is the dependence of the ZPEL on the parameter γ, which is the strength of the coupling between the system and the bath. Let us consider once again the Nb spectra reported in Figure 4.24. We observe that the leakage seems less pronounced, especially on the spectra of lattice, as γ increases. In Figure 4.28 we show then the difference $\Delta_{FDT}(\omega)$ for different values of γ in the case of the niobium lattice.

It is clear that the difference $\Delta_{FDT}(\omega)$ constant with γ, compared to the values of the spectra in Figure 4.24, which increases of one order of magnitude with γ. This is a remarkable result because it is in perfect accordance with what we expected from [45]. Indeed, we proved that the ZPEL is reduced with by increasing the strength of the coupling with the quantum bath i.e. by forcing the system to have the quantum energy distribution (3.37), as explained in Section 3.4.

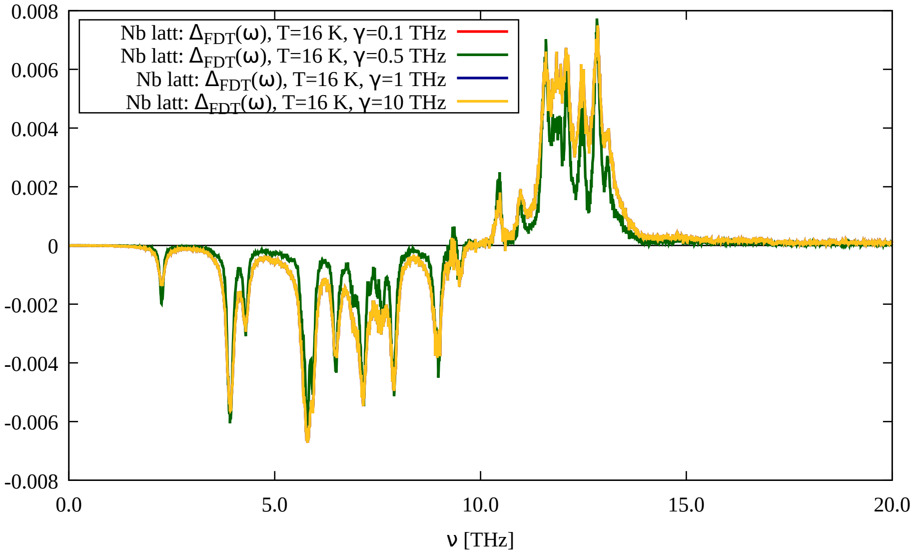

Figure 4.28: Difference between C_{vv} and C_{vR} for the Nb lattice spectra (see Figure 4.37) for different values of γ.

4.3.4 Couplings of modes

Of even more relevance to the problem of diffusion is the ZPEL observed from the hydrogen spectra. Let us consider fist the case of the Nb lattice: the hydrogen spectra and the difference Δ_{FDT} are shown in Figure 4.29. Here, Δ_{FDT} is positive for most of the frequencies, which means that the hydrogen mostly looses energy to the lattice. The same is true for the lead case, shown in Figure 4.30, in which again the two parts of the spectra are well separated.

In the case of the oxygen lattice instead, the modes of the hydrogen and the lattice are coupled, as is shown in Figure 4.31. This means that the hydrogen both loses (at high frequencies) and gains (at lower frequencies) energy interacting with the lattice. Therefore, in Figure 4.32, it is possible to see that $m\gamma C_{vv} > \Re\left[C_{vR}\right]$ for the low frequencies of the hydrogen in the oxygen lattice and vice-versa for the high frequencies. This is a very complex effect due to the high level of coupling between the two elements.

In Section 4.4 we will discuss again this problem and show how the adaptive QTB, presented in Section 3.5, can definitively solve the leakage problem.

4.3.5 Diffusion coefficient

As mentioned before, the QTB allows to introduce the quantum delocalization of the hydrogen into the dynamics of the classical system. Thus, we expect the emergence of NQEs, in particular the zero-point energy..

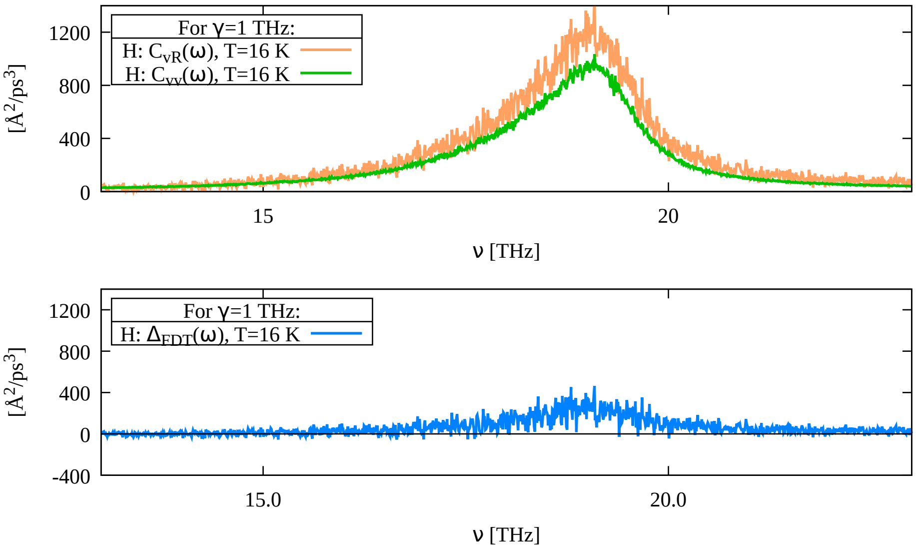

Figure 4.29: Spectra of the hydrogen in the Nb lattice and the corresponding difference between C_{vv} and C_{vF}

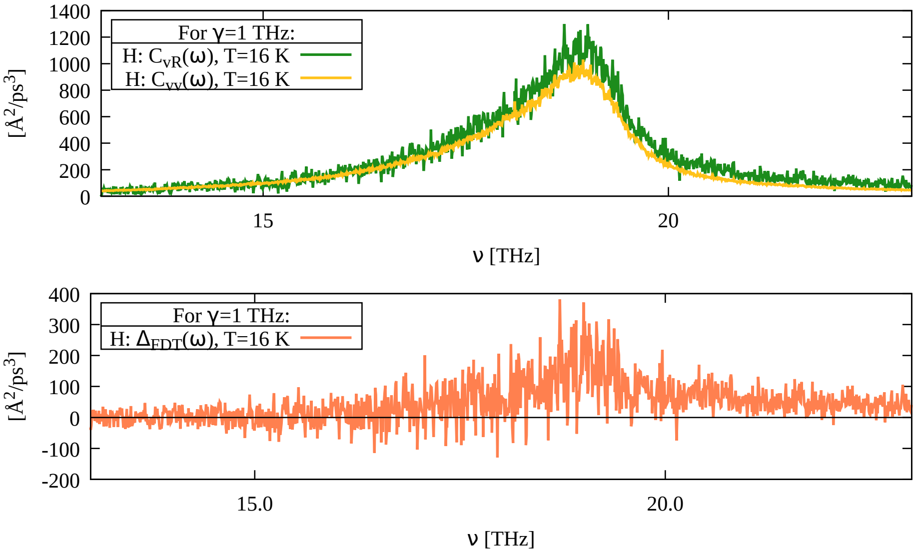

Figure 4.30: Spectra of the hydrogen in the Pb lattice and the corresponding difference between C_{vv} and C_{vF}

The perhaps most remarkable observation is obtained from the dynamical measure of the diffusion coefficients D_x as a function of $1/T$, which are shown in Figure 4.33, 4.34 and 4.35. Note that the Arrhenius behaviour is not expected anymore, since it was a purely classical law (although it should still be recovered

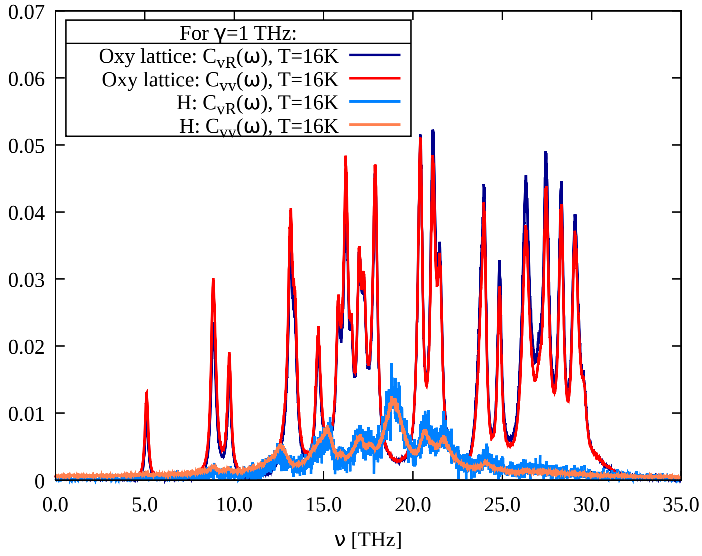

Figure 4.31: Comparison of the spectra of the hydrogen (lighter colours) in the oxygen lattice (darker colours) (in arbitrary units). Clear sight on the difference between the C_{vv} and the C_{vR} spectra, which is the sign of the ZPEL (see Section 3.4.3)

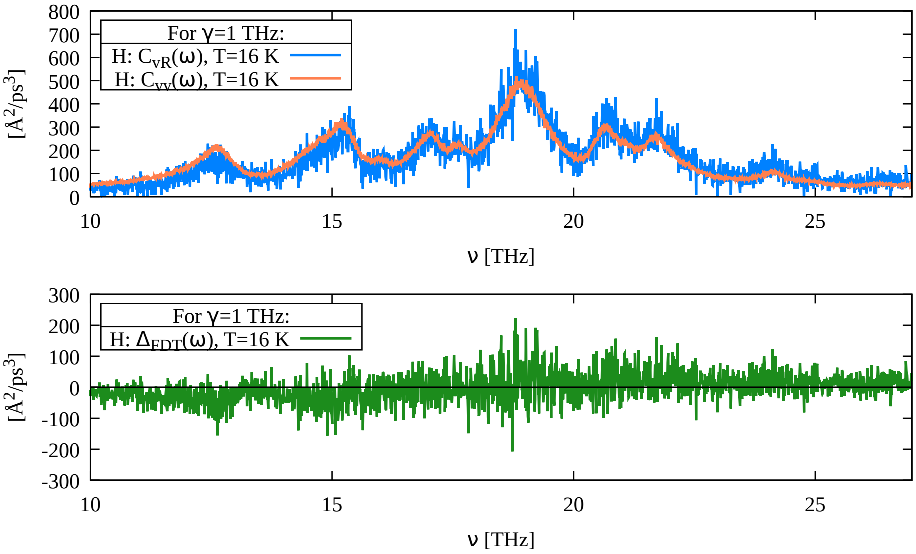

Figure 4.32: Spectra of the hydrogen in the oxygen lattice and the corresponding difference between $m\gamma C_{vv}$ and $\Re\left[C_{vR}\right]$

in the high temperature classical limit). However, we choose to plot the diffusion coefficient as in Section 4.2 in order to facilitate the comparison and show how, in the high temperature limit, the classical diffusion regime is recovered, given the

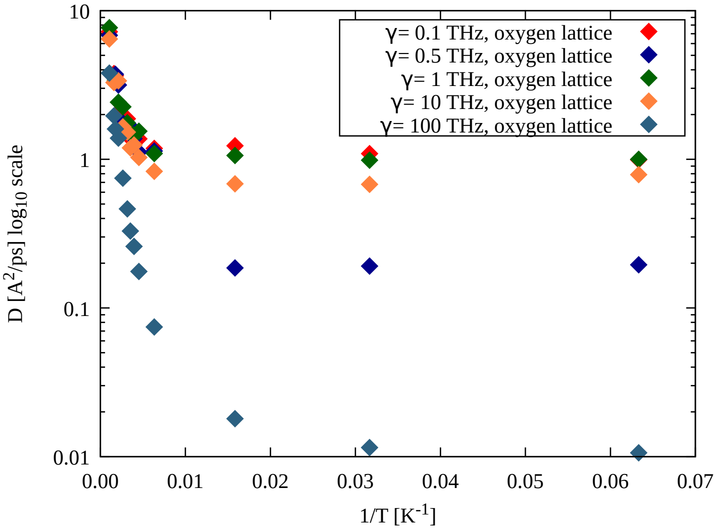

Figure 4.33: Oxygen lattice: Diffusion coefficient in logaritmic scale as a function of the inverse temperature for different values of γ.

characteristic of our system.

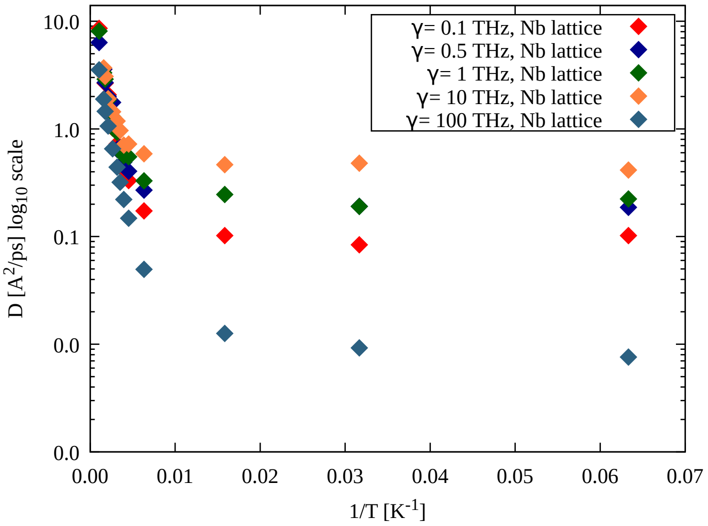

Figure 4.34: Nb lattice: Diffusion coefficient in logaritmic scale as a function of the inverse temperature for different values of γ.

The main NQE that is highlighted by this confront is the saturation of the quantum curves at low temperature. This means that the quantum delocalization of hydrogen and its zero temperature motion enhance diffusion, which is suppressed in the classical case because the classical proton cannot overcome the barrier and hop to one cell to the other if not helped by thermal fluctuations. These quantum fluctuations are thus at the origin of the saturation of the diffusion coefficient to a non-zero value .

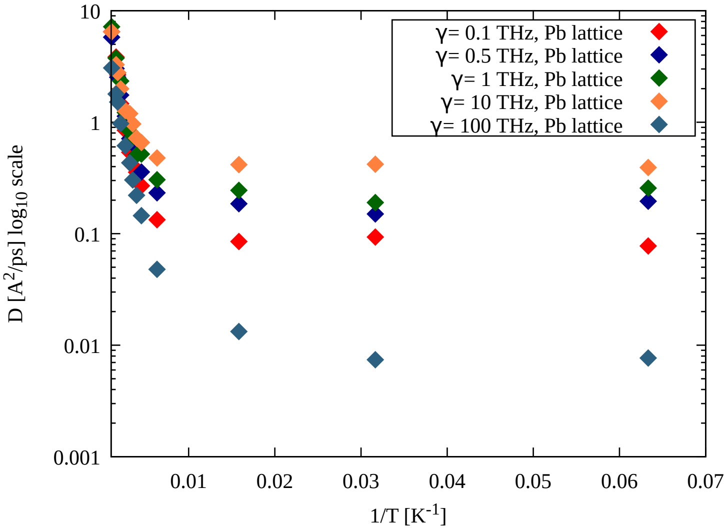

Figure 4.35: Pb lattice: Diffusion coefficient in logaritmic scale as a function of the inverse temperature for different values of γ.

This is an indication that, even for a simple model like the one we created, the QTB takes into account the quantum nature of the hydrogen and the correct qualitative trend is observed. In particular, we are able to reproduce the zero-point energy motion of the light nucleus with the same computational cost of a classical MD simulation.

As already explained in Section 3.4 and Section 4.3.3, when the values of γ increases, the system is forced to have the quantum energy distribution (3.37). In the results of the diffusion coefficients we observe another confirmation of this behaviour of the QTB method. Indeed, as γ increases, the values of D at low temperature saturates to an higher constant, which means the zero-point energy is a stronger NQEs in this case. However, once the γ is so large that we fall in the overdamped regime, this effect is completely reversed.

We notice that a quantitative confirmation of the accuracy of these results can be achieved only with a confront with results obtained with RPMD. In particular, the case of the oxygen, in which strong couplings are present, may hide interesting differences with respect to the other cases. Furthermore, we need still to take care of the ZPEL.

Finally, we observe that, for very large values of the friction parameter γ, it is very hard to recover any quantum behaviour. Indeed, in this overdamped regime, the spectra are so broaden and the dynamics so effected by the bath that no reliable measure can be obtained, even using the correct quantum distribution of energy.

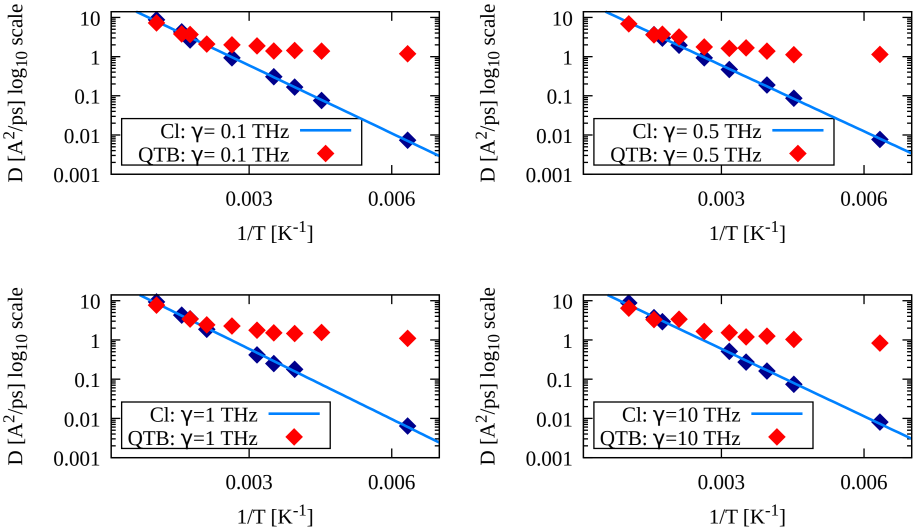

Figure 4.36: Oxygen lattice: comparison of diffusion coefficient in logaritmic scale as a function of the inverse temperature for classical (with Arrhenius fit) and QTB cases.

In Figure 4.36, 4.37 and 4.38 we confront QTB Pb lattice cases with the classical results. As expected, for high temperature, the values of the quantum diffusion coefficients tends to the classical values and, for temperature of the order of $500K$, and the diffusion of the hydrogen driven by nuclear quantum effects is indistinguishable from classical thermal diffusion.

However, the most important result is that at ambient temperature i.e. at about $300K$, the two behaviours start to diverge one from another. Therefore, in our system, we observe the action of NQEs not only in the limit of very low temperature but even at ambient conditions. It is worth noticing that this result depends on the interaction potential (4.2) and on the choice of the parameters which characterize the double-well shown in Figure 2.1. Indeed, for lower values of the barrier, classical diffusion can happen even at low temperature. On the other hand, for very high or very large barriers, also quantum-driven diffusion is suppressed, regardless of the presence of the zero-point energy.

We have concluded the presentation of QTB results. The main problem, as already discussed in Section 3.4 and Section 4.3, is still the ZPEL. We aim to solve this problem with the use of the adaptive QTB (see Section 3.5).

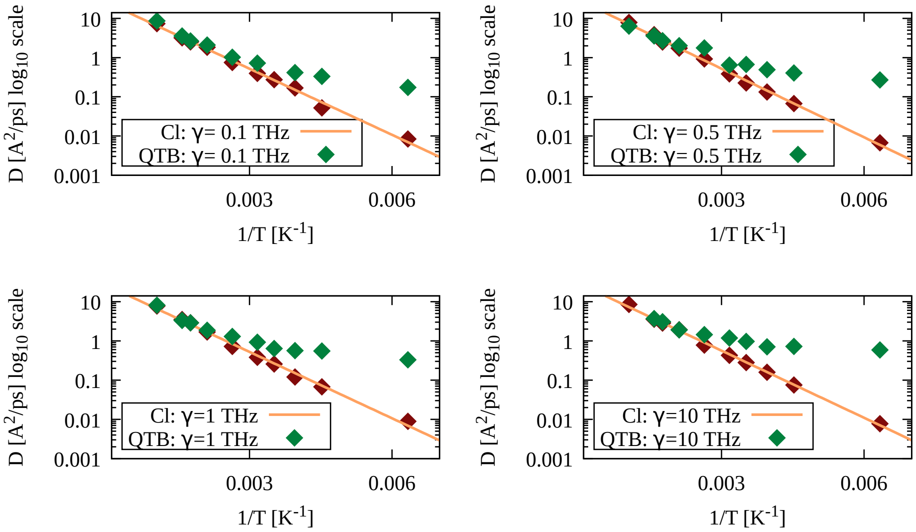

Figure 4.37: Nb lattice: comparison of diffusion coefficient in logaritmic scale as a function of the inverse temperature for classical (with Arrhenius fit) and QTB cases.

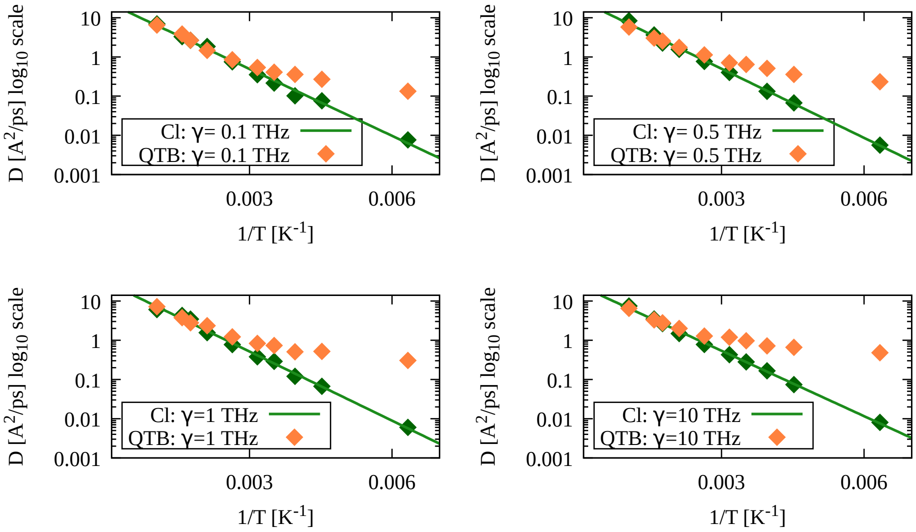

Figure 4.38: Pb lattice: comparison of diffusion coefficient in logaritmic scale as a function of the inverse temperature for classical (with Arrhenius fit) and QTB cases.

4.4 Adaptive QTB results

The main goal of the adaptive Quantum Thermal Bath (adQTB) is to recover the correct quantum energy distribution, given by the quantum FDT (3.38), by eliminating the problem of the ZPEL, as explained in Section 3.5.

Parameters	values $[a.u.]$
ω_{cut}	1×10^{-2}
N_{seg}	2×10^{3}
t	10^{5}
A_{γ}	10^{-6}
$A_{\gamma}^{(H)}$	10^{-7}
γ_0	5×10^{-5}

Table 4.6: Values of the parameters for the adQTB used in the simulations.

4.4.1 Adaptation of $\gamma(\omega)$

As explained in Section 3.5, the main new feature of the adQTB is the introduction of the frequencies depending function $\gamma(\omega)$. The algorithm adapts on the fly the values of this function for each frequency in order to compensate the difference $\Delta_{FDT}(\omega)$, which detects and quantify the ZPEL. Therefore, when convergence is reached, the quantum Fluctuation-Dissipation theorem (3.38) is satisfied and we expect to recover the correct energy distribution.

In Figures 4.39 and 4.40, the values of $\gamma(\omega)$ are shown as they evolve and adapt along the simulation (i.e. for different values of N_{seg}, which is the integration step for $\gamma(\omega)$. We expect to see a trend which is directly related to the difference Δ_{FDT}: at low frequencies, the adaptation will tend to compensate the dissipated energy by decreasing the C_{vv} values and eliminate the energy leaking from the highest modes, whereas in the high frequency regime, we expect the $\gamma(\omega)$ to increase the values of C_{vv} in order to counter the leakage and obtain the correct quantum distribution (3.37).

From Figure 4.39, we can observe that the adaptation for the lattice is relatively fast and after few hundreds of integration steps the initial trend is modified and we reach a configuration for $\gamma(\omega)$ which is mostly stable.

In the Figure 4.40 we have the same plot as before for the adaptation of $\gamma(\omega)$ for the hydrogen degree of freedom. First of all, we noticed that the adaptation requires much more time, due to the fact that the hydrogen is a single atom, while for the lattice we averaged over the number of particles. Moreover, we have used a smaller adaptation velocity $A_{\gamma}^{(H)}$ as reported in Table 4.6. After many hundreds of segments, the $\gamma(\omega)$ has acquired a peculiar shape, due to the fact that the potential in which the hydrogen diffuses is very anharmonic. In particular, for very low frequency, the values of $\gamma(\omega)$ reaches zero, whereas, at high frequencies they have very high values with respect to the initial $\gamma_0 = 2THz$. This fact indicates that the

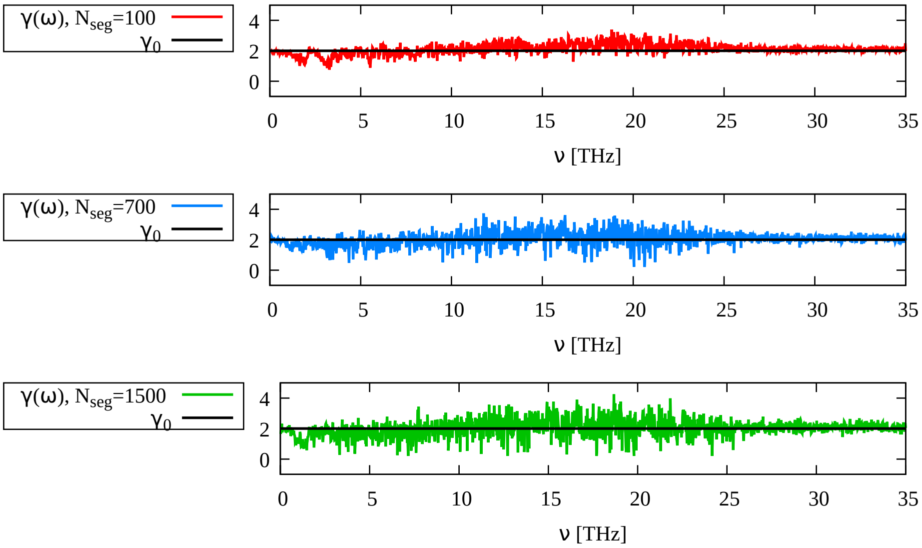

Figure 4.39: Nb lattice:

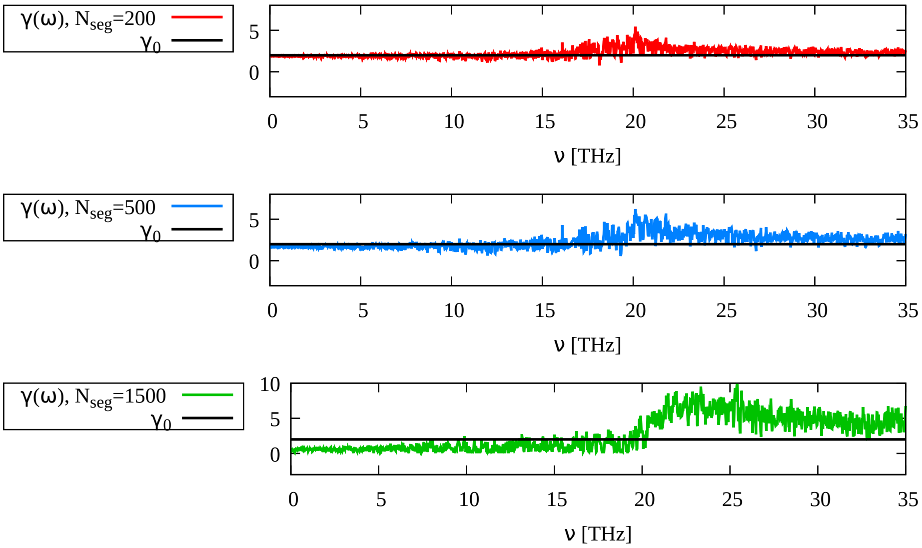

Figure 4.40: Nb lattice:

initial value γ_0 was chosen too low and further simulations are needed to explore this problem.

4.4.2 Spectral analysis

In Figure 4.41 we report the spectra of the hydrogen (light colour) and the Nb lattice (darker colour) after the adaptation of the $\gamma(\omega)$ (the same colour convention of previous section is maintained).

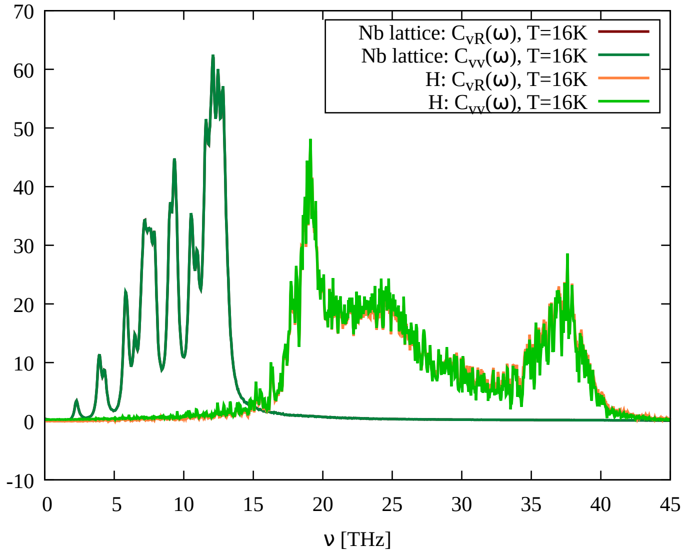

Figure 4.41: Nb lattice spectra (darker colour) and hydrogen spectra (lighter colour) at $T = 16K$

At first, we concentrate on the lattice spectrum. It is clear that the adaptation of γ effectively eliminated the ZPEL: the two power spectra $\Re\left[C_{vR}\right]$ and $m\gamma(\omega)C_{vv}$ (which is now different from the dissipated power spectrum $m\gamma C_{vv}$) are now superimposed and the difference Δ_{FDT} is almost zero.

In Figure 4.42, the removal of the ZPEL is depicted in detail. We note that still a small difference between the two spectra still persists but only consist on statistical fluctuations around zero. Moreover, we notice that the spectra are broader than what was shown previously for small values of γ. However, the feature of the peaks are still observed, which means that the adaptation process stabilize the gamma to values much lower than the overdamped regime.

We analyze now the spectra of the hydrogen, shown in more details in Figure 4.43, together with the difference Δ_{FDT}. Again, the adaptation process removes the ZPEL on the main peak of the hydrogen around $20THz$. We notice that, in order to recover this results for the hydrogen, the adaptation process needs more time and an adaptation velocity A_γ lower, at least of one order of magnitude, in accordance with [23].

The hydrogen spectra present an interesting feature with respect to its classical

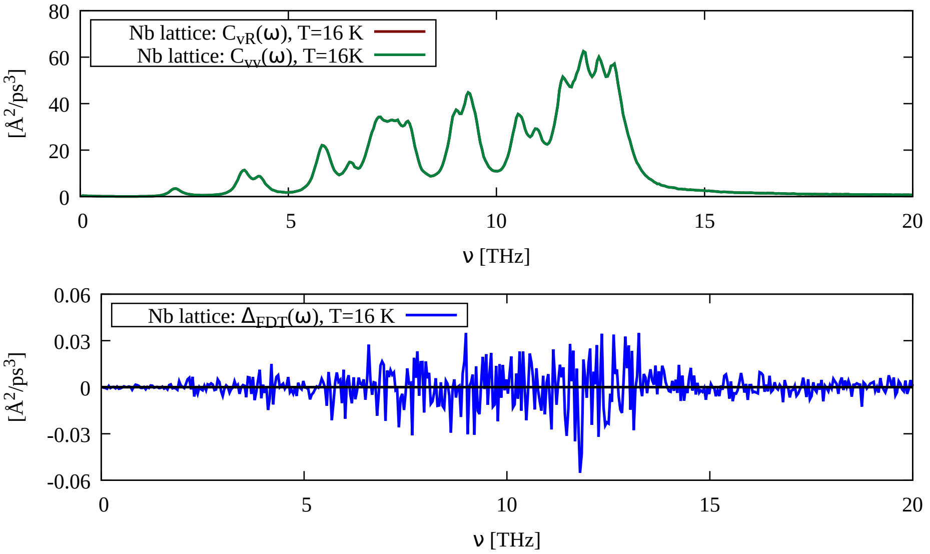

Figure 4.42: Nb lattice spectra and the corresponding difference Δ_{FDT}

and QTB counterparts. In Figure 4.43, we observe a strange asymmetric shape for frequencies higher than $20THz$ and we observe a peak at about $38THz$. This peak is an overtone peak. The overtone peaks are the results of the anharmonicity present in the system and their positions and features, such as symmetry and shape, depend in general on the type of interaction potential of the hydrogen with the lattice.

The presence of overtone peaks and other asymmetric features in the hydrogen spectra was not observed in previous QTB spectral analysis. This is because the $\gamma(\omega)C_{vv}$ is not physically accurate quantity, because $\gamma(\omega)$ is now only a computational tool. This means that the features after observed in the hydrogen's spectrum after $20THz$ are artificially enhanced by $\gamma(\omega)$.

The solutions to this problem are two: we can simply use a smaller ω_{cut}, such that the adaptation of $\gamma(\omega)$ does not reaches the frequencies of the overtone peaks and thus does not detect a grater difference Δ_{FDT}. However, this solution is not preferred since the we might lose some physical information from the spectrum at higher frequencies.

The second solution is to increase the initial value γ_0, which allows the adaptive $\gamma(\omega)$ not to reach zero. This solution is preferred in order to still reproduce the overtone peaks but must be applied carefully. Indeed, as we discussed in Section 4.3, the γ_0 cannot be increased arbitrarily because the overdamped regime must be avoided.

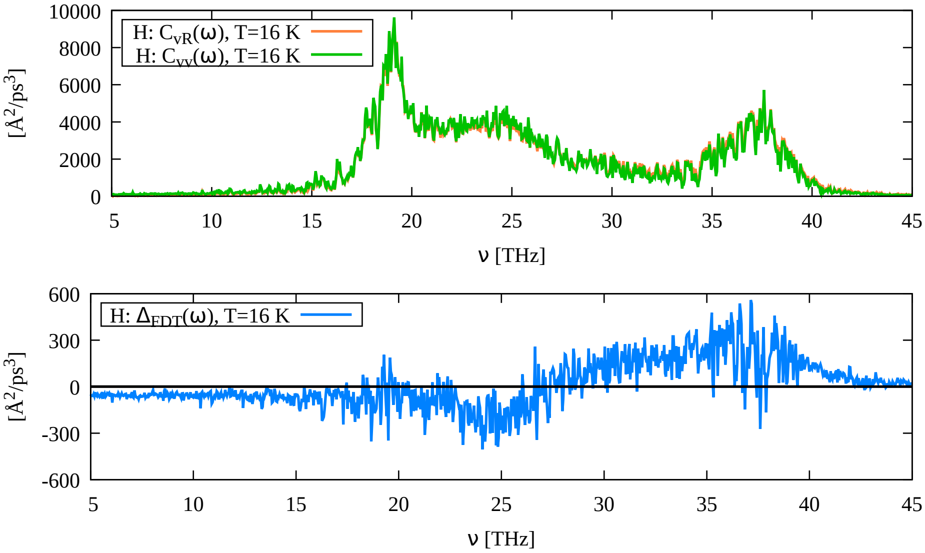

Figure 4.43: Hydrogen (diffusing in Nb lattice) spectra and the corresponding difference Δ_{FDT}

Chapter 5

Conclusions

The main goal of this work is to analyze different Langevin-based MD methods to simulate hydrogen and proton diffusion in which NQEs are present. In particular, the new Quantum Thermal Bath method and its refinement, the adaptive QTB, are discussed in details, from a theoretical, computational and practical point of view. Classical Langevin thermostat is also presented with particular interest because it constitute the very basis of the quantum methods, due to the presence of the same equations and the use of many classical concepts, such as trajectories and classical potential, in the quantum picture. In order to study in details the performances and the limits of these methods, a simple 2D triangular lattice is created and the diffusion problem of a single hydrogen particle is considered.

The results obtained from the simulations are divided in three parts. First, classical Langevin thermostat is used to study the dependence of spectra and diffusion coefficient from the frictional parameter γ. We found that for values of γ of the order of $10THz$, the spectra are broaden but still accurate dynamics results, such as the diffusion coefficient, can be obtained. Moreover, the static and dynamics measures are compared with the Arrhenius law and they are in agreement, as expected. Finally, the interesting and complex phenomenon of phonon assisted hopping was studied. Our results indicate that the presence of phonons enhances diffusion of the proton almost regardless on the values of the mass of the lattice's atoms. The appearance of this feature is a remarkable physical result for the simple model under study. Further developments of the classical simulations can include the study of the free energy profile of the saddle point and a more precise study of the effect of phonons on the diffusion coefficient.

Then, the QTB was implemented with the aim of computing the diffusion coefficient and find evidence of NQEs, in particular zero-point energy, which can play a role in the diffusion behaviour of the hydrogen. Moreover, we wanted to analyse the spectra and probe the Zero-Point Energy Leakage for different values of γ. For both objectives, we obtained interesting results: the ZPEL shows a strong dependence on the parameter γ, which strongly motivates the implementation of the adaptation. Then, we were able to correctly quantify this dependence and use it in the Adaptive QTB method, which is one of the most advanced MD method proposed to study efficiently NQEs in complex systems. Moreover, a clear sign of the zero-point energy was observed in both the spectral analysis and the dynamical measurements of the diffusion coefficients. Quantitative evaluation of the results of this work can be achieved by RPMD techniques, through which we will be also able to assess the effect of tunneling on hydrogen diffusion.

Overall, this work constitutes a first step for the study of quantum diffusion of the hydrogen, from both theoretical and computational points of view. Through a simple system and the problem of the diffusion of a quantum particle in a solid lattice, we had the opportunity to grasp the great complexity of modeling correctly quantum dynamical phenomena. This was achieved not only by the deepening on the state-of-the-art literature but also with the active challenge of implementing and assessing new quantum MD approach which are extremely advanced and promising in the future applications to real systems.

Bibliography

[1] Ian R. Sims. «Tunnelling in space». en. In: *Nature Chemistry* 5.9 (Sept. 2013), pp. 734–736. ISSN: 1755-4330, 1755-4349. DOI: `10.1038/nchem.1736`. URL: `http://www.nature.com/articles/nchem.1736` (cit. on p. 2).

[2] Yael Bronstein, Philippe Depondt, Fabio Finocchi, and Antonino Marco Saitta. «Quantum-driven phase transition in ice described via an efficient Langevin approach». en. In: *Physical Review B* 89.21 (June 2014), p. 214101. ISSN: 1098-0121, 1550-235X. DOI: `10.1103/PhysRevB.89.214101`. URL: `https://link.aps.org/doi/10.1103/PhysRevB.89.214101` (cit. on pp. 2, 3, 49, 59).

[3] Michele Ceriotti, Wei Fang, Peter G. Kusalik, Ross H. McKenzie, Angelos Michaelides, Miguel A. Morales, and Thomas E. Markland. «Nuclear Quantum Effects in Water and Aqueous Systems: Experiment, Theory, and Current Challenges». en. In: *Chemical Reviews* 116.13 (July 2016), pp. 7529–7550. ISSN: 0009-2665, 1520-6890. DOI: `10.1021/acs.chemrev.5b00674`. URL: `https://pubs.acs.org/doi/10.1021/acs.chemrev.5b00674` (cit. on p. 2).

[4] Kevin M. Hickson, Jean-Christophe Loison, Dianailys Nuñez-Reyes, and Raphaël Méreau. «Quantum Tunneling Enhancement of the C + H_2O and C + D_2O Reactions at Low Temperature». en. In: *The Journal of Physical Chemistry Letters* 7.18 (Sept. 2016), pp. 3641–3646. ISSN: 1948-7185. DOI: `10.1021/acs.jpclett.6b01637`. URL: `https://pubs.acs.org/doi/10.1021/acs.jpclett.6b01637` (cit. on p. 2).

[5] Yael Bronstein, Philippe Depondt, Livia E. Bove, Richard Gaal, Antonino Marco Saitta, and Fabio Finocchi. «Quantum versus classical protons in pure and salty ice under pressure». en. In: *Physical Review B* 93.2 (Jan. 2016), p. 024104. ISSN: 2469-9950, 2469-9969. DOI: `10.1103/PhysRevB.93.024104`. URL: `https://link.aps.org/doi/10.1103/PhysRevB.93.024104` (cit. on pp. 2, 3, 49).

[6] Wojciech Grochala and Peter P. Edwards. «Thermal Decomposition of the Non-Interstitial Hydrides for the Storage and Production of Hydrogen». en. In: *Chemical Reviews* 104.3 (Mar. 2004), pp. 1283–1316. ISSN: 0009-2665,

1520-6890. DOI: 10.1021/cr030691s. URL: https://pubs.acs.org/doi/10.1021/cr030691s (cit. on pp. 2, 4).

[7] Klaus-Dieter Kreuer, Stephen J. Paddison, Eckhard Spohr, and Michael Schuster. «Transport in Proton Conductors for Fuel-Cell Applications: Simulations, Elementary Reactions, and Phenomenology». en. In: *Chemical Reviews* 104.10 (Oct. 2004), pp. 4637–4678. ISSN: 0009-2665, 1520-6890. DOI: 10.1021/cr020715f. URL: https://pubs.acs.org/doi/10.1021/cr020715f (cit. on pp. 2, 4).

[8] Romain Dupuis, Jorge S. Dolado, Magali Benoit, Jose Surga, and Andrés Ayuela. «Quantum Nuclear Dynamics of Protons within Layered Hydroxides at High Pressure». en. In: *Scientific Reports* 7.1 (Dec. 2017), p. 4842. ISSN: 2045-2322. DOI: 10.1038/s41598-017-04080-2. URL: http://www.nature.com/articles/s41598-017-04080-2 (cit. on p. 2).

[9] Lei Zhang, Wei-Lie Zhong, and Wolfgang Kleemann. «A study of the quantum effect in BaTiO3». en. In: *Physics Letters A* 276.1-4 (Oct. 2000), pp. 162–166. ISSN: 03759601. DOI: 10.1016/S0375-9601(00)00632-0. URL: https://linkinghub.elsevier.com/retrieve/pii/S0375960100006320 (cit. on p. 2).

[10] Xianzhe Jia, Margaret G. Kivelson, Krishan K. Khurana, and Raymond J. Walker. «Magnetic Fields of the Satellites of Jupiter and Saturn». en. In: *Space Science Reviews* 152.1-4 (May 2010), pp. 271–305. ISSN: 0038-6308, 1572-9672. DOI: 10.1007/s11214-009-9507-8. URL: http://link.springer.com/10.1007/s11214-009-9507-8 (cit. on p. 2).

[11] Dongdong Kang, Huayang Sun, Jiayu Dai, Wenbo Chen, Zengxiu Zhao, Yong Hou, Jiaolong Zeng, and Jianmin Yuan. «Nuclear quantum dynamics in dense hydrogen». en. In: *Scientific Reports* 4.1 (May 2015), p. 5484. ISSN: 2045-2322. DOI: 10.1038/srep05484. URL: http://www.nature.com/articles/srep05484 (cit. on p. 2).

[12] Magali Benoit, Dominik Marx, and Michele Parrinello. «Tunnelling and zero-point motion in high-pressure ice». en. In: *Nature* 392.6673 (Mar. 1998), pp. 258–261. ISSN: 0028-0836, 1476-4687. DOI: 10.1038/32609. URL: http://www.nature.com/articles/32609 (cit. on p. 2).

[13] José Teixeira. «The double identity of ice X». en. In: *Nature* 392.6673 (Mar. 1998), pp. 232–233. ISSN: 0028-0836, 1476-4687. DOI: 10.1038/32542. URL: http://www.nature.com/articles/32542 (cit. on p. 3).

[14] L.D. Landau and E.M. Lifshitz. *Statistical Physics: Volume 5*. v. 5. Elsevier Science, 2013. ISBN: 9780080570464. URL: https://books.google.fr/books?id=VzgJN-XPTRsC (cit. on p. 3).

[15] Olivier May, Juraj Fedor, and Michael Allan. «Isotope effect in dissociative electron attachment cross sections in acetylene». en. In: *Journal of Physics: Conference Series* 194.5 (Nov. 2009), p. 052006. ISSN: 1742-6596. DOI: `10.1088/1742-6596/194/5/052006`. URL: `https://iopscience.iop.org/article/10.1088/1742-6596/194/5/052006` (cit. on p. 3).

[16] Hichem Dammak, Ekaterina Antoshchenkova, Marc Hayoun, and Fabio Finocchi. «Isotope effects in lithium hydride and lithium deuteride crystals by molecular dynamics simulations». en. In: *Journal of Physics: Condensed Matter* 24.43 (Oct. 2012), p. 435402. ISSN: 0953-8984, 1361-648X. DOI: `10.1088/0953-8984/24/43/435402`. URL: `https://iopscience.iop.org/article/10.1088/0953-8984/24/43/435402` (cit. on pp. 3, 49).

[17] K Liang and A Nowick. «High-temperature protonic conduction in mixed perovskite ceramics». en. In: *Solid State Ionics* 61.1-3 (May 1993), pp. 77–81. ISSN: 01672738. DOI: `10.1016/0167-2738(93)90337-3`. URL: `https://linkinghub.elsevier.com/retrieve/pii/0167273893903373` (cit. on p. 4).

[18] Sofiane Schaack, Philippe Depondt, Simon Huppert, and Fabio Finocchi. «Quantum driven proton diffusion in brucite-like minerals under high pressure». en. In: *Scientific Reports* 10.1 (Dec. 2020), p. 8123. ISSN: 2045-2322. DOI: `10.1038/s41598-020-64813-8`. URL: `http://www.nature.com/articles/s41598-020-64813-8` (cit. on p. 4).

[19] Mariana Rossi, Michele Ceriotti, and David E. Manolopoulos. «Nuclear Quantum Effects in H $^{+}$ and OH $^{-}$ Diffusion along Confined Water Wires». en. In: *The Journal of Physical Chemistry Letters* 7.15 (Aug. 2016), pp. 3001–3007. ISSN: 1948-7185. DOI: `10.1021/acs.jpclett.6b01093`. URL: `https://pubs.acs.org/doi/10.1021/acs.jpclett.6b01093` (cit. on p. 4).

[20] S. Glasstone, K.J. Laidler, H. Eyring, and L.P. Hammet. *The Theory of Rate Processes: The Kinetics of Chemical Reactions, Viscosity, Diffusion and Electrochemical Phenomena*. International chemical series. McGraw-Hill Book Company, Incorporated, 1941. URL: `https://books.google.fr/books?id=iv6TzQEACAAJ` (cit. on pp. 4, 25).

[21] Riccardo Spezia and Hichem Dammak. «On the Use of Quantum Thermal Bath in Unimolecular Fragmentation Simulation». en. In: *The Journal of Physical Chemistry A* 123.40 (Oct. 2019), pp. 8542–8551. ISSN: 1089-5639, 1520-5215. DOI: `10.1021/acs.jpca.9b06795`. URL: `https://pubs.acs.org/doi/10.1021/acs.jpca.9b06795` (cit. on pp. 5, 26).

[22] Hichem Dammak, Yann Chalopin, Marine Laroche, Marc Hayoun, and Jean-Jacques Greffet. «Quantum Thermal Bath for Molecular Dynamics Simulation». en. In: *Physical Review Letters* 103.19 (Nov. 2009), p. 190601. ISSN: 0031-9007, 1079-7114. DOI: `10.1103/PhysRevLett.103.190601`. URL: `https://link.aps.org/doi/10.1103/PhysRevLett.103.190601` (cit. on pp. 5, 45).

[23] Etienne Mangaud, Simon Huppert, Thomas Plé, Philippe Depondt, Sara Bonella, and Fabio Finocchi. «The Fluctuation–Dissipation Theorem as a Diagnosis and Cure for Zero-Point Energy Leakage in Quantum Thermal Bath Simulations». en. In: *Journal of Chemical Theory and Computation* 15.5 (May 2019), pp. 2863–2880. ISSN: 1549-9618, 1549-9626. DOI: `10.1021/acs.jctc.8b01164`. URL: `https://pubs.acs.org/doi/10.1021/acs.jctc.8b01164` (cit. on pp. 6, 47, 50–52, 89).

[24] J. L. Garcia-Palacios. «Introduction to the theory of stochastic processes and Brownian motion problems». en. In: *arXiv:cond-mat/0701242* (Jan. 2007). arXiv: cond-mat/0701242. URL: `http://arxiv.org/abs/cond-mat/0701242` (cit. on pp. 7–9).

[25] M.E. Tuckerman. *Statistical Mechanics: Theory and Molecular Simulation*. Oxford graduate texts. Oxford University Press, 2010. URL: `https://books.google.fr/books?id=UMM2NAEACAAJ` (cit. on pp. 7, 19, 22, 24, 37, 47).

[26] R Kubo. «The fluctuation-dissipation theorem». en. In: (1966), p. 31 (cit. on pp. 7, 8, 19, 46).

[27] N.G. Van Kampen. *Stochastic Processes in Physics and Chemistry*. North-Holland Personal Library. Elsevier Science, 2011. ISBN: 9780080475363. URL: `https://books.google.fr/books?id=N6II-6HlPxEC` (cit. on pp. 7, 12).

[28] Don S. Lemons and Anthony Gythiel. «Paul Langevin's 1908 paper "On the Theory of Brownian Motion" ["Sur la théorie du mouvement brownien," C. R. Acad. Sci. (Paris) **146** , 530–533 (1908)]». en. In: *American Journal of Physics* 65.11 (Nov. 1997), pp. 1079–1081. ISSN: 0002-9505, 1943-2909. DOI: `10.1119/1.18725`. URL: `http://aapt.scitation.org/doi/10.1119/1.18725` (cit. on p. 7).

[29] R. Brown and J.J. Bennett. *The Miscellaneous Botanical Works of Robert Brown*. Ray Society publication. Ray Society, 1866. URL: `https://books.google.fr/books?id=Dy6nz9VMsOcC` (cit. on p. 7).

[30] A. Einstein. «Über die von der molekularkinetischen Theorie der Wärme geforderte Bewegung von in ruhenden Flüssigkeiten suspendierten Teilchen». de. In: *Annalen der Physik* 322.8 (1905), pp. 549–560. ISSN: 00033804, 15213889. DOI: `10.1002/andp.19053220806`. URL: `http://doi.wiley.com/10.1002/andp.19053220806` (cit. on p. 7).

[31] J. Perrin. *Brownian Movement and Molecular Reality*. Taylor & Francis, 1910. URL: https://books.google.fr/books?id=eARJAAAAIAAJ (cit. on p. 7).

[32] R Zwanzig. «Time-Correlation Functions and Transport Coefficients in Statistical Mechanics». en. In: *Annual Review of Physical Chemistry* 16.1 (Oct. 1965), pp. 67–102. ISSN: 0066-426X, 1545-1593. DOI: 10.1146/annurev.pc.16.100165.000435. URL: http://www.annualreviews.org/doi/10.1146/annurev.pc.16.100165.000435 (cit. on p. 18).

[33] Ian R. Craig and David E. Manolopoulos. «Quantum statistics and classical mechanics: Real time correlation functions from ring polymer molecular dynamics». en. In: *The Journal of Chemical Physics* 121.8 (Aug. 2004), pp. 3368–3373. ISSN: 0021-9606, 1089-7690. DOI: 10.1063/1.1777575. URL: http://aip.scitation.org/doi/10.1063/1.1777575 (cit. on pp. 18, 19, 42).

[34] Scott Habershon, David E. Manolopoulos, Thomas E. Markland, and Thomas F. Miller. «Ring-Polymer Molecular Dynamics: Quantum Effects in Chemical Dynamics from Classical Trajectories in an Extended Phase Space». en. In: *Annual Review of Physical Chemistry* 64.1 (Apr. 2013), pp. 387–413. ISSN: 0066-426X, 1545-1593. DOI: 10.1146/annurev-physchem-040412-110122. URL: http://www.annualreviews.org/doi/10.1146/annurev-physchem-040412-110122 (cit. on pp. 19, 28, 42).

[35] N. Pottier. *Physique statistique hors d'équilibre: processus irréversibles linéaires*. Savoirs actuels. EDP Sciences, 2007. ISBN: 9782868839343. URL: https://books.google.fr/books?id=OY3JzcPOqu0C (cit. on p. 20).

[36] Richard P. Feynman, Laurie M. Brown, Richard P. Feynman, Richard P. Feynman, and P. A. M. Dirac. *Feynman's thesis: a new approach to quantum theory*. en. OCLC: ocm62332166. Hackensack, NJ: World Scientific, 2005. ISBN: 978-981-256-366-8 978-981-256-380-4 (cit. on p. 22).

[37] G. C. Wick. «Properties of Bethe-Salpeter Wave Functions». en. In: *Physical Review* 96.4 (Nov. 1954), pp. 1124–1134. ISSN: 0031-899X. DOI: 10.1103/PhysRev.96.1124. URL: https://link.aps.org/doi/10.1103/PhysRev.96.1124 (cit. on p. 23).

[38] Rüdiger Achilles and Andrea Bonfiglioli. «The early proofs of the theorem of Campbell, Baker, Hausdorff, and Dynkin». en. In: *Archive for History of Exact Sciences* 66.3 (May 2012), pp. 295–358. ISSN: 0003-9519, 1432-0657. DOI: 10.1007/s00407-012-0095-8. URL: http://link.springer.com/10.1007/s00407-012-0095-8 (cit. on pp. 24, 32).

[39] Sven Karsten, Sergei D. Ivanov, Sergey I. Bokarev, and Oliver Kühn. «Simulating vibronic spectra via Matsubara-like dynamics: Coping with the sign problem». en. In: *The Journal of Chemical Physics* 149.19 (Nov. 2018), p. 194103. ISSN: 0021-9606, 1089-7690. DOI: `10.1063/1.5046874`. URL: `http://aip.scitation.org/doi/10.1063/1.5046874` (cit. on p. 25).

[40] Gustav-Stresemann-Institut e.V. für Übernationale Bildung und Europäische Zusammenarbeit, John von Neumann-Institut für Computing, Johannes Gutenberg-Universität Mainz, Max-Planck-Institut für Biophysikalische Chemie, and Max-Planck-Institut für Polymerforschung, eds. *Computational soft matter: from synthetic polymers to proteins; Winter School, 29 February - 6 March 2004, Gustav-Stresemann-Institut, Bonn, Germany. 2: Lecture notes.* en. NIC series 23. Meeting Name: Winter School. Gustav-Stresemann-Institut OCLC: 253989746. Jülich: NIC, 2004. ISBN: 978-3-00-012641-3 (cit. on p. 28).

[41] Joseph E. Lawrence and David E. Manolopoulos. «Path integral methods for reaction rates in complex systems». en. In: *Faraday Discussions* 221 (2020), pp. 9–29. ISSN: 1359-6640, 1364-5498. DOI: `10.1039/C9FD00084D`. URL: `http://xlink.rsc.org/?DOI=C9FD00084D` (cit. on pp. 28, 42–44).

[42] Jian Liu, Dezhang Li, and Xinzijian Liu. «A simple and accurate algorithm for path integral molecular dynamics with the Langevin thermostat». en. In: *The Journal of Chemical Physics* 145.2 (July 2016), p. 024103. ISSN: 0021-9606, 1089-7690. DOI: `10.1063/1.4954990`. URL: `http://aip.scitation.org/doi/10.1063/1.4954990` (cit. on pp. 28, 42).

[43] Jianshu Cao and Gregory A. Voth. «The formulation of quantum statistical mechanics based on the Feynman path centroid density. III. Phase space formalism and analysis of centroid molecular dynamics». en. In: *The Journal of Chemical Physics* 101.7 (Oct. 1994), pp. 6157–6167. ISSN: 0021-9606, 1089-7690. DOI: `10.1063/1.468503`. URL: `http://aip.scitation.org/doi/10.1063/1.468503` (cit. on p. 28).

[44] Alexander Witt, Sergei D. Ivanov, Motoyuki Shiga, Harald Forbert, and Dominik Marx. «On the applicability of centroid and ring polymer path integral molecular dynamics for vibrational spectroscopy». en. In: *The Journal of Chemical Physics* 130.19 (May 2009), p. 194510. ISSN: 0021-9606, 1089-7690. DOI: `10.1063/1.3125009`. URL: `http://aip.scitation.org/doi/10.1063/1.3125009` (cit. on pp. 28, 44).

[45] Fabien Brieuc, Yael Bronstein, Hichem Dammak, Philippe Depondt, Fabio Finocchi, and Marc Hayoun. «Zero-Point Energy Leakage in Quantum Thermal Bath Molecular Dynamics Simulations». en. In: *Journal of Chemical Theory and Computation* 12.12 (Dec. 2016), pp. 5688–5697. ISSN: 1549-9618,

1549-9626. DOI: 10.1021/acs.jctc.6b00684. URL: https://pubs.acs.org/doi/10.1021/acs.jctc.6b00684 (cit. on pp. 29, 49, 50, 79).

[46] Mark E. Tuckerman, Bruce J. Berne, Glenn J. Martyna, and Michael L. Klein. «Efficient molecular dynamics and hybrid Monte Carlo algorithms for path integrals». en. In: *The Journal of Chemical Physics* 99.4 (Aug. 1993), pp. 2796–2808. ISSN: 0021-9606, 1089-7690. DOI: 10.1063/1.465188. URL: http://aip.scitation.org/doi/10.1063/1.465188 (cit. on p. 29).

[47] Loup Verlet. «Computer "Experiments" on Classical Fluids. I. Thermodynamical Properties of Lennard-Jones Molecules». en. In: *Physical Review* 159.1 (July 1967), pp. 98–103. ISSN: 0031-899X. DOI: 10.1103/PhysRev.159.98. URL: https://link.aps.org/doi/10.1103/PhysRev.159.98 (cit. on p. 30).

[48] Joel E. Cohen, Shmuel Friedland, Tosio Kato, and Frank P. Kelly. «Eigenvalue inequalities for products of matrix exponentials». en. In: *Linear Algebra and its Applications* 45 (June 1982), pp. 55–95. ISSN: 00243795. DOI: 10.1016/0024-3795(82)90211-7. URL: https://linkinghub.elsevier.com/retrieve/pii/0024379582902117 (cit. on p. 32).

[49] William C. Swope, Hans C. Andersen, Peter H. Berens, and Kent R. Wilson. «A computer simulation method for the calculation of equilibrium constants for the formation of physical clusters of molecules: Application to small water clusters». en. In: *The Journal of Chemical Physics* 76.1 (Jan. 1982), pp. 637–649. ISSN: 0021-9606, 1089-7690. DOI: 10.1063/1.442716. URL: http://aip.scitation.org/doi/10.1063/1.442716 (cit. on p. 32).

[50] H. J. C. Berendsen, J. P. M. Postma, W. F. van Gunsteren, A. DiNola, and J. R. Haak. «Molecular dynamics with coupling to an external bath». en. In: *The Journal of Chemical Physics* 81.8 (Oct. 1984), pp. 3684–3690. ISSN: 0021-9606, 1089-7690. DOI: 10.1063/1.448118. URL: http://aip.scitation.org/doi/10.1063/1.448118 (cit. on p. 33).

[51] William G. Hoover and Brad Lee Holian. «Kinetic moments method for the canonical ensemble distribution». en. In: *Physics Letters A* 211.5 (Feb. 1996), pp. 253–257. ISSN: 03759601. DOI: 10.1016/0375-9601(95)00973-6. URL: https://linkinghub.elsevier.com/retrieve/pii/0375960195009736 (visited on 10/07/2020) (cit. on p. 33).

[52] Glenn J. Martyna, Michael L. Klein, and Mark Tuckerman. «Nosé–Hoover chains: The canonical ensemble via continuous dynamics». en. In: *The Journal of Chemical Physics* 97.4 (Aug. 1992), pp. 2635–2643. ISSN: 0021-9606, 1089-7690. DOI: 10.1063/1.463940. URL: http://aip.scitation.org/doi/10.1063/1.463940 (cit. on p. 33).

[53] Hans C. Andersen. «Molecular dynamics simulations at constant pressure and/or temperature». en. In: *The Journal of Chemical Physics* 72.4 (Feb. 1980), pp. 2384–2393. ISSN: 0021-9606, 1089-7690. DOI: `10.1063/1.439486`. URL: `http://aip.scitation.org/doi/10.1063/1.439486` (cit. on p. 33).

[54] Giovanni Bussi, Davide Donadio, and Michele Parrinello. «Canonical sampling through velocity-rescaling». en. In: *The Journal of Chemical Physics* 126.1 (Jan. 2007). arXiv: 0803.4060, p. 014101. ISSN: 0021-9606, 1089-7690. DOI: `10.1063/1.2408420`. URL: `http://arxiv.org/abs/0803.4060` (cit. on p. 33).

[55] Shuichi Nosé. «A unified formulation of the constant temperature molecular dynamics methods». en. In: *The Journal of Chemical Physics* 81.1 (July 1984), pp. 511–519. ISSN: 0021-9606, 1089-7690. DOI: `10.1063/1.447334`. URL: `http://aip.scitation.org/doi/10.1063/1.447334` (cit. on p. 33).

[56] B. Leimkuhler and C. Matthews. «Rational Construction of Stochastic Numerical Methods for Molecular Sampling». en. In: *Applied Mathematics Research eXpress* (June 2012), abs010. ISSN: 1687-1200, 1687-1197. DOI: `10.1093/amrx/abs010`. URL: `https://academic.oup.com/amrx/article-lookup/doi/10.1093/amrx/abs010` (cit. on p. 33).

[57] Benedict Leimkuhler and Charles Matthews. «Robust and efficient configurational molecular sampling via Langevin dynamics». en. In: *The Journal of Chemical Physics* 138.17 (May 2013), p. 174102. ISSN: 0021-9606, 1089-7690. DOI: `10.1063/1.4802990`. URL: `http://aip.scitation.org/doi/10.1063/1.4802990` (cit. on p. 33).

[58] Benedict Leimkuhler and Charles Matthews. «Efficient molecular dynamics using geodesic integration and solvent–solute splitting». en. In: *Proceedings of the Royal Society A: Mathematical, Physical and Engineering Sciences* 472.2189 (May 2016), p. 20160138. ISSN: 1364-5021, 1471-2946. DOI: `10.1098/rspa.2016.0138`. URL: `https://royalsocietypublishing.org/doi/10.1098/rspa.2016.0138` (cit. on pp. 33, 34).

[59] E Kestemont and J Van Craen. «On the computation of correlation functions in molecular dynamics experiments». en. In: *Journal of Computational Physics* 22.4 (Dec. 1976), pp. 451–458. ISSN: 00219991. DOI: `10.1016/0021-9991(76)90043-7`. URL: `https://linkinghub.elsevier.com/retrieve/pii/0021999176900437` (cit. on p. 39).

[60] Timothy J. H. Hele, Michael J. Willatt, Andrea Muolo, and Stuart C. Althorpe. «Communication: Relation of centroid molecular dynamics and ring-polymer molecular dynamics to exact quantum dynamics». en. In: *The Journal of Chemical Physics* 142.19 (May 2015), p. 191101. ISSN: 0021-9606, 1089-7690.

DOI: 10.1063/1.4921234. URL: http://aip.scitation.org/doi/10.1063/1.4921234 (cit. on pp. 42, 44).

[61] William H. Miller. «The Semiclassical Initial Value Representation: A Potentially Practical Way for Adding Quantum Effects to Classical Molecular Dynamics Simulations». en. In: *The Journal of Physical Chemistry A* 105.13 (Apr. 2001), pp. 2942–2955. ISSN: 1089-5639, 1520-5215. DOI: 10.1021/jp003712k. URL: https://pubs.acs.org/doi/10.1021/jp003712k (visited on 10/09/2020) (cit. on p. 44).

[62] Michele Ceriotti, Giovanni Bussi, and Michele Parrinello. «Nuclear Quantum Effects in Solids Using a Colored-Noise Thermostat». en. In: *Physical Review Letters* 103.3 (July 2009), p. 030603. ISSN: 0031-9007, 1079-7114. DOI: 10.1103/PhysRevLett.103.030603. URL: https://link.aps.org/doi/10.1103/PhysRevLett.103.030603 (cit. on p. 45).

[63] Michele Ceriotti, Giovanni Bussi, and Michele Parrinello. «Colored-Noise Thermostats à la Carte». en. In: *Journal of Chemical Theory and Computation* 6.4 (Apr. 2010), pp. 1170–1180. ISSN: 1549-9618, 1549-9626. DOI: 10.1021/ct900563s. URL: https://pubs.acs.org/doi/10.1021/ct900563s (cit. on p. 45).

[64] Herbert B. Callen and Theodore A. Welton. «Irreversibility and Generalized Noise». en. In: *Physical Review* 83.1 (July 1951), pp. 34–40. ISSN: 0031-899X. DOI: 10.1103/PhysRev.83.34. URL: https://link.aps.org/doi/10.1103/PhysRev.83.34 (cit. on pp. 46, 47).

[65] Jean-Louis Barrat and David Rodney. «Portable Implementation of a Quantum Thermal Bath for Molecular Dynamics Simulations». en. In: *Journal of Statistical Physics* 144.3 (Aug. 2011), pp. 679–689. ISSN: 0022-4715, 1572-9613. DOI: 10.1007/s10955-011-0193-z. URL: http://link.springer.com/10.1007/s10955-011-0193-z (cit. on p. 48).

[66] Philip M. Morse. «Diatomic Molecules According to the Wave Mechanics. II. Vibrational Levels». In: *Phys. Rev.* 34 (1 July 1929), pp. 57–64. DOI: 10.1103/PhysRev.34.57. URL: https://link.aps.org/doi/10.1103/PhysRev.34.57 (cit. on p. 57).